Data-Driven Applications for Connected Vehicle Based Traffic Signal Systems

by

Jianfeng Zheng

A dissertation submitted in partial fulfillment
of the requirements for the degree of
Doctor of Philosophy
(Civil Engineering)
in the University of Michigan
2016

Doctoral Committee:

Professor Henry X. Liu, Chair
Assistant Professor Branko Kerkez
Professor Huei Peng
Research Scientist James Sayer

Acknowledgments

First and foremost, I would like to express my deepest gratitude to my adviser, Prof. Henry X. Liu. His unwavering support, patient guidance and astute mentorship are deeply appreciated. Prof. Liu has the distinctive ability to "see the big picture" and always expertly guided me to the right research direction with great vision and research passion. The constant encouragements and constructive suggestions from Prof. Liu make it not only possible, but also aspiring, for overcoming many hurdles of the research. His personal generosity, genuine kindness and endearing friendship also help make my journey as a Ph.D student enjoyable and fruitful, for which I am greatly indebted.

I would also like to thank Prof. Huei Peng, Prof. Branko Kerkez and Dr. James Sayer for taking interest in this research and serving in my committee. Their insightful suggestions and critical feedback have improved this research. Also, courses from Prof. Kerkez were greatly beneficial and inspiring for me. I am also thankful for Dr. Sayer for leading the Safety Pilot Model Deployment project, which creates the very foundation for the work in this dissertation.

My special thanks go to my fellow colleagues in Prof. Liu's research group, i.e. the Michigan Traffic Lab (MTL): Prof. Xuan Di (now in Columbia University), Dr. Yiheng Feng, Dr. Weili Sun, Mr. Shihong Huang, Mr. Shengyin Shen, and Mr. Yan Zhao for their advice and help. This dissertation would not be made possible without their friendships, inspiration and encouragement over these years.

Last but not least, my gratitude goes to the unconditional love and support from my families: my parents, Mr. Quanshun Zheng and Mrs. Zhujiao Lin, my sisters, Mrs. Surong Zheng and Mrs. Suting Zheng. My sincere gratitude also goes to my dear friend, Miss Hanyue Li, who walked all the way with me for the past 8 years.

Contents

List of Figures

List of Tables

Abstract

Massive deployment of connected vehicles (CVs) is now on the horizon, and will undoubtedly introduce paradigm shifts to the transportation system. At signalized intersections, CV can receive real-time traffic information from roadside equipment (RSE) so that driver can be advised for safer driving, while signal controllers can receive vehicle position and speed information for more effective operation. Considering signalized intersections are often hot-spots of traffic congestion and driver frustration, tremendous opportunities exist to improve the effectiveness and efficiency of traffic signal operation with CV data. However, due to the lack of real-world CVs, the benefit of CV data for signal operation has yet been explored. This limitation has now been partially overcome with the safety pilot model deployment (SPMD) project, the world's first large-scale CV deployment project with around 2,800 CVs.

Through leveraging the SPMD project, this dissertation is the first-ever effort of analyzing large amount real-world CV data to improve traffic signal system operation. Three innovative traffic signal applications are developed to explore the benefit of CV data with low penetration rates. Firstly, to

facilitate the deployment of Vehicle-to-Infrastructure (V2I) systems at intersections, a procedure is developed for automatic generation of intersection map, a critical element of many CV applications. Using data from RSE, the proposed approach can automatically estimate intersection geometry and lane-phase mapping, and serve as a cost-effective alternative to prepare input for RSE deployment. Secondly, to pave the way for detector-free signal operation, an algorithm is developed for estimating traffic volumes with CV data. This application could help reduce the dependency of traffic signals on vehicle detectors, and would be particularly beneficial for signal operation. Lastly, to explore the benefit of V2I communication for driving assistance, a speed advisory system is proposed to help drivers reduce fuel consumption when driving through intersections, using information from RSEs. An efficient algorithm is proposed based on Pontryagin's maximum principle for real time implementation.

With the three applications to improve traffic signal system in three different perspectives, the ultimate objective of this dissertation is to facilitate development and deployment of CV-based traffic signal system in the near future.

Chapter 1

Introduction

With a number of large scale connected vehicle (CV) deployment projects underway, ubiquitous presence of CVs is now on the horizon. This will undoubtedly introduce paradigm shifts to the transportation system. CVs are vehicles equipped with dedicated short range communication (DSRC) devices and can communicate with each other to exchange vehicle positions and status. They can also communicate with roadside equipment (RSE) deployed at the road infrastructure to receive situational awareness information that may not be detected by on-board sensors. With the Vehicle-to-Vehicle (V2V) and Vehicle-to-Infrastructure (V2I) communication, drivers can be better informed of surrounding environment for safer and more efficient driving. Considering its potential to improve safety and mobility performance as well as reducing environmental impact of the vehicular traffic, the CV technology is considered a critical part of next generation transportation system

[2].

At urban intersections, CV systems introduce both opportunities and challenges to traffic signal systems. With V2I communication, CV can receive real-time traffic signal information and advise drivers of safer and more fuel-efficient driving, e.g., red light violation warning or eco-driving advisory. At the same time, traffic signal controllers can receive real-time vehicle position and speed information and have better estimation of overall traffic condition, so that traffic signals can be operated more effectively. Considering signalized intersections are frequent hot-spots of traffic congestion and driver frustration, causing 295 million vehicle-hours of delay occurred annually [3], significant potential exists for CV-based traffic signal system to improve efficiency and effectiveness of intersection operation.

However, despite the promise held by CV systems, their benefits for improving signal operation have yet been explored. Thus far, existing efforts only focus on the concept demonstration through simulation experiments, because of the lack of CVs and relevant data in the real world. This limitation has now been partially overcome by the safety pilot model deployment (SPMD) project, the world's first large-scale CV deployment project with around 2,800 vehicles outfitted with DSRC devices.

Through leveraging the SPMD project, this dissertation is the first-ever effort of analyzing large amount real-world CV data to improve traffic signal systems. Three innovative traffic signal applications are developed to explore the benefits of CV under a low penetration rate environment. Firstly,

to facilitate the deployment of Vehicle-to-Infrastructure (V2I) systems at intersections, a procedure is developed for automatic generation of intersection map. Secondly, to pave the way for detector-free signal operation, an algorithm is developed for estimating traffic volumes with data from CVs. Lastly, to explore the benefit of V2I communication for driving assistance, a speed advisory system is proposed to help drivers reduce fuel consumption when driving through signalized intersections based on information received from RSEs. With the three applications for improving CV-based traffic signal system in three different perspectives, the ultimate goal of this dissertation is to facilitate both development and deployment of CV-based traffic signal system in the near future.

1.1 Background

1.1.1 Connected Vehicle Technology

The concept of vehicle connectivity started with the Automated Highway System (AHS) program in the early 1990s. The objective of AHS program was to achieve safer and more efficient driving based on the concept that vehicles could be guided by highway infrastructure through in-pavement sensors, instead of being driven by human drivers [4]. However, due to the deficit in federal research funds and concerns on the feasibility of full scale AHS applications, in 1997, US Department of Transportation (USDOT) decided to shift the focus to vehicle based safety system and introduced the Intelligent

Vehicle Initiative [5]. In 2005, the Vehicle Infrastructure Integration (VII) program was announced to develop standardized V2V communication and V2I communication for safety and mobility applications [6]. Over the last several years, the development and standardization of vehicular communication technology has gradually matured for commercialization, exemplified by the publication of IEEE 802.11p and 1609.x standards, as well as SAE J2735 DSRC dictionary set.

More recently, substantial progress has been made for the deployment of the CV technology. In USDOT's ITS 2015-2019 strategic plan, "realizing connected vehicle implementation" is listed as one of the two primary strategic priorities, with a focus on adopting and deploying CV systems in large scale [7]. Along with the strategic plan, active deployment efforts have also been funded. A major milestone is marked by the completion of the SPMD project, the first large-scale CV deployment project implemented in the City of Ann Arbor, Michigan. With around 2,800 vehicles equipped with DSRC devices, the project successfully demonstrated the applicability of V2V and V2I communication technology, as well as CV based safety applications. In 2015, three additional CV pilot deployment projects were awarded by the USDOT, with sites located in New York, Florida and Wyoming [8]. Columbus, Ohio, the winner of the $40 million Smart City Challenge, also announced plans of implementing CV technology in city fleets, transit vehicles and intersections to improve traffic flow efficiency and safety [9].

To facilitate the deployment of CV technology and further improve traffic

safety, the U.S. National Highway Traffic Safety Administration (NHTSA) has announced the rule-making intent for mandating CV technology on all light-duty vehicles [10]. At the same time, auto manufacturers are also actively developing and implementing the CV technology, exemplified by the announcement from General Motors (GM) that V2V technology will be equipped in Cadillac by 2017 [11]. With both public and private sectors pacing aggressively for the deployment of CV technology, there is no doubt that ubiquity of CVs are just around the corner.

1.1.2 Traffic Signal System

Traffic signal system has been in operation since its invention in the mid-19th century. The first traffic signal appeared as a mechanical semaphore operated manually in 1800s [12]. The first electric traffic light, consisting of red and green lights, was installed in Cleveland, Ohio, in 1914. It was later extended by adding yellow lights in 1920. In 1923, the fixed-time traffic light was invented by Garrett A. Morgan [13]. Since then, the fixed-time traffic signal has become the basic form of modern traffic signal systems.

After the invention of fixed-time traffic signals, two important components were introduced into the traffic signal operation: vehicle actuation and coordination. In order for traffic signal to respond to demand fluctuation, vehicle detector, as well as vehicle-actuated traffic signal, were invented. The first vehicle detector consisted of a microphone mounted near utility pole for the detection of horn sounds from vehicles. The system was first installed

in Baltimore in 1928. Shortly after, the pressure sensor was invented to detect vehicle presence using two metal plates as electrical contacts buried in pavement [14]. After 30 years of wide use, the pressure sensor was later replaced by loop detectors, the most common traffic detectors nowadays. On the other hand, the concept of signal coordination was proposed in 1917 with the first installation in Utah, consisting of 6 signal lights that were electrically connected [15]. These two components, vehicle actuation and coordination, complete the basic form of modern traffic signal system.

Over the decades, extensive research has been conducted on the optimization of traffic signal timing parameters. Early studies were primarily concentrated on parameter optimization for fixed-time signal control [16, 17, 18, 19, 20]. Later on, along with the increasing implementation of demand responsive signal control, numerous studies were conducted to optimize parameters for vehicle-actuated signals [21, 22, 23, 24]. More recently, with the availability of high-resolution traffic signal data, attention was drawn to estimate intersection performance measures [25, 26, 27, 28, 29, 30, 31, 32, 33, 34, 35]. Nonetheless, research in data mining for traffic signal operation is still in its infancy. Substantial work is needed for the development of analysis tools to help traffic engineers improve signal operation [30].

Today, over 300,000 traffic signals exist in the U.S, accounting for $82.7 billion public investment [3]. Signalized intersections have become indispensable parts of the transportation networks, with two-thirds of urban vehicle miles traveled on signal controlled roads [36]. Traffic signal has also be-

come one of the main causes for driver frustration [37]. With shrinking funding and resources nowadays, maintaining efficient traffic signal operation becomes more and more challenging for traffic management agencies. According to the National Traffic Signal Report Card, the traffic signal operation was graded as D+ in 2012 [3]. Significant room exists to improve the practice of signal operation.

1.2 Fundamentals of V2I System at Signalized Intersections

To set the stage, here, we will discuss several important types of communication messages used in the V2I system, and also briefly introduce the SPMD project as well as the data collected in the project.

1.2.1 Communication Messages used in V2I Systems

The illustration of a typical V2I system at an signalized intersection is shown in Figure 1.1. The hardware components at infrastructure mainly include traffic signal devices and the RSE. The RSE connects with a signal controller to obtain traffic signal information, and broadcast two important types of messages to CVs: MAP messages and Signal Phase and Timing (SPaT) messages, for geometry information and signal information, respectively. At the same time, the CVs broadcast the Basic Safety Messages (BSMs) containing

information of vehicle position and speed to their surrounding CVs as well as to RSEs. Besides of the three types of messages, there are also other types of messages used in CV system, such as Road Side Alert message or Traveler Information messages. Considering their infrequent use at intersections, these messages will not be discussed in this dissertation. The three frequently used messages will be briefly introduced in the next. For details of the messages, readers are referred to [38].

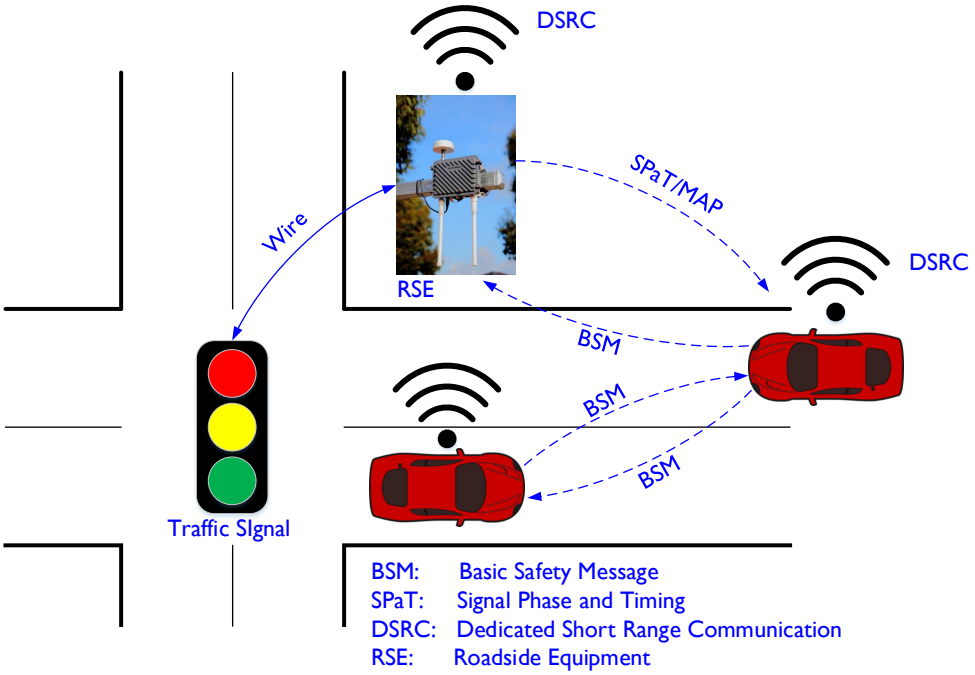

Figure 1.1: Illustration of V2I system

BSM Message

The BSM message is the most important message broadcast by CVs, indicating "here I am" information to other CVs and RSEs. The data elements in the BSM mainly include time, position, motion, braking status, and vehicle size as the required elements. The position information includes Latitude, Longitude, Elevation and position accuracy of the vehicle location. The motion information includes speed, heading, steering wheel angle and acceleration of the vehicle. Optional data elements in the message include: safety extension elements such as path history and path prediction, and vehicle status such as wiper state and traction control state.

MAP Message

The MAP message contains the information of lane-level geometry map of the intersection. The core data elements of the MAP message are shown in Figure 1.2. There are three levels of information in the MAP message, organized hierarchically: intersection level, approach level and lane level. Elements in the lane level are the most basic, including information of vehicle lanes regarding lane width, allowable vehicle maneuvers, and a node list indicating the centerline positions of each lane. The information in the MAP message provides the basic location input for many V2I applications.

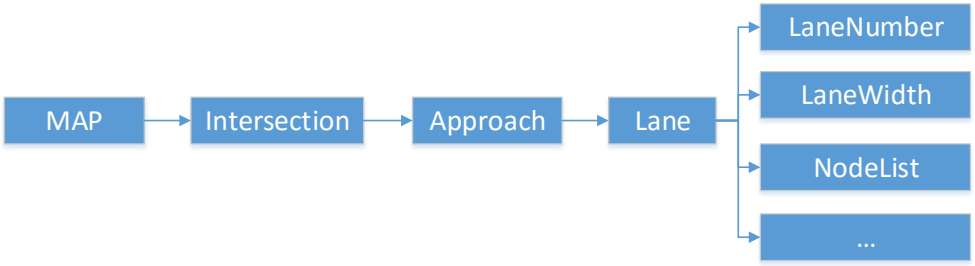

Figure 1.2: Core elements of MAP message

SPaT Message

The SPaT message conveys traffic signal status information, with the intersection state as the key data element in the message. The elements of the intersection state include: intersection ID, status of signal controller, time, and movement state as the required data elements, as well as priority state, preempt state and regional extension as the optional data elements. Among the required data elements, the movement state is the most important element, consisting of data entries of signal group ID and traffic signal status. The signal group ID maps lists of vehicle lanes to their corresponding signal light, so that traffic signal status can be correctly associated to vehicle lanes in the MAP messages. The mapping between vehicle lanes and signal phases is also termed as the lane-phase mapping. In the movement state, there are also optional data entries such as descriptive name of the intersection, and advisory speed for driving. In this dissertation, we primarily utilize the data entries of time, signal group ID and signal status, in our analysis.

1.2.2 The SPMD Project and CV Data

One of the major milestones of CV technology deployment is the recent completion of the SPMD project, the first large-scale CV deployment project in the world. The SPMD project was conducted by the University of Michigan Transportation Research Institute (UMTRI) for evaluating operation applicability of CV technology in a real-world, concentrated environment, and also for quantifying the benefits of CV safety applications and user acceptance. In the project, since August 2012, UMTRI has equipped about 2,800 vehicles with DSRC devices and deployed RSEs at 27 locations including 19 intersections. An illustration of RSE deployment in the project is shown in Figure 1.3. For more details of the SPMD project, readers are referred to [1, 39].

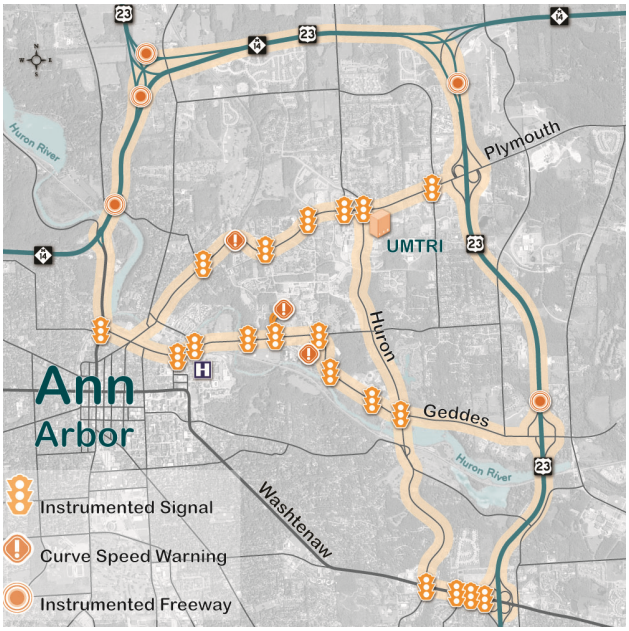

Figure 1.3: Deployments of RSEs in the SPMD project (source: [1])

In the SPMD project, four different types of vehicle-based devices are used: vehicle awareness device (VAD), aftermarket safety device (ASD), retrofit safety device (RSD) and integrated safety device (ISD). Of these four types of devices, VAD can only broadcast BSM, but cannot receive DSRC messages. ASD, RSD and ISD all can broadcast and receive DSRC messages simultaneously. In addition, RSD or ISD in a vehicle is connected to the vehicle data bus, and thus can access information from in-vehicle sensors, while VAD and ASD can only obtain GPS data. In the deployment, about 2,500 CVs were equipped with VADs, and about 300 CVs were equipped with ASDs, with around 80 CVs using either RSD or ISD [1].

A number of different types of data are collected and archived in the UMTRI database, since 2012. For vehicle-based devices, BSM data that were broadcast are all archived, as well as the received BSM data by ASD, RSD and ISD. For RSE, SPaT messages that were broadcast are archived, as well as received BSMs. The illustration of data from the SPMD project is shown in the following. Sample data are also available at the Research Data Exchange[1].

BSM messages received by RSEs

A sample of BSM data received by a RSE is shown in Figure 1.4. Only

[1] FHWA Research Data Exchange: www.its-rde.net

a subset of data fields are used in our investigation, including device ID of a RSE (RxDevice), device ID of a CV sending the BSMs (TxDevice), GPS position and speed of the CV, and timestamp when the BSM was received by a RSE.

RxDevice	TxDevice	Gentime	Latitude	Longitude	Speed	Heading
18013	35	281203941949171	42.30465	-83.70778	4.78	88.4125
18013	35	281203942249243	42.30465	-83.70776	4.7	88.7125
18013	35	281203942349227	42.30465	-83.70776	4.66	88.4
18013	35	281203942449212	42.30465	-83.70775	4.68	88.5
18013	35	281203942549207	42.30465	-83.70774	4.68	88.5

Figure 1.4: Sample BSM data received by RSEs

SPaT message broadcast by RSEs

A sample of SPaT data is shown in Figure 1.5. Here, only a portion of the data fields in the SPaT are used, including: timestamp when a message was generated, signal phase ID and signal status.

Time Stamp	Phase ID	Phase Status
2015-9-1,0:6:48.837	2	Red
2015-9-1,0:6:48.837	2	Red
2015-9-1,0:6:48.837	1	Green
2015-9-1,0:6:48.837	1	Green

Figure 1.5: Sample SPaT data broadcast by RSEs

1.3 Research Scope and Contributions

As we discussed above, CV technology holds great potential to revolutionize the traffic signal system. With CVs in the traffic stream, traffic signal system can rely on CVs self-reporting their status for traffic demand estimation, without using fixed location detectors. In this way, the signal control system would be less sensitive to frequent detector failures or errors, and be operated with higher reliability. For example, even if a small number of CVs fail to communicate with RSE, the signal control system can still obtain information from the rest of CV fleet for traffic demand information. In contrast, for a detector-based signal system, if a detector fails at one approach, then there is no other alternative for the signal system to obtain traffic demand information.

Despite the great potential of the V2I systems, substantial research gaps exist to improve traffic signal system with CVs. Although numerous studies have proposed adaptive signal control algorithms based on CV data, most of the proposed signal control algorithms focus on scenarios with relatively high CV penetration rates, e.g., 25%. The high penetration rate may not be achieved in the near future. Under a low penetration rate environment, how to utilize CVs for signal operation remains an open question. Moreover, these studies are primarily based on simulated CV data which cannot fully capture characteristics of real-world system, e.g., communication performance. Therefore, the proposed algorithms may not be transferable to real-world

implementation. In addition, many CV applications relies on MAP messages and Signal Phase and Timing (SPaT) messages from RSE for the information of intersection geometry and signal status. However, few studies have addressed the problem of how to prepare these messages. Considering the number of existing traffic signals in the US, the preparation of these messages would be particularly challenging with large scale deployment.

To fill in these research gaps, in this dissertation, we aim at developing innovative applications using CV data at signalized intersections. Considering CV system deployment is still in its early stage, we focus on data-driven approaches that can leverage CV data with low penetration rates. Three different applications will be developed according to three different aspects of CV-based traffic signal systems. An overview of the three applications is shown in Figure 1.6.

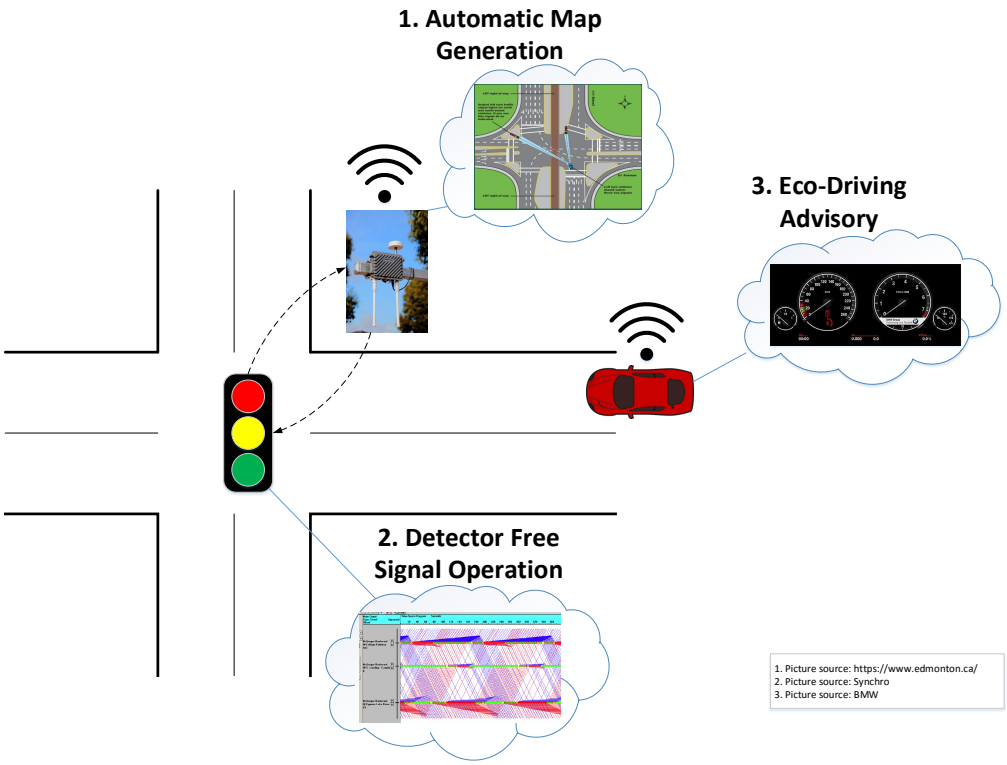

Figure 1.6: Overview of the applications for CV-based traffic signal system

In the first application, a procedure is developed for automatic generation of intersection map, which is a critical element of many CV applications. Using data from RSE, the proposed procedure can automatically estimate intersection geometry and lane-phase mapping. Therefore, it could serve as a cost-effective alternative of conventional manual survey approach to prepare data input for RSE deployment. Therefore, it could be of significant help to the deployment and maintenance of RSEs at signalized intersections.

In the second application, an algorithm is developed for estimating traffic volumes with data from CVs under a low penetration rate. In the proposed

approach, we model the vehicle arrivals as time-dependent Poisson arrivals to account for signal coordination, and formulate the likelihood function for the volume estimation. An Expectation-Maximization (EM) procedure is derived for solving the estimation problem. With the estimated volume information, this application could help reduce the dependency of traffic signals on vehicle detectors. Therefore, the proposed application would be particularly beneficial to improve the current practice of signal operation, and also build the foundation for the development of the detector-free signal operation.

In the last application, a speed advisory system is proposed to help drivers reduce fuel consumption when driving through signalized intersections. The proposed system leverages the historical driving data to obtain acceleration/deceleration characteristics of drivers as well as fuel consumption characteristics of a vehicle. Using these information, an efficient algorithm is proposed based on Pontryagin's maximum principle so that it can be implemented on-board in real time. Through leveraging V2I communication, this applications could help promote more fuel-efficient driving of the vehicular traffic.

Overall, by analyzing data from the SPMD project, this dissertation is the first-ever effort of leveraging large amount of CV data for traffic signal systems in the real world. By aggregating historical data and extracting relevant information contained in CV trajectories, the proposed applications are advantageous to accommodate existing CV systems with low penetration

rates. With the three proposed applications, this dissertation could be of significant help to facilitate both development and deployment of CV-based traffic signal system in the near future.

1.4 Thesis Organization

The rest of this thesis is organized as follows: Chapter 2 presents the application of using CV data for automatic generation of intersection map. The algorithm for estimating geometry of approaches and lanes will be presented, with evaluation results based on benchmark data from Light Detection and Ranging (LiDAR) surveys. The algorithm for lane-phase mapping estimation will also be presented with a case study.

Chapter 3 presents the application for volume estimation at signalized intersections. The derivation of likelihood function for the estimation will be described. Two case studies will be presented: one using CV data from RSEs, and the other using GPS trajectory data from navigation service users.

Chapter 4 presents the application for eco-driving advisory with V2I information. We will first present the problem formulation, and then illustrate the derivation of the solution algorithm based on the Pontryagin's maximum principle (PMP). For evaluation, a case study based on data from a participant in the SPMD project will also be presented.

Finally, conclusions and future research are summarized in Chapter 5.

Chapter 2

Intersection Map Generation

2.1 Introduction

For many CV applications at intersections, one crucial element is an accurate representation of road segments (i.e., a location map). Only with accurate maps, CV can be aware of its position in the driving environment and properly generate warnings to the drivers. In the SAE J2735 standard for DSRC message set dictionary, location maps are conveyed in the MAP message, one of the basic messages broadcast by a roadside equipment (RSE) [40, 38]. To prepare MAP messages, the conventional approach would rely on manual surveying which is time consuming and costly. Considering approximately 300,000 intersections exist in the U.S [3], the manual surveying approach could be challenging for large-scale deployment of V2I systems. The high costs also prevent the MAP from being updated frequently and could re-

sult in outdated information in the messages. As a consequence, availability and performance of CV applications could be compromised. Clear needs exist for more efficient approaches to generate and maintain intersection maps for CV systems.

To fulfill this need, this chapter presents an innovative approach to automatically estimate intersection map information using BSMs received by RSEs. Our estimation will focus on estimating lane information including allowable maneuvers and lane centerline geometry, which are the most important parts of MAP messages. In essence, the proposed approach will first identify directions of approaches of an intersection and estimate centerline geometries of the approaches. Then, for each approach, the number of traffic lanes, allowable vehicle maneuvers and centerline geometries of different lanes will be estimated. In addition to the geometry map estimation, a procedure is also proposed to automatically estimate lane-phase mapping, i.e., the mapping between traffic movements and lanes with traffic signal phases, using BSMs together with signal status data. This lane-phase mapping associates MAP messages and Signal Phase and Timing (SPaT) messages at intersections, and is vital for signal-aware CV applications at intersections, e.g., red light violation warning. With the potential to reduce labor costs of preparing infrastructure related messages, the proposed procedure could be helpful for deploying and maintaining CV systems in the near future.

2.2 Relevant Work

The presenting work lies within the literature on using GPS traces for estimating traffic network maps, which has emerged over the last two decades thanks to the increasing availability of GPS units. Overall, existing methodologies can be categorized into 3 main types.

The first type of algorithms focus on refining an existing map with GPS data. Schroedl et al. proposed a procedure to refine an existing map using GPS traces from differential GPS units [41]. First, raw GPS data were filtered based on GPS signal availability or quality, and then projected to existing road segments with a map matching method. In [42], GPS data were first smoothed by a 2D Gaussian smoother and then used to refine existing road segments with spline curve fitting. Zhang et al. proposed to first characterize road geometries from an existing map with sequential, perpendicular lines, then segment and merge GPS traces with the existing map [43]. Baier et al. proposed the MapCorrect system that collected GPS traces from cellphones to correct or validate an existing map [44]. Torre et al. applied a Hidden Markov Chain based map matching algorithm to identify missing segments of an existing map and then estimated these missing segments correspondingly [45]. Similarly, in the CrowdAtlas system [46], data were first partitioned based on location proximity and direction similarities into point clusters. Then, a polygonal principal curve algorithm was used to extract the centerline of road in each cluster. Restricted by their dependence of existing

maps, these approaches are more suitable for map refinement rather than map generation.

The second type of algorithms generate density images using GPS points and then apply image processing techniques to extract road geometries. Chen et al. proposed to first generate binary images for GPS locations, and then applied morphological operation to process the binary images into nodes of road [47]. Then, a post process was performed to remove redundant nodes and to connect nodes for generating graph for the network. Instead of binary images, Shi et al. proposed to generate density images similar to energy contours and then extract skeleton to form a road network [48]. Steiner & Leonhardt applied a Gaussian kernel to process raw GPS data, then used a watershed transformation to generate the map [49]. This type of algorithms have advantages for generating maps using data with low sampling frequencies. However, the lane-level accuracy is often compromised.

The third type of algorithms apply clustering techniques for map generation and are the ones that inspire the procedure proposed in this chapter. Generally, the idea is to first cluster GPS data based on locations or headings and then estimate nodes in each cluster for road geometries. Worrall & Nebot proposed to segment GPS data into sequential clusters based on similarity of headings, and then link clusters based on distances, bearing and heading difference to complete the road graph [50]. Jang et al. proposed to first separate targeted regions into grid cells, and then aggregate data within each cell into nodes which are later connected as links [51]. In [52],

they assigned artificial "forces" to raw GPS points based on locations and relative distance, and then merged the points based on these forces into road segments. In [53], nodes of road segments were first estimated by incrementally merging GPS points. Then, a constrained optimization problem was formulated to link road points as a graph for the network. Karagiorgou & Pfoser proposed to first identify intersections based on turnings and locations of GPS trajectories, and then connect these intersection nodes for links [54]. Li et al. also developed an incremental approach for map estimation [55]. They first segmented GPS traces into small trajectories based on distance and time difference between consecutive GPS points, and then incrementally merged the trajectories to estimate road geometries.

Overall, several limitations exist in the aforementioned studies restricting their applicability of generating map for the CV systems. First, the focuses of the approaches are mostly on estimating the topology of a road network in relatively large scales, and are not suitable for estimating lane-level map with high accuracy required by CV systems. While some efforts also focus on identifying number of lanes and lane positions [56, 57, 58], their applicability is limited due to dependence on knowing the network topology. Additionally, in the existing studies, data are mostly from probe vehicles with substantially different sampling rates and coverage than CV data received by the RSEs. Lastly, none of the existing research has tackled the problem of estimating lane-phase mapping, an indispensable piece of information associating lanes geometries with traffic signals. This application intends to address these

limitations.

In this application, by extending the existing clustering based approaches, an innovative procedure is developed to estimate lane-level intersection map for CV systems using BSM received by the RSE at an intersection. To the best of our knowledge, this is the first attempt of using real-world CV data to generate map for V2I systems. In this way, MAP messages in the RSEs could be generated or updated in a timely manner.

2.3 Investigated Intersections for Map Generation

For the map generation, we primarily utilize CV data received by RSEs in the SPMD project. Among the deployed intersections from the SPMD project, five intersections are selected for investigation in this research. The illustration of the selected intersections is shown in Figure 2.1.

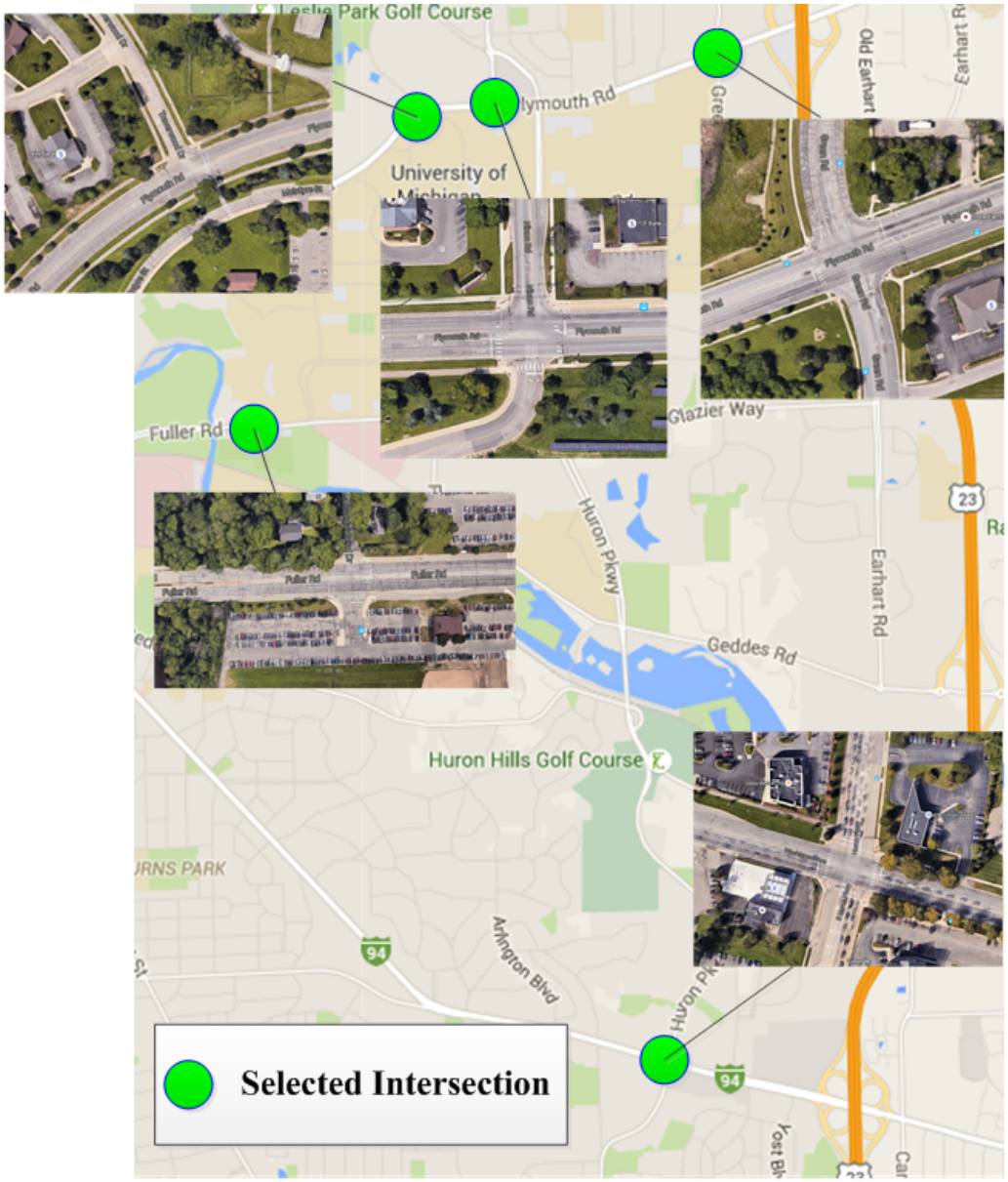

Figure 2.1: Illustration of selected intersections

As shown in Figure 2.1, different intersections are selected including 4-arm intersection, T intersection, etc. These 5 intersections could be considered as

proper representatives of typical traffic intersections. At these intersections, three types of data are prepared: 1. BSMs received by RSEs; 2. Signal status; and 3. Reference map as the ground truth of the estimation. To obtain the reference map, a high-resolution LiDAR survey was conducted to obtain geometries of the 5 intersections. The LiDAR system uses laser light for detection and has the capability to measure both range and intensity of light return, thus combining advantages of both radar and vision detection systems. With these advantages, the LiDAR system can be used to detect road edges as well as lane markers accurately [47, 59, 60]. In the field survey system, the LiDAR system is integrated with differential GPS to generate point lists of GPS coordinates for lane geometries. Accuracy of 0.06 foot (0.02m) can be achieved by the survey system [61]. The illustration of the reference maps is shown in Figure 2.2.

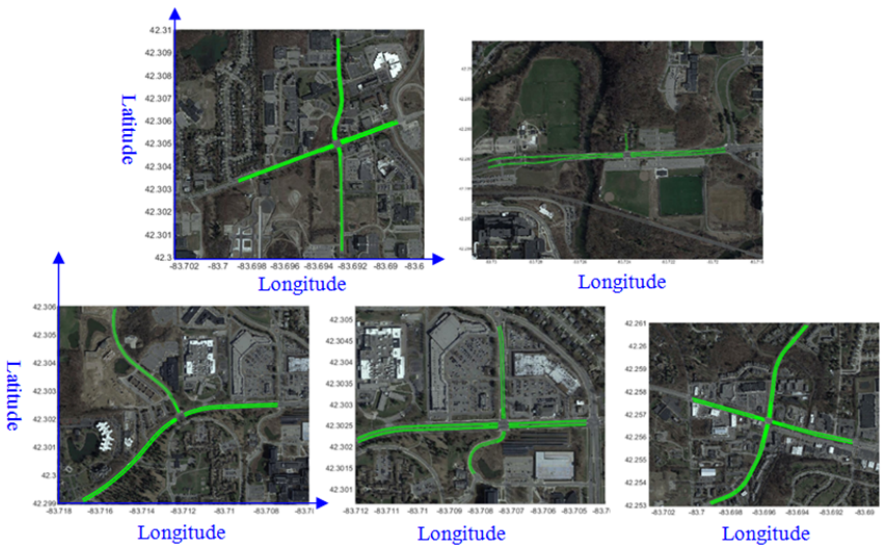

Figure 2.2: Illustration of reference MAP form field survey

2.4 Estimating Intersection Geometry

The proposed procedure consists of three main steps: 1. Pre-processing step, 2. Geometry estimation step, and 3. Post-processing step, shown in Figure 2.3. The pre-processing step cleans raw GPS data using a geofence and then categorizes vehicle trips based on their traveling directions and trip movements, e.g., northbound through movement or westbound left-turn movement. After the vehicle trips are categorized, step 2 is to aggregate GPS points of trips based on the movement, then estimate the geometry of a driving path for each movement, and then centerline positions of different lanes along each driving path. Finally, step 3 estimates the stop bar location for each lanes and organizes the geometry data to be compatible with the MAP message format.

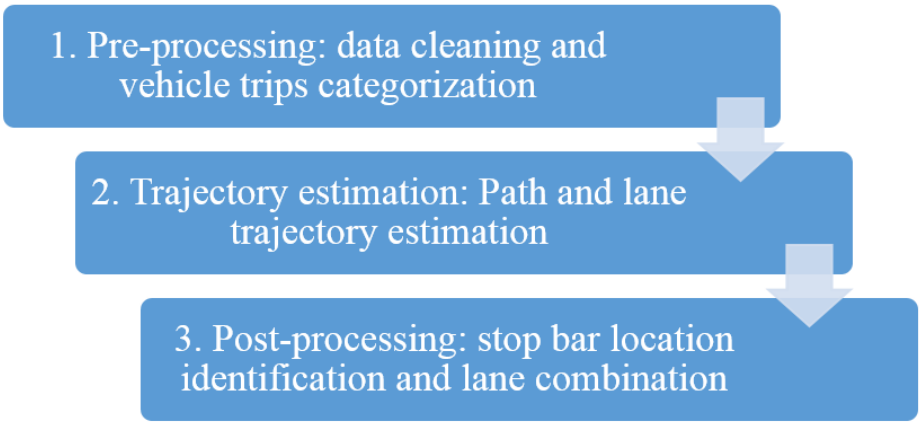

Figure 2.3: Three steps for estimation procedure

Pre-processing Step: Data Cleaning and Trip Categorization

In the pre-processing step, data are first cleaned use a geofence defined as a square with the RSE at the center and 0.01 units extension (roughly 780 m) for both latitude and longitude. Then, to identify the directions of approaches entering or exiting from the intersection, the root square distance (RS-Distance) between a CV and the RSE is defined based on their GPS coordinates as:

$$d_i^{(j)} = \sqrt{(x_i^{(j)} - x_r)^2 + (y_i^{(j)} - y_r)^2} \tag{2.1}$$

Where $d_i^{(j)}$ is the distance of i-th GPS point of CV trip j to the RSE at an intersection; $x_i^{(j)}$, $y_i^{(j)}$ are the latitude and longitude of the GPS point; and subscript r denotes RSE.

Based on the RS-Distance, next, a circle with the RSE at the center can be defined as the "intersection center area". The radius of the circle, r_c, is selected that the circle is large enough so that entering and exiting points of CVs on different approaches are sufficiently far from each other, but not too large that CV trips entering and exiting the circle are insufficient.

The illustration of the circle is shown in Figure 2.4, using data sample from Int. Green & Plymouth. In the figure, the red mark indicates the

position of the RSE and the purple circle indicates the intersection area. The blue points are GPS points of CVs from BSMs received by the RSE. A sample CV trip is also shown, depicted by the red, yellow and green lines, representing the 3 portions of the trip: approaching, traversing, and leaving the circle, respectively.

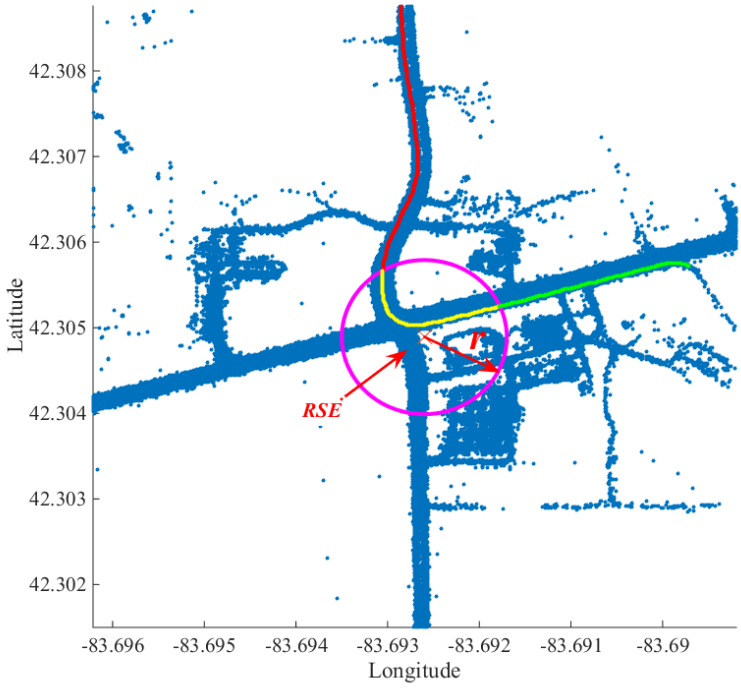

Figure 2.4: Illustration of the circle for intersection center area

Based on the intersection circle, two sets of data (entering set and exiting set) are prepared. The entering set includes the first point of a CV entering the intersection circle for each CV. The exiting set includes the last point of

a CV before it leaves the circle. The two sets are expressed as:

$$U_{en} = \left\{ \left[x_{i_{en}}^{(j)}, y_{i_{en}}^{(j)} \right] | i_{en} = \min \left\{ i | d_i^{(j)} \leq r_c \right\}, \ \forall j \right\}$$

$$U_{ex} = \left\{ \left[x_{i_{ex}}^{(j)}, y_{i_{ex}}^{(j)} \right] | i_{ex} = \max \left\{ i | d_i^{(j)} \leq r_c \right\}, \ \forall j \right\}$$

Points in both sets are further clustered into different groups representing different vehicle approaches. For clustering, the K-Means method is used, considering its simplicity [62]. The results for Int. Green & Plymouth are shown in Figure 2.5. In the figure, the red and green points are entering and exiting points, respectively. For both entering and exiting points, four groups are identified corresponding to four approaches of the intersection, labeled as 1-4 clockwise.

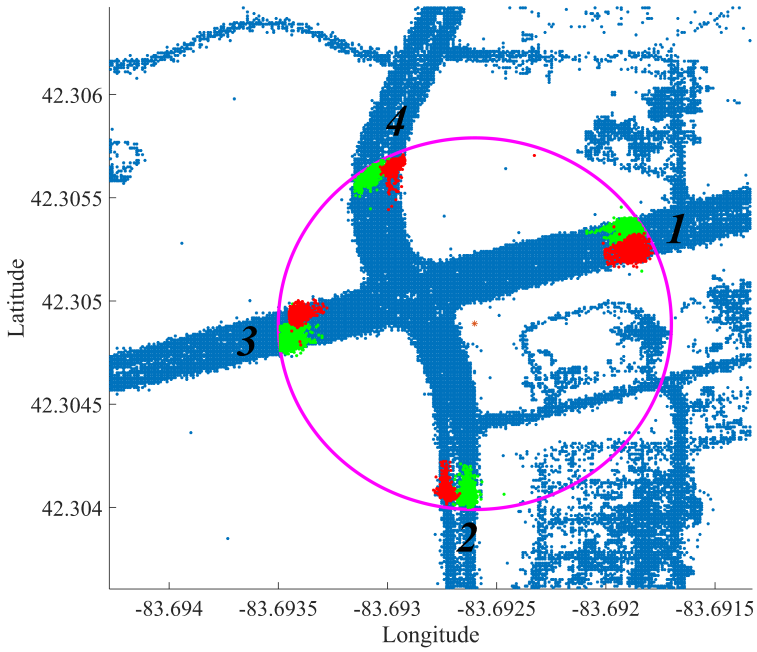

Figure 2.5: Illustration of clustering the entering and exiting points

After clustering, CV trips are categorized according to the group of their entering points and exiting points. For an intersection with N approaches, trips can be categorized into $N \times (N-1)$ groups, excluding U-turn trips. In the example in Figure 2.5, trips are grouped into twelve categories. These categories are labeled as "N in, M out" category, where N is the group ID of an entry point of the trip, and M is the group ID of an exit point of the trip. For example, "2 in, 1 out" indicates CVs that enter through Group 2, and exit through Group 1, which represents westbound right-turning (WB-RT) trips in Figure 2.5.

Trajectory Estimation: Path Centerline Geometry and Lane Position Estimation

Estimating Path Centerline Geometry

After trip categorization, step 2 is to estimate path and lane geometry. For each category, the GPS data are aggregated to estimate the approach (or driving path) centerline geometry. Based on the intersection circle, each trip is divided into 3 segments for approaching, traversing, and leaving the circle, respectively. Approach geometry are then estimated according to the three segments. In specific, for each segment, data are grouped into bins based on accumulated distance from either the entry point or the exit point. The illustration is shown in Figure 2.6.

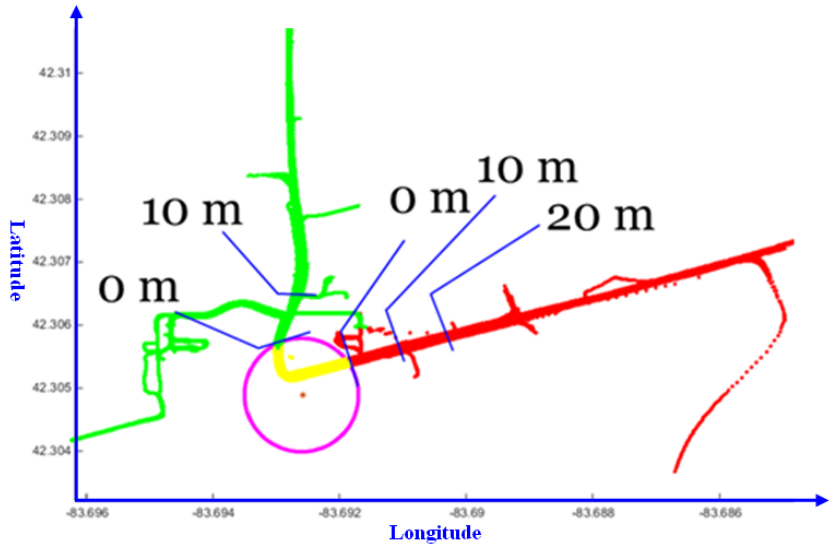

Figure 2.6: Illustration of calculating accumulated distance and grouping data based on distance

Then, for GPS data in each bin, mean values weighted by speed are calculated as node points of the approach trajectory. The calculation is expressed as:

$$\bar{x}_{m,k} = \frac{1}{\sum_{(i,j)\in\Omega_{m,k}} v_i^{(j)}} \sum v_i^{(j)} x_i^{(j)},\ \bar{y}_{m,k} = \frac{1}{\sum_{(i,j)\in\Omega_{m,k}} v_i^{(j)}} \sum v_i^{(j)} y_i^{(j)} \quad (2.2)$$

Where m is the index of an approach, k is the index of data bin, $v_i^{(j)}$ is the speed of i GPS data point of trip j, $\Omega_{m,k}$is the set of index (i, j) of GPS points in k data bin of m approach. $\bar{x}_{m,k}, \bar{y}_{m,k}$ are the estimated coordinates for the node point of the approach path.

The calculation aims at placing greater weight on data points with higher speed for CVs more likely traveling on main approaches, so that the impact of data on driveways or in parking lots nearby, typically with low speed, could be reduced. The calculation is repeated for each bin for all three parts of the driving path to obtain path geometry of each trip category. The illustration is shown in Figure 2.7.

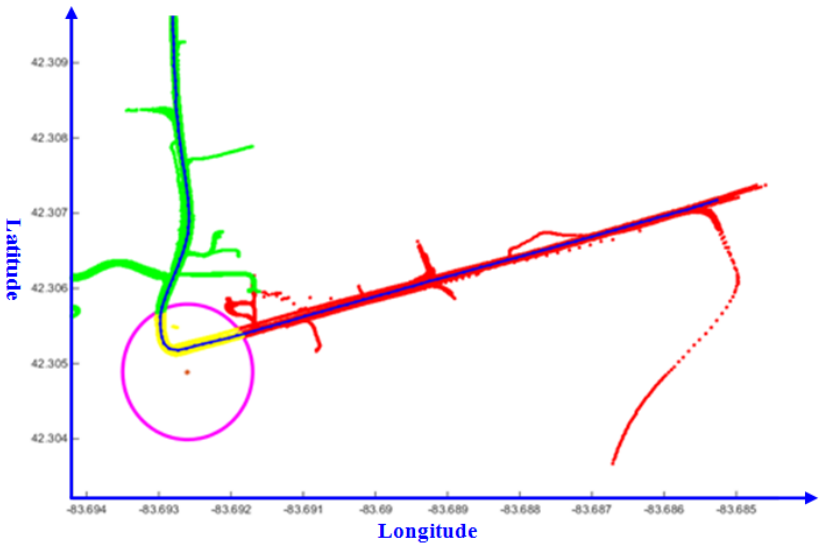

Figure 2.7: Estimating path trajectory based on weighted mean

Estimating Number of Lanes and Centerline Positions

Next, we estimate number of lanes on the path and the centerline positions of the lanes. Along the path geometry, we estimate the relative shift of lane position to the path geometry. An illustration of lane position estimation is shown in Figure 2.8. The histogram on the right in Figure 2.8 shows the distribution of vehicle positions in the local coordinate system. The histogram shows two peaks indicating positions of the lane center-line. The procedure here aims at estimating the number and positions of these peaks.

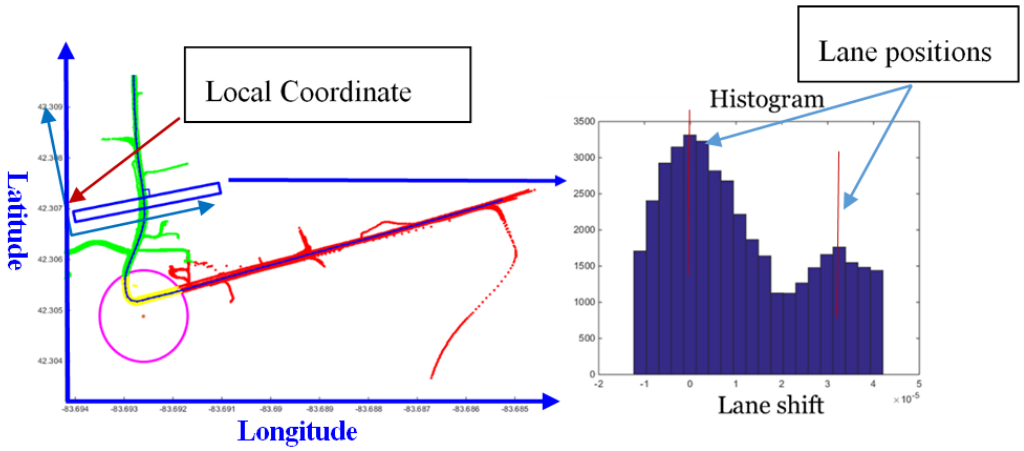

Figure 2.8: Illustration of estimating lane position

We first take a slice of data vertical to the path geometry, and then transform the data into individual local coordinates in which the vertical axis is the shift of CV position to the center of the approach. The coordinate transformation is performed as follows: we first find the slope θ_i of the vehicles' travel direction of k-th slice from the approach geometry, as:

$$\theta_{m,k} = \arctan\left\{\frac{\bar{y}_{m,k+1} - \bar{y}_{m,k}}{\bar{x}_{m,k+1} - \bar{x}_{m,k}}\right\} + \frac{\pi}{2} \tag{2.3}$$

Then, we calculate the coordinate transformation matrix:

$$M_{m,k} = \begin{bmatrix} \cos\theta & \sin\theta \\ -\sin\theta & \cos\theta \end{bmatrix} \tag{2.4}$$

The vehicle location in the local coordinate system is calculated as:

$$\begin{bmatrix} \hat{x}_{m,k}(i) \\ \hat{y}_{m,k}(i) \end{bmatrix} = M_{m,k} \times \begin{bmatrix} x_{m,k}(i) - \bar{x}_{m,k} \\ y_{m,k}(i) - \bar{y}_{m,k} \end{bmatrix} \tag{2.5}$$

Where $\begin{bmatrix} \hat{x}_{m,k}(i) \\ \hat{y}_{m,k}(i) \end{bmatrix}$ is the transformed location in the local coordinate system of a GPS point.

The number of lanes is determined based on the "spread" of vehicle locations, i.e., difference between maximum and minimum value [57]. The calculation of spread $S_{m,k}$ is expressed as:

$$S_{m,k} = \max\left(X_{m,k}\right) - \min\left(X_{m,k}\right) \tag{2.6}$$

Where $X_{m,k} = (\hat{x}_{m,k}(1), \hat{x}_{m,k}(2)...)$

Then, the following criteria is used to determine the number of vehicle lanes, $N_{m,k}$. The threshold is determined based on visual inspection of a small number of data samples with known lane numbers. Here, we assume at most 3 lanes exist on an approach. The assumption could be relaxed with additional configurations without difficulty.

$$N_{m,k} = \begin{cases} 1 & if\ S_{m,k} \in (0,\ 4.5 \times 10^{-5}] \\ 2 & if\ S_{m,k} \in (4.5, 7.5] \times 10^{-5} \\ 3 & if\ S_{m,k} \in (7.5 \times 10^{-5}, +\infty) \end{cases} \tag{2.7}$$

Based on the number of lanes, we utilize the K-mean clustering to esti-

mate the position of the individual lanes.

Post-process: Stop Bar Location Identification and Lane Combination

After lane positions are estimated, the last step is to organize the estimated data to be compatible with MAP message format. Here, the key is to identify the stop bar location so that the path trajectory can be divided into ingress lanes and egress lanes. Here, the focus is on ingress lanes which are mandatory in the MAP message [38]. Estimation of egress lanes is left for future investigation.

To identify stop bar locations, we only consider points of centerline geometry inside the intersection circle as possible locations. Of these points, the one with minimum speed is selected as the stop bar location. The illustration is shown in Figure 2.9.

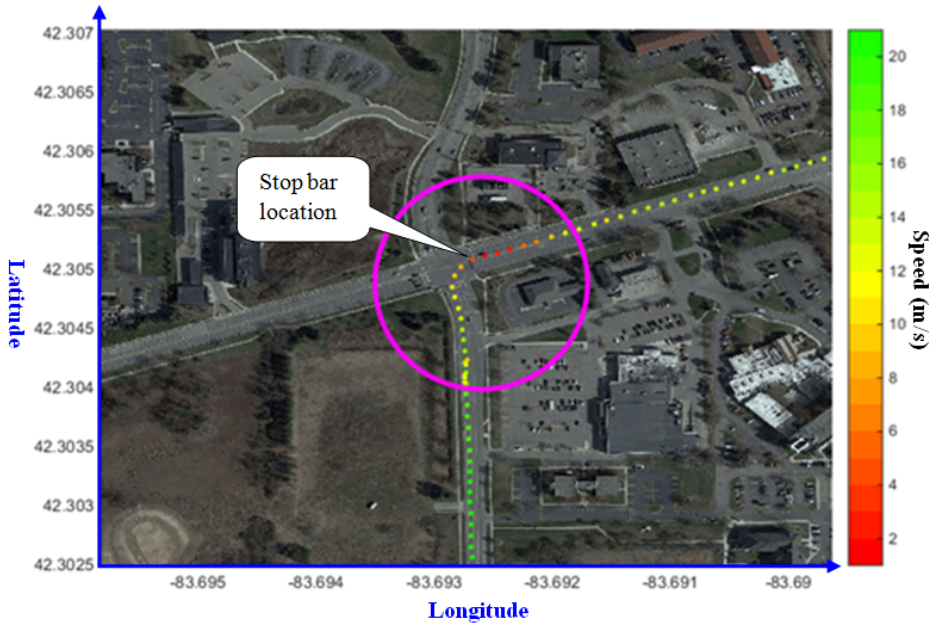

Figure 2.9: Illustration of estimating the stop bar location

Based on the stop bar location, the ingress lane portion is retrieved from the path trajectory. Then, lane positions in adjacent bins are connected along the driving path to form lane centerline geometries. We assume that number of lanes will not increase upstream, i.e., maximum number of lanes exists at the stop bar location. Then, starting from the stop bar, lane positions at adjacent bins are connected upstream, based on the following equation:

$$I^*(m,i) = \arg\min_m \sqrt{(x_{m,i} - x_{m,i-1})^2 + (y_{m,i} - y_{m,i-1})^2} \tag{2.8}$$

Where $I^*(m,i)$ is the index of lane position in bin i-1 that will be connected to n lane position of i bin.

However, cases exist that number of lanes are different over two adjacent

bins and decrease upstream. In these cases, lane positions with maximum distance to the adjacent bin are not connected. After connecting the node points together, finally, a local regression smoothing is applied to reduce outliers in the lane centerline geometry.

2.5 Evaluation of Geometry Estimation

2.5.1 Measurement of Accuracy

This section presents results of the accuracy evaluation by comparing the estimated map with the reference map. The comparison is conducted at two levels. The first level compares the structure of an intersection regarding the number of lanes for each approach and the vehicle movement. The second level compares the difference in individual lane centerline geometries between the estimated map and the reference map.

Two types of measurements are used, one for the average accuracy and the other for the worst accuracy, of the estimations. The first measurement is the Mean Distance of node points between estimated lane centerline geometries and surveyed lane centerline geometries. The second measurement is the Max Distance of node points between estimated lane centerline geometries and surveyed lane centerline geometries. The max distance is also called the Hausdorff Distance [63]. The calculations are:

$$Mean\ Distance:\ D_{mean}(\mathbf{X_a}, \mathbf{X_b}) = \frac{1}{n_a} \sum_{X_a \in \mathbf{X_a}} \left\{ \min_{X_b \in \mathbf{X_b}} \{f_d(X_a, X_b)\} \right\} \quad (2.9)$$

$$Max\ Distance:\ D_{max}(\mathbf{X_a}, \mathbf{X_b}) = \max_{X_a \in \boldsymbol{X_a}} \left\{ \min_{X_b \in \boldsymbol{X_b}} \{f_d(X_a, X_b)\} \right\} \quad (2.10)$$

Where $\mathbf{X_a}$, $\mathbf{X_b}$ indicate collections of node points for lane centerline geometries of the estimated and surveyed map. $X_a = (x_a, y_a)$,$X_b = (x_b, y_b)$, denoting GPS coordinates of node points. n_a is the number of node points in an estimated map. $f_d(\cdot)$ is the function calculating the distance between two GPS points, using the Haversine formula [64] as:

$$\begin{cases} f_d\left(X_a, X_b\right) & = 2R \times \arcsin\sqrt{h} \\ h & = \sin^2\left(\frac{x_a - x_b}{2}\right) + \cos\left(x_a\right)\cos\left(x_b\right)\sin^2\left(\frac{y_a - y_b}{2}\right) \end{cases}$$

Where R is mean radius of earth, as 6,371 km.

2.5.2 Evaluation of Accuracy for Selected Intersections

The estimated maps and reference maps are shown in Figure 2.10 for the selected intersections. In the figure, red dots indicate the estimated geometries of lane centerline and yellow curves for the surveyed geometry. Overall, most of the estimated lane geometries match well with the surveyed lane geometries. There are still several limitations with the estimated maps. For

Int. Fuller & Cedar Bend, the proposed procedure correctly identifies the lanes for WB and EB through movement, but fails to identify the rest of the lanes. This is because there are insufficient trips entering/exiting the SB approach, which is a small driveway. Also, the NB approach contains the access to a parking lot. The CV trajectories collected from this approach scattered widely within the parking lot and could not be used to identify traffic lanes. As a consequence, only the WB and EB approaches are estimated from the data.

For Int. Plymouth & Traverwood, the NB approach is incorrectly identified as a 1-lane road instead of a 2-lane road. This is most likely because that the lane markers of the NB approach is blurred and would confuse the drivers. For Int. Plymouth & Green and Int. Washtenaw & Huron, the right-turn lanes of the SB approach are also not identified, mainly due to a lack of data for the right-turn traffic for the approach at these two intersections. In these cases, manual corrections are needed to obtain final maps.

(a) Int. Fuller & Cedar Bend

(b) Int. Plymouth-Traverwood

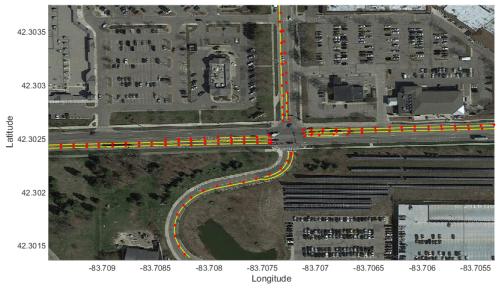

(c) Int. Plymouth- Nixon

(d) Int. Plymouth-Green

(e) Int. Washtenaw-Huron

Figure 2.10: Estimated map and reference map for selected intersections

The results of evaluations are summarized in Table 2.1. The first level evaluates the estimated number of lanes for each movement of the intersection. The second level evaluate the accuracy of the estimated lane geometry

for each successfully identified lane.

In the table, a yellow cell indicates that this is a false identification of the number of lanes for a movement. The number outside the bracket is the number of lanes incorrectly identified, and number in the bracket is the correct number of lanes. For lane geometry accuracy, each cell shows an accuracy measurement for each of the lanes, ordered from the leftmost lane to the rightmost lane. The value outside the bracket is the mean distance (D_{mean}) of node points between the estimated geometry with the surveyed geometry, while the value in the bracket is the max distance (D_{max}), based on Eq. 2.9 and Eq. 2.10.

False Identification

Performance Measure		WB	NB	EB	SB
Int. Fuller & Cedar Bend					
Intersection Structure	LT lane	0(1)*	N/A	0(1)	N/A
	Through lane	2	N/A	2	N/A
	RT lane	0(1)	N/A	0(1)	N/A
	LT, through shared	0	N/A	0	N/A
	RT, through shared	0(1)	N/A	0(1)	N/A
	LT, RT shared	0	N/A	0	N/A
Accuracy of Estimated Geometry of Lane Centerline	Distance (unit: m)	0.4 (1.9)**	N/A	0.4 (1.2)	N/A
		0.4 (1.1)	N/A	1.2 (2.4)	N/A
Int. Plymouth & Traverwood					
Intersection Structure	LT lane	0	N/A	1	1
	Through lane	2	N/A	2	0
	RT lane	1	N/A	0	1
	LT, through shared	0	N/A	0	0
	RT, through shared	1	N/A	0	0
	LT, RT shared	0	N/A	0	0
Accuracy of Estimated Geometry of Lane Centerline	Distance (unit: m)	0.8 (3.3)	N/A	0.2 (0.4)	1.5 (2.2)
		0.7 (1.1)	N/A	0.2 (0.6)	0.7 (1.3)
			N/A	0.2 (0.9)	
Int. Plymouth & Nixon					
Intersection Structure	LT lane	1	1	1	1
	Through lane	2	1	2	1
	RT lane	1	1	1	1
	LT, through shared	0	1(0)	0	0
	RT, through shared	1	1	1	1
	LT, RT shared	0	0	0	0
Accuracy of Estimated Geometry of Lane Centerline	Distance (unit: m)	0.9 (1.3)	0.5 (1.4)	0.3 (0.7)	0.5 (0.7)
		1.0 (2.1)		0.2 (0.6)	0.6 (0.9)
		1.2 (1.7)		0.8 (1.7)	
Int. Plymouth & Green					
Intersection Structure	LT lane	1	1	1	2
	Through lane	2	1	3	2
	RT lane	1	1	1	0(1)
	LT, through shared	0	0	0	1
	RT, through shared	0	0	1	0(1)
	LT, RT shared	0	0	0	0
Accuracy of Estimated Geometry of Lane Centerline	Distance (unit: m)	0.6 (0.9)	0.2 (0.4)	0.4 (1.0)	0.2 (0.5)
		0.5 (1.0)	0.3 (0.7)	0.2 (0.6)	0.5 (1.7)
		0.3 (1.1)	0.4 (0.5)	0.7 (1.3)	0.8 (1.9)
		1.1 (1.7)		1.3 (1.9)	
Int. Washtenaw & Huron					
Intersection Structure	LT lane	1	2	1	2
	Through lane	2	2	2	2
	RT lane	1	1	1	0(1)
	LT, through shared	0	0	0	0
	RT, through shared	1	1	1	0(1)
	LT, RT shared	0	0	0	0
Accuracy of Estimated Geometry of Lane Centerline	Distance (unit: m)	0.4 (0.9)	1.4 (3.2)	0.4 (1.1)	0.5 (1.7)
		0.8 (2.3)	0.8 (1.7)	0.6 (0.9)	0.2 (0.4)
		0.2 (0.8)	0.3 (0.8)	1.2 (1.5)	0.3 (0.7)
			1.0 (1.7)		0.6 (1.1)

*estimated No. of lanes (True No. of lanes); ** D_{mean} (D_{max});

Table 2.1: Comparison of intersection structure and accuracy for selected intersections.

As shown in the table, the mean distances between the estimation and reference map are from 0.2 to 1.5 m, while max distances from 0.5 to 3.3 m. Figure 2.11 further shows histograms for the mean distances and the max distances of all identified lanes. The average of mean distances,D_{mean}, for all estimated lane geometries is 0.6 m, and the average of the max distances, D_{max}, is 1.3 m. Moreover, 90% of D_{mean} are within 1.2 m, and 90% of D_{max} within 2.2 m.Considering that the accuracy of common GPS devices from 1-3 m [65] and the observation that in our investigation vehicle GPS position could deviate from the lane centerline as much as 3 m, the average accuracy of the estimated lanes for 0.6 m is encouraging. In addition, the accuracy on average is well below typical lane width of 3.6 m, and the worst estimations are mostly within reasonable accuracy. This would indicate the potential of using the estimated map for navigation or driving assistance in CV applications.

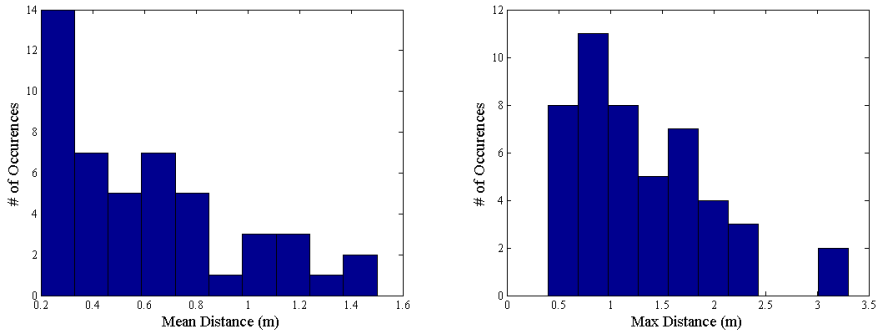

	Mean Distance (m)	Max Distance (m)
Average	0.6	1.3
90 Percentile	1.2	2.2

Figure 2.11: Summaries of mean distances and max distances

2.5.3 Discussion regarding Estimation Errors

To further interpret the estimation errors, two factors need to be considered. One factor is the different geodetic systems used in the Geo-referencing survey system and the CV system. Currently, two geodetic systems are mostly used for localization: World Geodetic System 1984 (WGS84) and North America Datum 1983 (NAD83). WGS84 is an Earth-centered Earth-fixed geodetic system, which is not fixed to any tectonic plate. NAD83, however, is fixed to the North American Tectonic plate. Due to the tectonic forces of Earth, in WGS84, the coordinate references of the North American tectonic plate will move gradually, while the coordinate references in NAD83 will remain static. Therefore, the WGS84 and NAD83 will gradually shift from each other over time, or after severe events of tectonic motion (e.g., an earthquake). In

Geo-referencing surveys, the NAD83 are mostly used so that the surveyed coordinates will not shift over time, while commercial GPS units use WGS84 Datum. In this work, the CV data are based on WGS84. However, the reference MAP obtained from Geo-referencing survey is based on NAD83 and then transformed to WGS84. The coordinate transformation between the two geodetic systems may result in limited accuracy of the surveyed map.

The second factor is the impact from pavement condition on driver's driving. To avoid driving on the cracks of the road, the drivers may choose not to drive along lane centerline defined by lane markers, but rather remain on part of lane with better pavement condition. In the tested intersections along the Plymouth Road, it is observed that drivers tended to drive on the left part of certain lanes, due to pavement cracks at right half of the lanes. Correspondingly, the estimated lane trajectories also deviate from the lane centerline to the left. This would indicate that additional caution should be taken when applying the proposed estimation procedure with presence of pavement cracks.

2.6 Estimating Lane-Phase Mapping

The lane-phase mapping indicates the allowable vehicle movements for traffic signal phases at the intersection, with an example shown in Figure 2.12. Currently, the lane-phase mapping can be only retrieved from the signal timing plans manually. Here, the objective is to develop an automatic process

as an alternative to the manual approach, thereby reducing the labor costs in the process. For simplicity, we only focus on 4-arm intersections operating NEMA signal settings, and assume right-turn movement is permitted at all approaches with rest movements being protected.

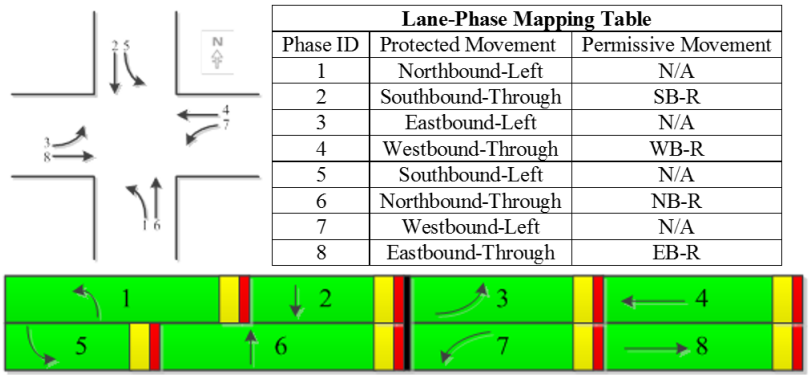

Lane-Phase Mapping Table

Phase ID	Protected Movement	Permissive Movement
1	Northbound-Left	N/A
2	Southbound-Through	SB-R
3	Eastbound-Left	N/A
4	Westbound-Through	WB-R
5	Southbound-Left	N/A
6	Northbound-Through	NB-R
7	Westbound-Left	N/A
8	Eastbound-Through	EB-R

Figure 2.12: Illustration of lane-phase mapping

Assuming that BSM data from the RSEs and signal status data are available, the problem of estimating lane-phase mapping can be stated as follows:

Given a sequence of starting time of green and red signal of different phases, as:

$$\{G_{i,1}, R_{i,1}, G_{i,2}, R_{i,2} \ldots, G_{i,n}, R_{i,n} \ldots\}, \ for\ i = 1, 2, \ldots, N_s$$

Where G, R denote starting time of the green and red signal, respectively. Subscript i denotes signal phase ID, n for the index of signal cycles, and N_s is the total number of the signal phases. For simplicity, we treat yellow signal as part of green.

The time instances when CVs travel through the intersection can be calculated from the CV trajectory data, as:

$$\{A_{j,1}, A_{j,2} \ldots, A_{j,m}, \ldots\}, \ for\ j = 1, 2, \ldots, N_v$$

Where A is the time when a CV passed the stop bar. Subscript j is for movement ID, e.g., EB through movement; m for the index of CV arrivals; N_v for the total number of vehicle movements at a selected intersection.

Denoting the set of associated vehicle movements for signal phase i as $S(i)$:

$$S(i) = \{j | movement\ j\ is\ allowed\ during\ phase\ i\}$$

The objective is to estimate the probability that a vehicle movement j is allowed with signal phase i, $P(j \in S(i))$ based on observed CV data, hence identifying the best estimator of $S(i)$.

To do so, it is assumed that a small likelihood, p_r, exists for CVs passing a stop bar during red signal either due to red light running or data errors, and also only one signal phase is associated with one and only one movement. For initialization, we use a uniform prior probability that a movement j is equally associated with any signal phases, expressed as:

$$P\left(j \in S(i)\right) = \frac{1}{N_s}, \ for\ i = 1, 2, \ldots, N_s, \ j = 1, 2, \ldots, N_v$$

For brevity, we define an indicator denoting whether a vehicle passed the

stop bar during green of a selected phase, as:

$$I_{j,m}^{i} = \begin{cases} 1 & if\ A_{j,m} \in [G_{i,k},\ R_{i,k}] \\ 0 & O.W. \end{cases}$$

Where k is the index of signal cycle when CV arrived, i.e., $k = \min\ j_{|A_{j,m} \geq G_{i,k}}$. For all CV arrivals of a selected movement, we have the sequence for arrivals as:

$$\mathbf{I}_j^i = \left\{ I_{j,1}^i, I_{j,2}^i ..., I_{j,N_v}^i \right\}$$

With the observations, we can calculate the posterior distribution of lane-phase mapping based on the Bayes theorem, as:

$$P\left(j \in S(i) | \mathbf{I}_j^i\right) = \frac{P\left(\mathbf{I}_j^i | j \in S(i)\right) \times P\left(j \in S(i)\right)}{P(\mathbf{I}_j^i)} \propto P\left(\mathbf{I}_j^i | j \in S(i)\right) \quad (2.11)$$

With the red light running probability p_r, we have:

$$P\left(\mathbf{I}_j^i | j \in S(i)\right) = (1 - p_r)^{N_g} p_r^{m - N_g}$$

Where $N_g = \sum_k I_{j,k}^i$, denoting the total number of green arrivals.

Overall, the posterior probability of a particular lane-phase mapping can be expressed as:

$$P\left(j \in S(i)|\mathbf{I}_j^i\right) \propto (1-p_r)^{N_g} p_r^{m-N_g} \propto N_g \ln(1-p_r) + (m-N_g)\ln p_r \quad (2.12)$$

We use the maximum a posteriori probability estimate, i.e., the one maximizing total green arrivals, as the estimator of lane-phase mapping. Based on this formula, next, we consider signal sequences compatible with NEMA signal conventions for a typical 4-arm intersection. To do so, we first associate main phase groups with movement groups for the two crossing roads, and then associate individual signal phase in each main phase group.

Associating Phase Groups with Movement Groups

The first step is to identify two main phase groups for the two crossing roads, referred as the main-street group and the side-street group. The road with larger through volume is indicated as the main street and the other as the side street. Then, we identify signal phases associated with the two groups, respectively. First, we would identify two barrier phases of which the barriers are at green start of the phases. Two conditions are checked to identify applicable barrier phases: 1. between two applicable break points, at most 2 signal phases of a ring exist; 2. at the green start of the barrier phases, no other phases are in active green. The illustration is shown in Figure 2.13. In the figure, phase 1 and 5 or phase 3 and 7 are applicable

pairs of barrier phases. Phase 2 or 6 are not applicable as phase 6 and 1 can be in green together. Afterwards, we combine signal phases between the barriers as phase groups and combine traffic movements on each road as movement groups.

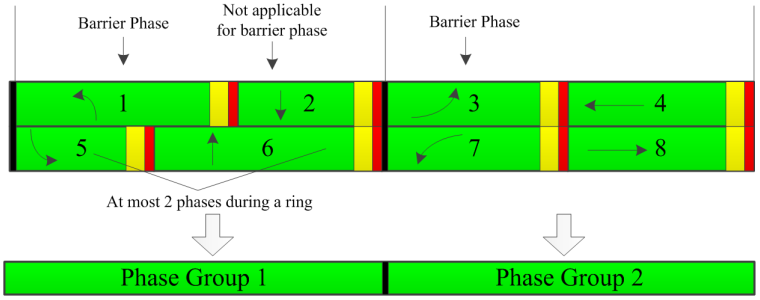

Figure 2.13: Illustration of barrier phase

To estimate association between phase groups and movement groups, we calculate the joint probability for the combined phases and arrivals:

$$P\left(j_1 = S(1),\ j_2 = S(2)|\mathbf{I}^1_{j1}, \mathbf{I}^2_{j2}\right) \propto \tilde{N}_g \ln(1-p_r) + (m - \tilde{N}_g)\ln p_r \quad (2.13)$$

Where $(j_1, j_2) = (1,2)$ *or* $(2,1)$, and $1,\ 2$ are indexes for the groups. $\hat{N}_g$ is the total green arrivals for a selected group association.

Based on the formula, we iterate all applicable pairs of barrier phases and identify the ones with the highest joint probability to find the best associations.

Associating Individual Phase with Movement in Each Group

After the phase groups and movement groups are associated, we associate phases with movements in each group. If there are 4 signal phases in a phase group between the identified barriers, then 8 possible combinations exist, shown in Figure 2.14a. If there are only 2 phases, then 4 possible combinations exist, shown in Figure 2.14b. For each combination, we can calculate its joint probability:

$$P(j_1 = S(i_1)\ , j_2 = S(i_2), \ldots, |I_{j_1}^1, I_{j_2}^2, \ldots) \propto \hat{N}_g \ln(1 - p_r) + (m - \hat{N}_g) Ln(p_r) \tag{2.14}$$

Where i_1,$i_2 \ldots$ are the signal phase IDs for a selected combination, and j_1,$j_2 \ldots$ are movement IDs of the combination, and $\hat{N}_g$ is the total green arrivals of the combination.

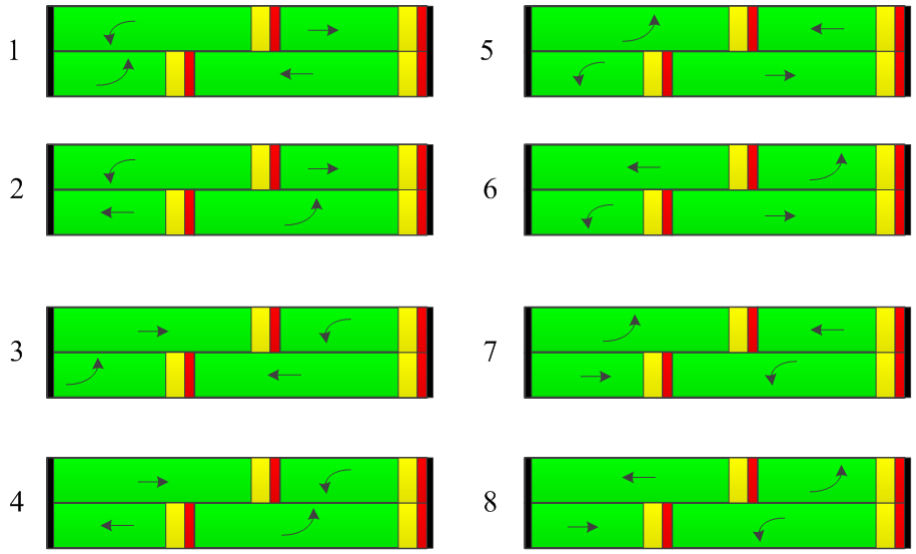

(a) 4 phases in a group

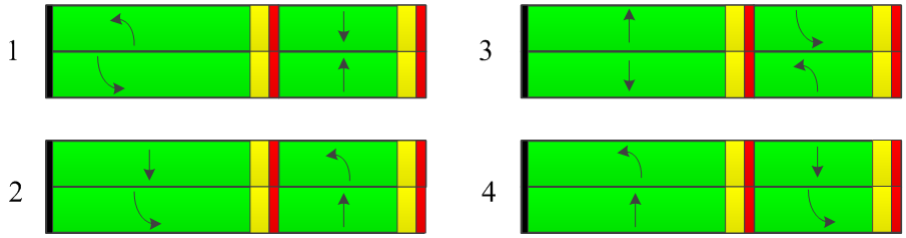

(b) 2 phases in a group

Figure 2.14: Possible combinations of phases and movements

2.7 Case Study for Lane-Phase Mapping Estimation

We select Int. Green & Plymouth to test the proposed procedure for lane-phase mapping estimation. The intersection geometry and ring-and-barrier diagram are shown in Figure 2.15. We use data collected during the afternoon

peak hour, 3:00 PM to 7 PM, for 2 weeks from 09/01/2015 to 09/15/2015. In the figure, the vehicle movements are indexed by the ID of input-output approaches of the movement path. For example, "1-4" indicates movement entering through approach 1 and leaving through approach 4, i.e., WB right-turn movement. Here, the objective is to infer allowable vehicle movements for each signal phases, so that we can associate signal phases with the geometry map.

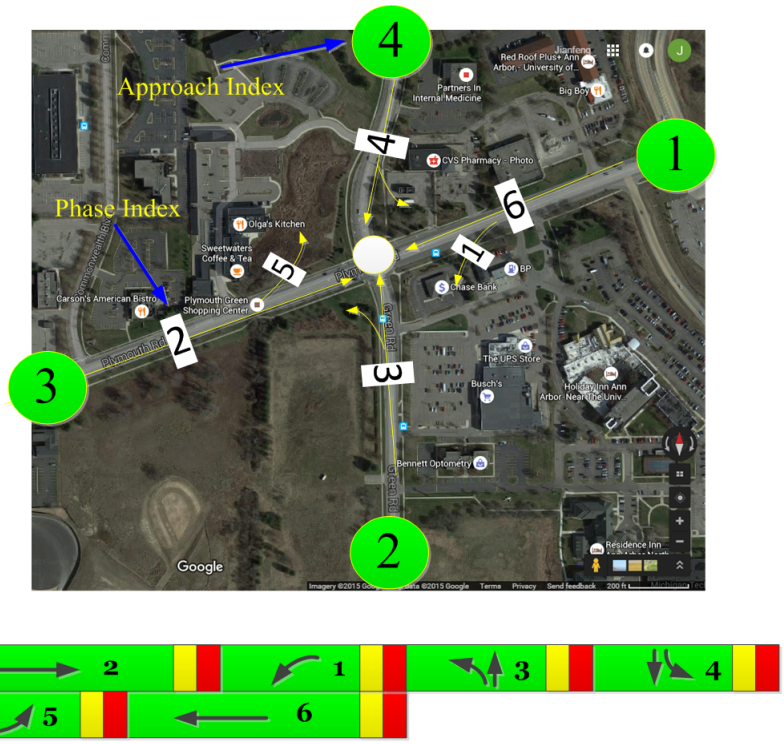

Figure 2.15: Intersection layout and ring-and-barrier diagram

For illustration, the signal sequence data are aggregated as green probability on time in signal cycle, shown in Figure 2.16a. This intersection is

currently operating SCOOT adaptive signal control system, and does not hold a fixed cycle clock. For simplicity, we select the start of phase 2 as the start of signal cycles. Total arrivals of CVs for each movement are shown in Figure 2.16b.

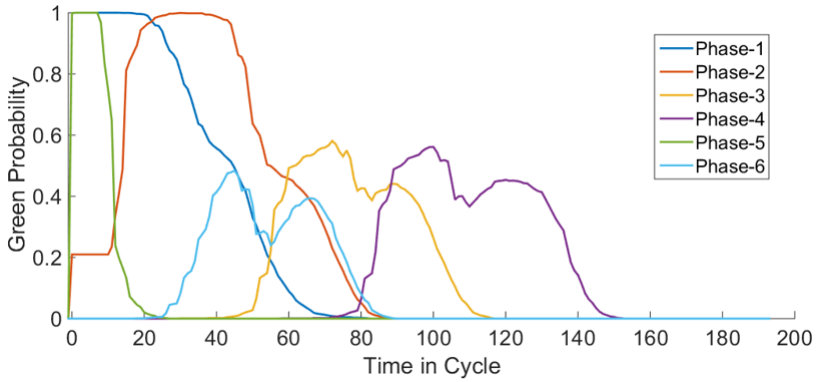

(a) Probability of green on time in cycle for different phases

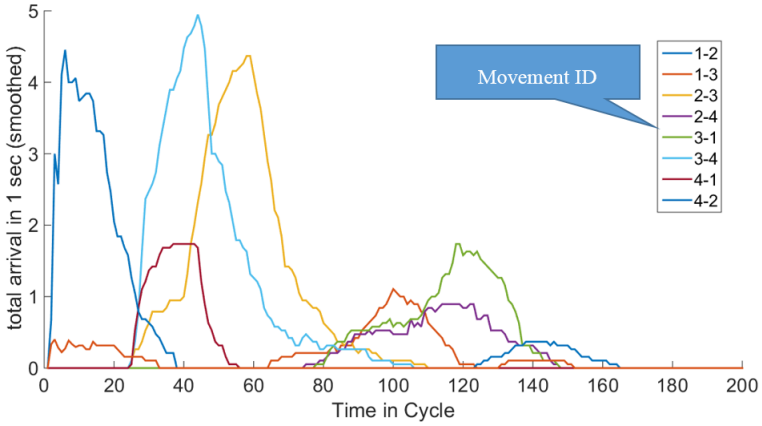

(b) Total arrivals of CV on time in cycle for different movements

Figure 2.16: Illustration of data used for lane-phase mapping

Using this data, we first identify the phase groups and movement groups and associate the groups. Based on the criteria for barrier identification,

phase 2 (or phase 5) and phase 3 are applicable pair for barrier phases. Hence, we group phase 1, 2, 5 and 6 as phase group 1, phase 3 & 4 as the phase group 2. For vehicle movements, we group movement (1-3,1-2, 3-1,3-4) as movement group for EB-WB trips on Plymouth road, and movement (2-4, 2-3, 4-2, 4-1) as the other movement group. Since more traffic are observed traveling on Plymouth Road (63.5% of all traffic), we indicate movement (1-3, 1-2, 3-1, 3-4) as the main-street movement, with the rest movement as the side-street movement.

For associating groups, two possible combinations exist: 1. phase group 1 (phase 1, 2, 5 & 6) for main-street movement, with phase group 2 (phase 3 & 4) for side-street movement, and vice versa. For simplicity, in the calculation of likelihood, we assume green arrival probability as 0.9, indicating 0.1 red light running probability. For the two combinations, the corresponding log-likelihoods are shown in Table 2.2. Apparently, association 1 with higher log-likelihood is the best estimate, colored in red in the table. Therefore, we associate phase group 1 for the main street, i.e., phase 1, 2, 5, and 6 for the Plymouth Road, and group 2 for the side street, i.e., phase 3 & 4 for Green road.

Combination ID	Green Arrival	Red Arrival	Log-Likelihood
1	**221**	**56**	**-66.1**
2	30	247	-248.4

Table 2.2: Log-Likelihood for associating main phase group with main movement

Next, we associate individual movement and signal phase in each phase and movement group. There are 4 phases in phase group 1, thus 8 possible combinations exist, shown in Figure 2.14a. For each combination, the corresponding log-likelihoods are shown in Table 2.3a. Here, the combination 3 is the best estimate for associating phases in main phase group 1. As there are 2 phases within the group, then 4 possible combinations exist. Based on the table, the combination 4 is the best estimate for associating phases in main phase group 2. The selected combinations are all consistent with the associations obtained from signal timing plans. That is, the lane-phase mapping has been correctly estimated at this intersection using the BSM and signal status data.

Combination ID	Green Arrival	Red Arrival	Log-Likelihood
1	150	148	-154.9
2	0	298	-298.0
3	**287**	**11**	**-24.1**
4	137	161	-167.3
5	101	197	-201.6
6	170	128	-135.8
7	103	195	-199.7
8	172	126	-133.9

(a) Log-likelihood for lane-phase mapping for main phase group 1

Combination ID	Green Arrival	Red Arrival	Log-Likelihood
1	42	149	-150.9
2	0	191	-191.0
3	127	64	-69.8
4	**169**	**22**	**-29.7**

(b) Log-Likelihood for lane-phase mapping for main phase group 2

Table 2.3: Log-Likelihood for lane-phase mapping for each main phase group

2.8 Chapter Summary

In this research, a new approach is developed to automatically generate intersection map using BSMs received by the RSEs. The proposed approach is applied for estimating map information at five intersections from the SPMD project. The estimated maps are then compared with surveyed maps obtained from highly accurate LiDAR surveys, to evaluate the accuracy of the proposed approach. Overall, encouraging results are obtained for the proposed approach, with some limitations of the estimation. Using 1-month BSM data collected at each of the intersections, the estimation approach correctly identify the most of the intersection structure regarding number of lanes for different movements. However, five out of 48 lanes are not correctly identified for the selected intersections. The miss-identification would be primarily due to the lack of CV data in these lanes. For the identified lanes, the accuracy of estimated lane geometries is 0.6 m on average, with the majority (90%) of the estimation under 1.2 m. The accuracy of the worst estimations is 1.3 m on average, with majority (90%) within 2.2 m. The accuracy on average is well below the typical lane width of 3.6 m, while the worst estimations within each lane geometry are also within reasonable accuracy, which would indicate the potential of using the estimated map for CV applications.

In addition to map estimation, the estimation of lane-phase mapping

is also investigated using signal status data and BSM data. A simple-yet-effective procedure is developed for the estimation by matching vehicle departures with traffic signal status, i.e., maximizing green departures. A case study is conducted using data from one of the five intersections for analysis. For the selected intersection, the proposed procedure is able to correctly associate vehicle movements to all applicable signal phases, confirming the validity of the lane-phase mapping estimation.

Chapter 3

Traffic Volume Estimation at Signalized Intersections

3.1 Introduction

Recent advent of CV introduces great opportunities of reforming the conventional traffic signal operation. Currently, many traffic signals in the U.S. are still fixed-time signals, which are not responsive to fluctuated traffic demands. For traffic signals to accommodate varying demands, vehicle detectors, e.g., inductance loop detectors or video detectors, need to be installed and maintained properly. This inevitably incurs significant cost for the public agencies. With the vehicle-to-infrastructure (V2I) communication, CVs can continuously report their status to roadside equipment (RSE) at intersections, working as mobile sensors. Therefore, CVs hold great potential to

reduce or even eliminate the needs for fixed-location detectors in the existing signal systems. When penetration rates are low, the CV data could be used to generate performance measures for fine-tuning traffic signals periodically. When penetration rates are high, it becomes viable to operate adaptive signal control that solely depends on CV input.

Considering these potentials, deploying V2I systems at signalized intersections has been an important part of CV pilot deployment, exemplified by the installation of RSEs at intersections in the Safety Pilot Model Deployment (SPMD) project [66], the upcoming CV pilot deployment [8], as well as in the Smart City development [9] supported by the US Department of Transportation (USDOT). Along with the deployment efforts, a number of CV-based signal control algorithms have also been proposed. However, the signal control algorithms proposed in the previous studies mainly focus on scenarios that penetration rates of CVs reach certain levels, e.g., 25%, which may not be feasible in the near future. In addition, most of the existing studies rely on simulated data which may not capture real-world characteristics of CVs, e.g. communication performance or GPS accuracy. Therefore, the proposed algorithms may not be transferable to the practice. How to utilize real-world CV data under low penetration rate environment to improve traffic signal operation remains as an open question.

Aiming to answer this question, this work develops an innovative approach that uses data from CVs to estimate traffic arrivals at signalized intersections, particularly under low penetration rate environment. It has been

well known that traffic volumes are the very key inputs to designing and optimizing traffic signal operation. In conventional signal systems, vehicle arrival information can only be obtained from detectors at fixed locations. Different from the detector data, CV data provide detailed trajectories, albeit from a small percentage of vehicles. The comparison is illustrated in Figure 3.1. The challenge here is to estimate overall arrival information using limited CV trajectories.

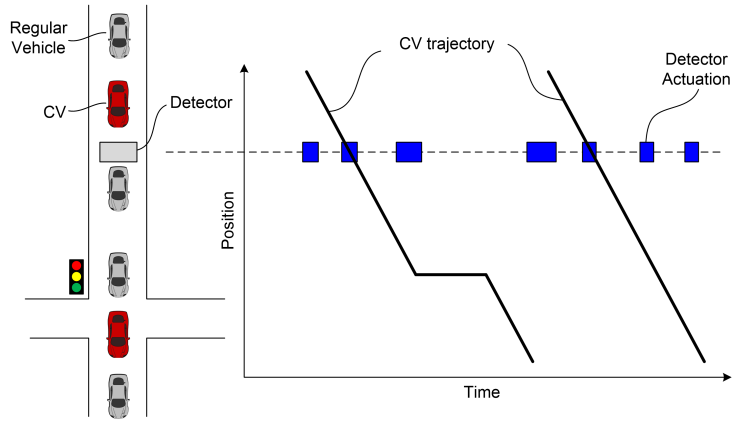

Figure 3.1: Illustration of CV data versus detector data

In this application, the above challenge will be addressed through leveraging historical CV data and the repetitive patterns of vehicle arrivals at signalized intersections. In the proposed algorithm, vehicle arrivals at intersections are modeled as a time-dependent Poisson process with a time dependent factor characterizing arrival types. For volume estimation, an expectation maximization (EM) procedure is derived that can incorporate

different types of CV trajectories. To evaluate the performance of the proposed algorithm, two case studies were conducted: the first case study utilized real-world CV data received by a RSE in the SPMD project; the second case study utilized vehicle trajectory data from users of a route navigation service. To the best of our knowledge, this research is the first attempt of exploring real-world CV or GPS trajectory data under low penetration rate environment for volume estimation at signalized intersections. Our ultimate goal is to use CV data to develop a detector-free signal control system in the future.

3.2 Relevant Work

Traffic signal control with CVs has captured substantial attention in the past several years. Many existing studies focus on developing real-time traffic signal control with CVs, through either extending signal actuation mechanism or minimizing vehicle delay based on a traffic model [67, 68, 69, 70, 71, 72, 73, 74, 75]. However, most of the proposed adaptive signal control algorithms require high penetration rates of CVs, e.g., 25%. Such high penetration rates may not be achievable in the near future. A notable exception is [76] which conducted a proof-of-concept study using CV data in a low penetration rate environment for optimizing signal coordination. However, the data used in [76] were sampled from fixed location vehicle detectors so vehicle trajectories were not used in their study. The problem of estimating traffic volume from

vehicle trajectories, which is a fundamental input for signal operation, is also not tackled.

On the other hand, with increasing availability of GPS data from cell phones and navigation units, substantial efforts have been carried out for traffic state estimation using vehicle trajectory data. Exemplified by the Mobile Century project [77, 78, 79], a large group of existing studies used GPS data to estimate traffic speed and travel time [80, 81, 82, 83, 84, 85, 86, 87]. Recently, several studies have also been conducted for real-time queue length estimation at signalized intersections. These approaches can be grouped into two main categories, one based on a probabilistic approach and the other using shockwave theory. Comert and his colleague derived analytical expressions of conditional probability of queue length based on the probability of observing probe vehicles in a queue [88, 89, 90]. Hao et al. proposed a Bayesian Network based model for estimating the probability of probe vehicle positions in vehicle arrivals [91, 92]. Another category focuses on applying the shock-wave theory by [93, 94] for queue length estimation with vehicle trajectory data. Cetin proposed a procedure for queue length estimation with over-saturated traffic conditions by identifying critical points of traffic shockwave [95]. Christofa et al. proposed a procedure to detect queue spillback using trajectory data with signal status information at both subject and upstream intersections [96]. Li et al. proposed a data fusion procedure for queue length estimation, leveraging data from both probe vehicles and loop detectors [97]. Sun & Ban applied the variation formulation of traffic

flow model by [98] for reconstructing all vehicle trajectories based on probe vehicle data [99]. Their key idea was to obtain flow information based on probe vehicle speeds, assuming that arrivals between two probe vehicles were uniform.

In the aforementioned studies, the primary focus is on estimating real-time performance measures at isolated intersections. However, estimating traffic volumes, which are critical for offline optimization of signal operation, has yet been studied. This work aims to fill in this gap. We believe that the proposed methodology would be an important building block of utilizing CV or vehicle trajectory data for traffic signal re-timing, and eventually achieving detector-free signal operation in the future.

3.3 Methodology for Traffic Volume Estimation

In order to estimate traffic volume, our basic idea is to take advantage of vehicle arrival information in vehicle trajectories. The arrival information can be reflected from the status whether a vehicle stopped or not. An example is shown in Figure 3.2. In the figure, CV1 passed the intersection with a stop and CV2 without a stop. Then, based on CV1's stopping position or departure time, we can calculate number of vehicles queuing in front of it. For CV2, we know that the vehicle queue is not long enough to impact CV2. In other words, the upper bound of possible vehicle arrivals between CV1

and CV2 can be calculated. By combining these arrival information from vehicle trajectories, volume of overall vehicle arrivals can be estimated.

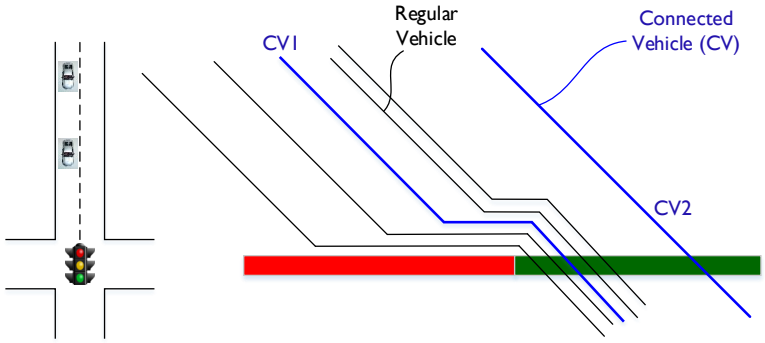

Figure 3.2: Illustration of vehicle arrival information in trajectories

The inputs to our estimation algorithm include vehicle trajectories approaching to an intersection as well as traffic signal status. For a CV trajectory, the information being utilized includes its projected arrival time with free flow speed at the stop bar $t_{f,i}$, its departure time at the stop bar $t_{d,i}$, the type of event indicating whether a CV stopped or not s_i, and the subscript i as the index of the event. For each CV trajectory, we have the following vector:

$$X_i = (t_{f,i}, t_{d,i}, s_i)^T$$

For CV without a stop, the projected arrival time at stop bar is equal to the departure time, as: $t_{f,i} = t_{d,i}$. For a CV with a stop, we can estimate its projected arrival time $t_{f,i}$ as:

$$t_{f,i} = t_{s,i} + \frac{y_i}{v_f} \tag{3.1}$$

Where $t_{s,i}$ is time when the CV came to a stop, y_i is the distance of its stopping position to the stop bar, and v_f is the free flow speed.

To incorporate signal information, we also treat the red signals as a type of events. Here, we assume that no residual queue exists at the start of red signal. With this assumption, we only focus on estimation with non-saturated traffic conditions, leaving estimation with over-saturated traffic conditions in our future research. For each red signal, we have the following vector:

$$X_j = (t_{f,j}, t_{d,j}, s_j)^T, with\, t_{f,j} = t_{r,j}, t_{d,j} = t_{g,j}$$

Where $t_{r,j}$ is the time of red start for cycle j, and $t_{g,j}$ for green start. Here, s_j is set as -1, indicating that this event is corresponding to a red signal. Denoting red signal as an event is for the ease of data processing so that we can calculate inter arrival period between arrivals of CVs and starting time of red signals easily.

These two vectors constitute the main input to the estimation process presented in the next section.

3.3.1 Modeling Traffic Arrivals as a Time-Dependent Poisson Process

During a selected Time of Day (TOD) period, we assume that traffic arrivals follow a time-dependent Poisson process with an arrival rate of $\lambda p(t^{(c)})$. Here, $t^{(c)}$ indicates time within a signal cycle, the superscript (c) indicates that the time is measured using a signal clock, λ denotes the mean arrival rate, and $p(t^{(c)})$ is the time dependent factor proportional to the arrival rate at $t^{(c)}$, i.e., the fraction of total arrivals at $t^{(c)}$ over the entire signal cycle. In traffic engineering literature, Poisson process is a common choice to model traffic arrivals at intersections. The additional assumption that arrival rates are dependent on the time in a signal cycle is to account for impacts from signal coordination with which mean arrival rate could not be treated as a constant.

Defining $N(t_1, t_2)$ as the accumulative number of arrivals from time t_1 to t_2, we have:

$$N(t_1,\ t_2) \sim Poisson\left(\Lambda(t_1,\ t_2)\right)$$

Where $\Lambda(t_1,\ t_2) = \int_{t_1}^{t_2} \lambda p\left(C(t)\right) dt = \lambda \int_{t_1}^{t_2} p\left(C(t)\right) dt$, and $C\ :\ t \to t^{(c)}$, mapping the time of a day, t, to time in signal cycle clock, $t^{(c)}$.

By aggregating CV trajectories, we can calculate the time dependent factor $p(t^{(c)})$ based on the following equation.:

$$p(t^{(c)}) = \frac{1}{N} \sum_{i=1}^{N} I\{C(t_{f,i}) = t^{(c)}\} \tag{3.2}$$

Where $I\{C(t_{f,i}) = t^{(c)}\}$ is an indicator that is 1 if the projected arrival time is $t^{(c)}$, and 0 otherwise, and N is the total number of CV trajectories. For the ease of data processing, we discretize time with 1-sec interval.

Given the Poisson arrival process, the likelihood function for observing all valid CV trajectories can be formulated by taking advantage of the inter-arrival time and the corresponding number of non-CV arrivals between two consecutive CV trajectories received at RSE. As mentioned earlier, two types of CV trajectories are considered: 1. CV trajectory with a stop at an intersection, and 2. CV trajectory that traverses the intersection without a stop. Between the projected arrival times of two stopped CVs, or between the projected arrival time of one stopped CV and the start of a red signal, the number of non-CV arrivals can be calculated based on the CVs' departure time. If a CV without a stop is observed, then queues at intersection, if exist, are not long enough to affect the non-stopped CV. Thus, the maximum number of vehicle arrivals before the CV can be calculated. Illustrations of the two types of CVs are shown in Figure 3.3, along with notations for calculation later on.

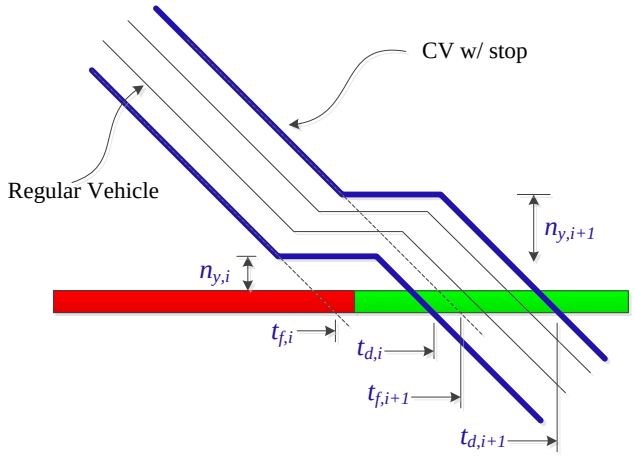

(a) CV with a stop

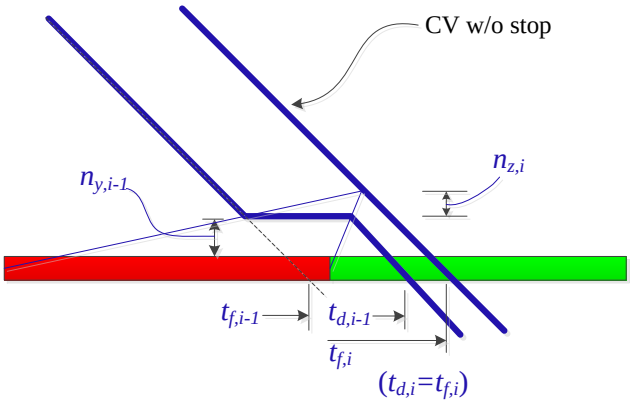

(b) CV without stop

Figure 3.3: Illustrations of two different types of CV trajectories

We further define $G(t_i, t_j)$ as the effective green time from time t_i, to t_j. For each CV trajectory, we can calculate the probability of occurrence

according to the following cases:

Case 1. If $s_i = 1$, $s_{i-1} = -1$ *or* 1, indicating a CV trajectory with a stop is observed after red start or after the arrival of another stopped CV, we have:

$$N(t_{f,i-1}, t_{f,i}) = n_{y,i},\ N(t_{f,i-1}, t_{f,i}) \sim Poisson\left(\lambda P_{y,i}\right)$$

Where $n_{y,i} = \left\lfloor \frac{G(t_{d,i-1}, t_{d,i})}{h_s} \right\rfloor$, denoting the number of departures during the inter-arrival period $[t_{f,i-1}, t_{f,i}]$, h_s is the saturated headway, and $P_{y,i} = \frac{\Lambda(t_{f,i-1}, t_{f,i})}{\lambda} = \int_{t_{f,i}}^{t_{f,i-1}} p\left(C(t)\right) dt$, denoting accumulated time dependent factor, for simplifying notations. The subscript y denotes that the observations are for stopped CVs. The illustration is also shown in Figure 3.3a.

Case 2. If $s_i = 2$, $s_{i-1} = -1$ *or* 1, indicating a CV trajectory without a stop is observed after red start or after a stopped CV. Accordingly, we have:

$$N(t_{f,i-1}, t_{f,i}) \leq n_{z,i},\ N(t_{f,i-1}, t_{f,i}) \sim Poisson\left(\lambda P_{z,i}\right)$$

Where $n_{z,i} = \left\lfloor \frac{G(t_{d,i-1}, t_{d,i})}{h_s} \right\rfloor$, $P_{z,i} = \frac{\Lambda(t_{f,i-1}, t_{f,i})}{\lambda} = \int_{t_{f,i}}^{t_{f,i-1}} p\left(C(t)\right) dt$. The subscript z denotes that the observations are for non-stopped CVs. The illustration is also shown in Figure 3.3b.

Besides these two cases, two other cases of trajectories also exist: 1. stopped CV arriving after a non-stopped CV in the same cycle, and 2. non-stopped CV arriving after another non-stopped CV, also in the same cycle. For the first case, the stop of the CV would not be caused by queues or red

signal, but likely by other factors, e.g., mid-block entry of other vehicles. For the second case, after the arrival of a non-stopped CV, we know that the queues must have been cleared and the rest of CVs in the same cycle would travel with free-flow speed. The trajectory therefore does not provide useful information for volume estimation. Accordingly, both cases are considered as invalid or trivial observations, and are not used in the estimation.

Based on the discussion, the likelihood of observing all valid CV trajectories can be calculated with the following equation, with $\mathbf{Y}$ as the collection of observations for all stopped CVs, and $\mathbf{Z}$ for all non-stopped CVs.

$$L(Y, Z|\lambda) = \prod_{i=1}^{n} \left\{ \frac{(\lambda P_{y,i})^{n_{y,i}} e^{-(\lambda P_{y,i})}}{n_{y,i}!} \right\} \prod_{j=1}^{m} \left\{ \sum_{k=0}^{n_{z,i}} \frac{(\lambda P_{z,i})^{n_{z,i}} e^{-(\lambda P_{z,i})}}{n_{z,i}!} \right\} \quad (3.3)$$

Now, we can estimate λ for the traffic volume using maximum likelihood estimator (MLE). However, due to the summation inside the product operation in Equation 3.3, it is difficult to obtain a closed form of the MLE. Instead of seeking for a closed form, we use the Expectation Maximization (EM) algorithm for the estimation.

3.3.2 Estimating Parameter Using Expectation Maximization (EM)

The Expectation Maximization (EM) algorithm is an iterative procedure to find the MLE mostly suitable when unobserved or partially observed variables exist. The EM algorithm consists of two main steps: the E-step and the M-step. The E-step calculates the conditional expectation of unobserved or partially observed variables based on initialized parameters, and the conditional expectation of the likelihood. Then, the M-step searches for an optimal update of the parameters through maximizing the likelihood. The two steps are iterated until updates converge. For the details of the EM algorithm, interested readers are referred to [100]. In our case, CV trajectories with stop provide direct information of number of arrivals, while trajectories without a stop only provide information of upper bounds of the number of arrivals, i.e., partial information. Considering this, the EM algorithm would be a proper choice for our estimation.

For the E-Step, denoting $\tilde{n}_{z,i}$ as the true value of accumulated number of arrivals by time $t_{z,i}$ corresponding to a CV trajectory without a stop, we have the log-likelihood for the complete data sequence as:

$$
\begin{aligned}
LL^c &= \sum_{i=1}^{n} \ln p(n_{y,i}|\lambda P_{y,i}) + \sum_{i=1}^{m} \ln p(\tilde{n}_{z,i}|\lambda P_{z,i}) \\
&= \sum_{i=1}^{n} \left[\ln \frac{(\lambda P_{y,i})^{n_{y,i}} e^{-\lambda P_{y,i}}}{n_{y,i}!} \right] + \sum_{i=1}^{m} \left[\ln \frac{(\lambda P_{z,i})^{\tilde{n}_{z,i}} e^{-\lambda P_{z,i}}}{\tilde{n}_{z,i}!} \right] \\
&= \sum_{i=1}^{n} \left[n_{y,i} \left(\ln \lambda + \ln P_{y,i} \right) - \lambda P_{y,i} - \ln n_{y,i}! \right] \\
&\quad + \sum_{i=1}^{m} \left[\tilde{n}_{z,i} \left(\ln \lambda + \ln P_{z,i} \right) - \lambda P_{z,i} - \ln \tilde{n}_{z,i}! \right] \qquad (3.4)
\end{aligned}
$$

Then, the expectation of the log-likelihood can be expressed as:

$$
Q(\lambda|\lambda^{(s)}) = E(LL^c|\lambda^{(s)}) = C + \sum_{i=1}^{n} \left[n_{y,i} \ln \lambda - \lambda P_{y,i} \right] + \sum_{i=1}^{m} \left[\overline{n}_{z,i} \ln \lambda - \lambda P_{z,i} \right] \qquad (3.5)
$$

The conditional mean of the unobserved variable $n_{z,i}$ is given by:

$$
\overline{n}_{z,i}|n_{z,i}, \lambda^{(s)} = \sum_{k=0}^{n_{z,i}} k \frac{\frac{(\lambda^{(s)} P_{z,i})^k}{k!}}{\sum_{l=0}^{n_{z,i}} l \frac{(\lambda^{(s)} P_{z,i})^l}{l!}} \qquad (3.6)
$$

Finally, in the M-step, by setting the derivative of $Q(\lambda|\lambda^{(s)})$ with respect to λ as zero, we have an equation for updating λ, as:

$$
\lambda^{(s+1)} = \frac{\sum_{i=1}^{n} n_{y,i} + \sum_{i=1}^{m} \overline{n}_{z,i}}{\sum_{i=1}^{n} P_{y,i} + \sum_{i=1}^{m} P_{z,i}} \qquad (3.7)
$$

Equation 3.6, Equation 3.7 complete the EM iteration for the estimation.

3.3.3 Overall Processing Procedure

The overview of the processing procedure is shown in Figure 3.4. First, the GPS data associated with an interested approach and signal phase will be selected during a particular time period, and converted to longitudinal data along the road, i.e., time-space trajectories. Then, the time-space trajectories are aggregated based on the signal status. With the aggregated data, we can calculate the time dependent factor, similar to the cyclic profile generated from vehicle detectors [76, 25]. The time dependent factor is then used together with vehicle trajectories to estimate traffic volumes. Finally, the time dependent factor and traffic volumes can be used to reconstruct overall traffic arrivals including both connected and non-connected vehicles, for further use in traffic signal operation.

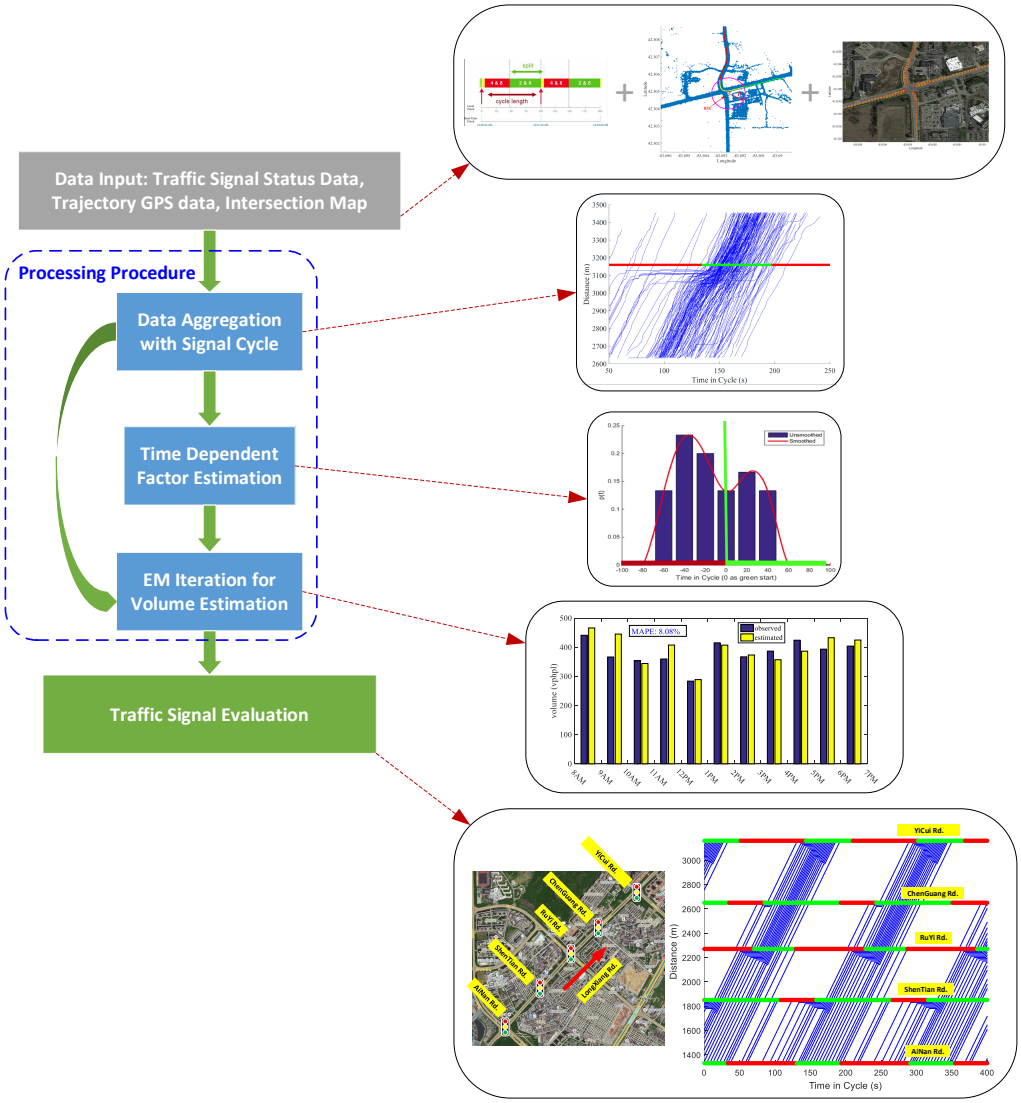

Figure 3.4: Overview of data processing procedure

3.4 Case Studies

To evaluate the proposed estimation algorithm, two case studies were conducted. The first case study utilized CV data received by a RSE in the SPMD project. The second case study utilized GPS data from users of a navigation service. These two types of data essentially contain similar information. However, data from CV are in 10 Hz sampling frequency while data from navigation devices are in 1 Hz frequency. Also, the studied intersection in the first study was controlled by the SCOOT adaptive signal system, while in the second case study, the intersection was controlled by a fixed-time signal.

3.4.1 Case 1: Using CV Data from a RSE

In the first case study, the analysis is conducted using CV data from Intersection Plymouth Rd. & Green Rd., one of the intersections deployed with a RSE in the SPMD project. The data used were received from 04/25/16 to 05/13/16 at the intersection. Sample data have been shown in Figure **??** earlier in Chapter 2. Note that, only data from Monday to Thursday are used, as these four weekdays typically posses similar traffic patterns which are different from the rest days. An illustration of the intersection geometry is shown in Figure 3.5, together with the ring-and-barrier diagram for traffic signal in operation. Here, the investigation focused on EB through, WB through, as well as SB through and left-turn traffic, corresponding to phase 1, 2 and 4. The NB approach is a single-lane road adjacent to the parking

lot of a shopping plaza. At the NB approach, traffic from the driveways and parking lots frequently affect vehicles traveling at the NB approach, resulting in additional queues and vehicle-stops not caused by the traffic signal. Since the stop and queuing information play key roles in the volume estimation, the analysis for the NB traffic is excluded, considering the noises caused by the traffics from the parking lots.

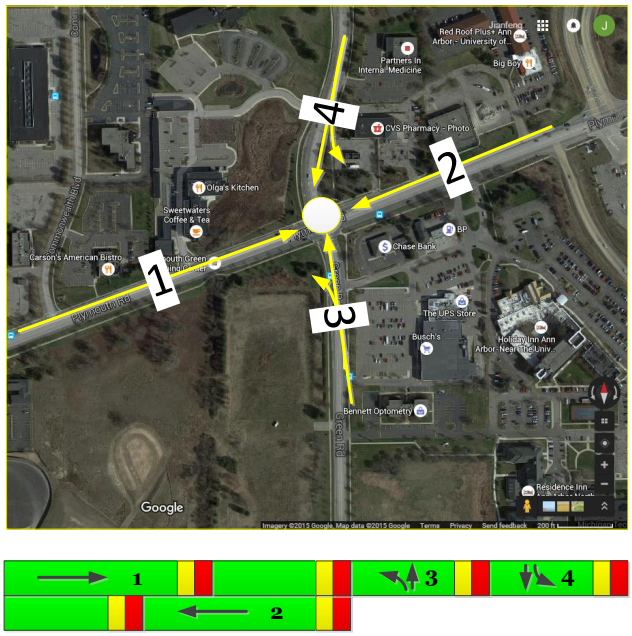

Figure 3.5: Illustration of investigated intersections

For each interested approach, trajectories of CVs were first processed as time-space plots with time as the horizontal axis and distance to the stop bar as the vertical axis. The trajectories are shown in Figure 3.6a. With

the SCOOT adaptive signal system, at this intersection, the cycle length, red and green duration all varied from cycle to cycle. To select a common reference point in a signal cycle, we use the start of green as time 0 in the plot for simplicity.

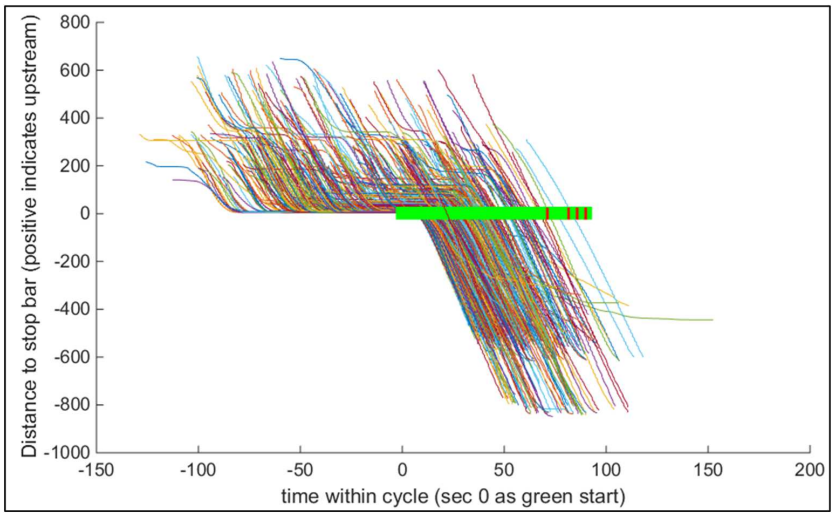

(a) Sample CV trajectories

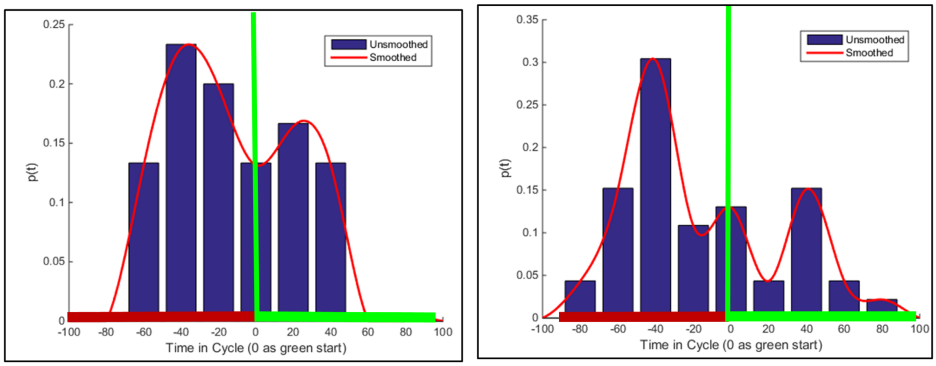

(b) Time dependent factor for 11AM-12 PM period (left) and 6 PM-7 PM period (right)

Figure 3.6: Illustration of CV trajectories (a) and time dependent factor (b) for EB through movement

The CV trajectories were aggregated according to different TOD periods with 1-hour intervals across different days, to first calculate time-dependent factors $p(t)$. For different TOD periods, substantially different $p(t)$ were observed with two examples shown in Figure 3.6b. The differences in $p(t)$ should be due to differences in both traffic patterns and signal settings in the two different TOD periods. Along with $p(t)$, observation lists were also prepared based on the CV trajectories. Finally, the EM procedure was implemented for the estimation.

For validation purpose, hourly volumes were also manually collected for two days, i.e., 04/25/16 and 04/26/16, from 11:00 AM to 7:00 PM. Using the measured volumes, we calculated the penetration rates of CVs, shown in Figure 3.7. Overall, the penetration rates ranged from 3% to 12%, varying over the selected periods. The rates also varied substantially at different approaches, with lower CV penetration rates at the EB and WB approach, i.e., the main approaches, and higher rates at the SB approach, a minor approach. This variation could be due to that the SB approach connects to residential areas close to the University of Michigan that have larger population of participants of the SPMD project.

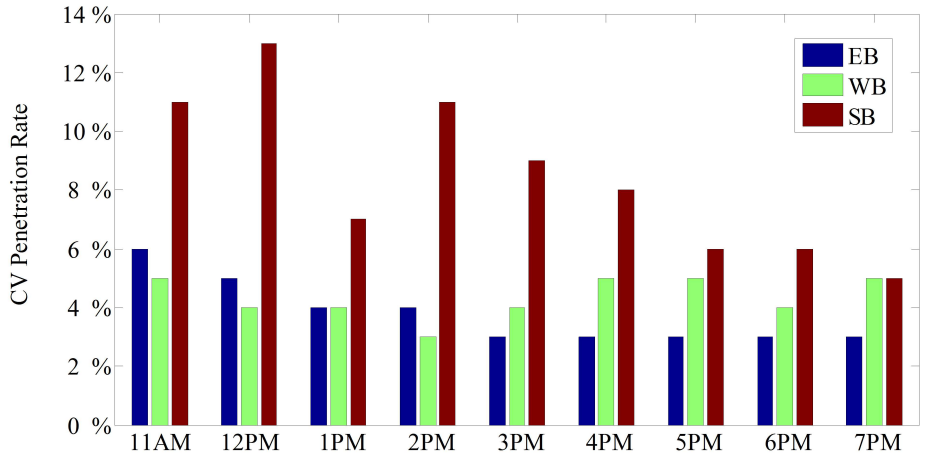

Figure 3.7: CV penetration rates over time of day

The observed volumes were then used for comparing with the estimated volumes, with results shown in Figure 3.8. To quantify the accuracy, we calculated the Mean Absolute Percentage Error (MAPE) for the estimation based on the following formula, indicated as well in the figure.

$$MAPE = \frac{1}{N}\sum_{i=1}^{N}\frac{|Vol_{o,i} - Vol_{e,i}|}{Vol_{o,i}} \tag{3.8}$$

Where $Vol_{o,i}$ is the observed volume, and $Vol_{e,i}$ is the estimated volume, during i-th interval.

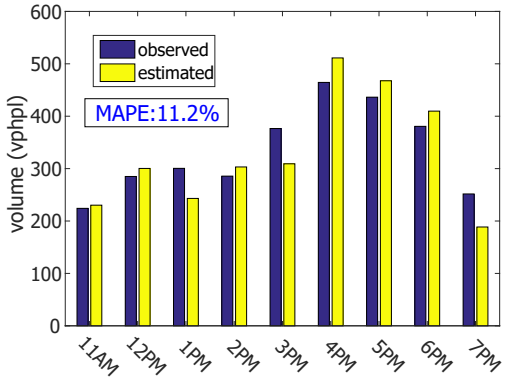

(a) EB-Through movement

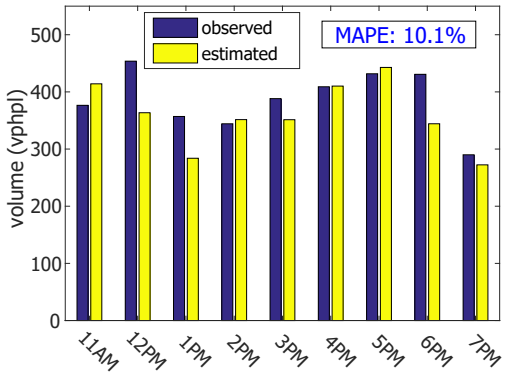

(b) WB-Through movement

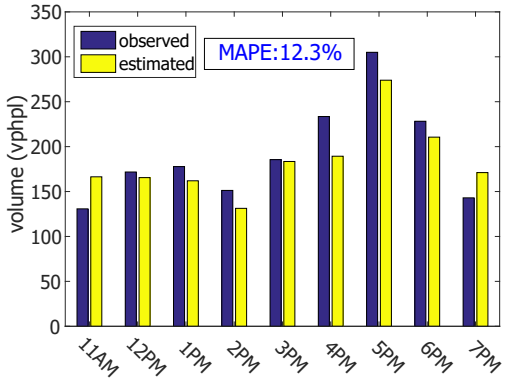

(c) SB-Through and Left-Turn movement

Figure 3.8: Comparison between observed volume and estimated volume using SPMD data

As shown in the figure, the estimated volumes are generally close to the observed volumes over different TOD periods. The MAPEs are 11.2%, 10.1% and 12.3% for EB, WB and SB approach, respectively, indicating reasonable accuracy of the proposed procedure. Among the 3 approaches, however, the estimation for the SB approach performs the worst among all three phases, despite the largest CV penetration rates. This is likely due to that the arrival patterns are more stable at the EB and WB approaches with signal coordination, than that at the SB approach, i.e., a minor approach. Additionally, with the lowest traffic volumes at the SB approach, the total number of observed CV trajectories at the SB approach is similar to that at the EB and WB approach, which could imply that the sample size also play an important role rather than the penetration rate alone. Nonetheless, the results are still encouraging, considering the overall low penetration rates mostly under 10% in the investigated cases.

3.4.2 Case 2: Using Data from Users of a Navigation Service

In the second case study, we utilized data collected from drivers using a navigation service in the City of Shenzhen, China. The data were collected on workdays between 06/13/2016 and 06/30/2016 on LongXiang Rd. The

illustration of data sample is shown in Figure 3.9, in which the color indicates vehicle speed. For the analysis, we focused on a selected approach at an intersection and estimated traffic volumes using the proposed procedure. The estimation was then validated using data from loop detectors for the approach. The selected approach and intersection are indicated with the purple arrow and circle in Figure 3.9.

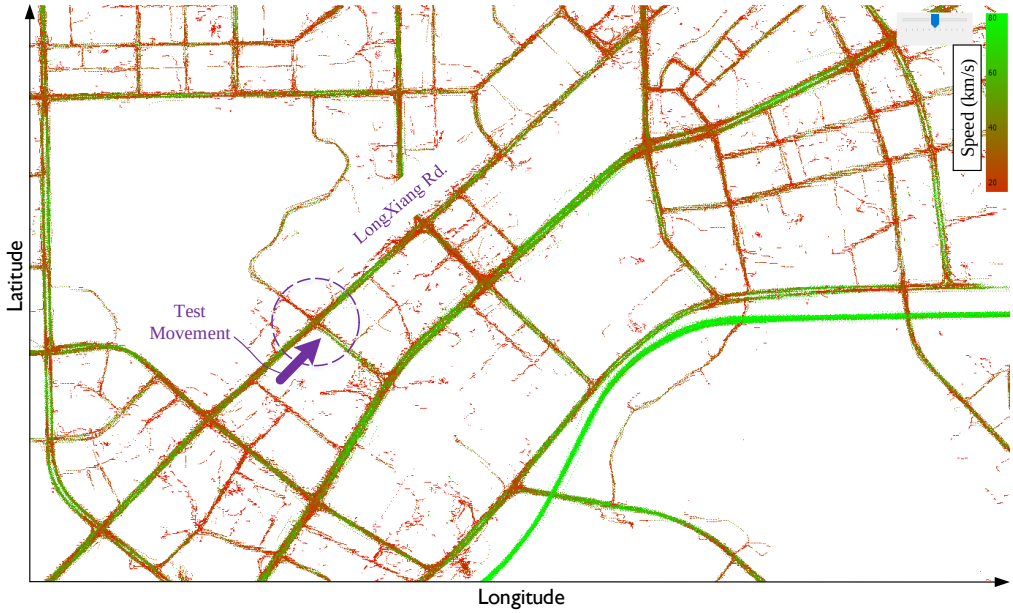

Figure 3.9: Illustration of GPS data from navigation service users

At the selected intersection, Intersection LongXiang Rd. & YiCui Rd., a sample set of the GPS trajectories between the adjacent upstream and downstream intersections for the through movement is shown in Figure 3.10. The time of each GPS data point was also converted to time within a signal cycle.

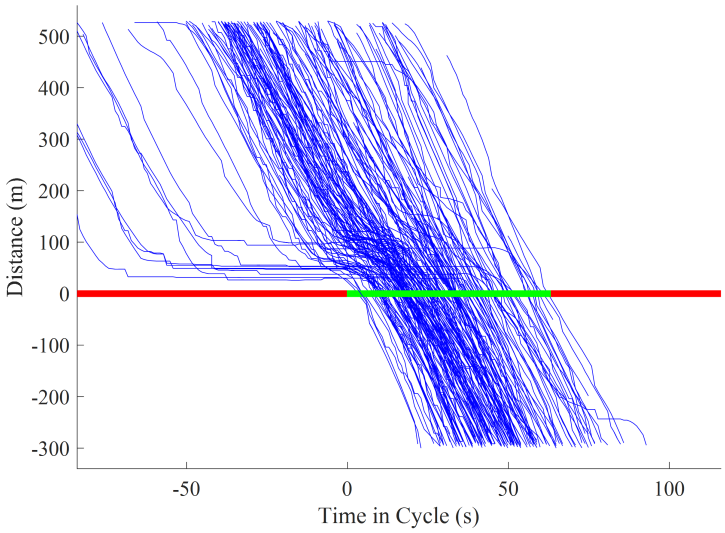

Figure 3.10: Trajectories of converted trajectory data from navigation user

For validation purposes, volume data were also obtained for the selected approach from loop detectors on 07/12/2016. Based on the detector data, we calculated the penetration rates of the navigation users for the through movement. The results are shown in Figure 3.11. While the penetration rate varied over time of day, generally, it stayed within the range of 0.5% to 2%.

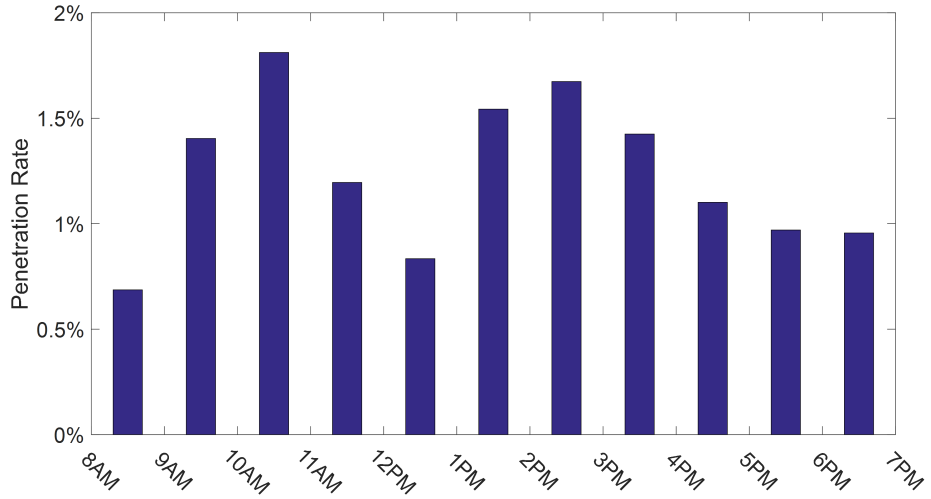

Figure 3.11: Penetration rates of navigation service users

The volume estimation results are shown in Figure 3.12. As we can see in the figure, similar to Case Study 1, the estimated volumes are generally close to the observed volumes. The MAPE of the estimation is 8.1% for the selected approach. Intriguingly, the estimation errors in Case Study 2 are even smaller than those in Case Study 1, despite lower penetration rates. This would be mainly because that the traffic signal in Case Study 2 was in a fixed-timed mode, while in Case Study 1 the signal was controlled by the SCOOT adaptive control system. With the SCOOT system, the green start and green end varies substantially from cycle to cycle. Due to such variation in signal status, the cyclic profiles are less consistent than that with fixed-timed signals. This inconsistency is difficult to be modeled by the time-dependent Poisson process used in the proposed estimation methodology. Therefore, Case Study 2 would likely yield better estimation results than

Case Study 1. In addition, the selected road in the Case Study 2 is a larger highway with 6 lanes for through movement than that in the Case Study 1 with 2 lanes. Although the penetration rate is lower in the Case Study 2, the sample sizes of CV trajectories in the two case studies are at similar levels. This may also contribute to the better estimation results observed in Case Study 2.

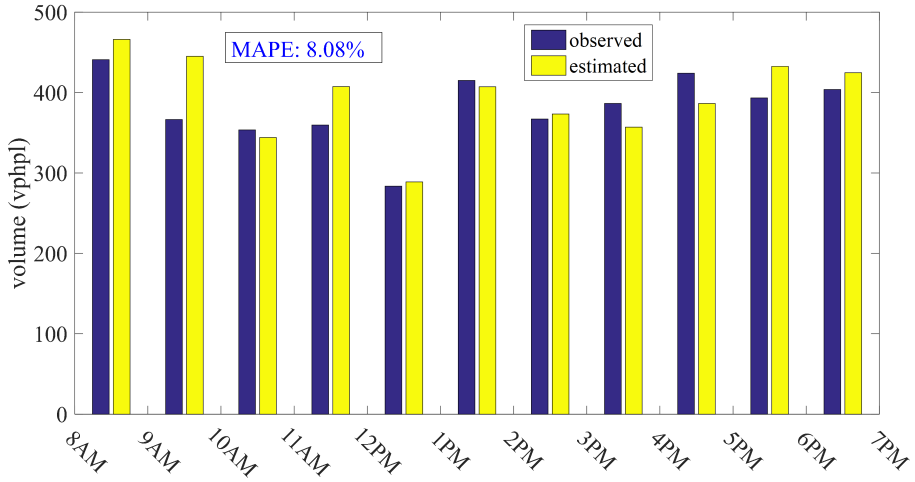

Figure 3.12: Comparison between observed volume with estimated volume using data from navigation users

To illustrate the use of the estimated volume data for assisting signal operation, we repeated the same procedure for four other intersections along the LongXiang Rd and generated a time-space diagram (TS-Diagram) based on the estimated volumes with the time dependent factors. The TS-Diagram is a convenient and popular tool for traffic engineers to evaluate performance of signal coordination, and to fine-tune signal settings if necessary. The

procedure to construct TS-Diagram is based on [35], and the result is shown in Figure 3.13 for the LongXiang corridor with the 5 intersections for time period 8 AM-9 AM.

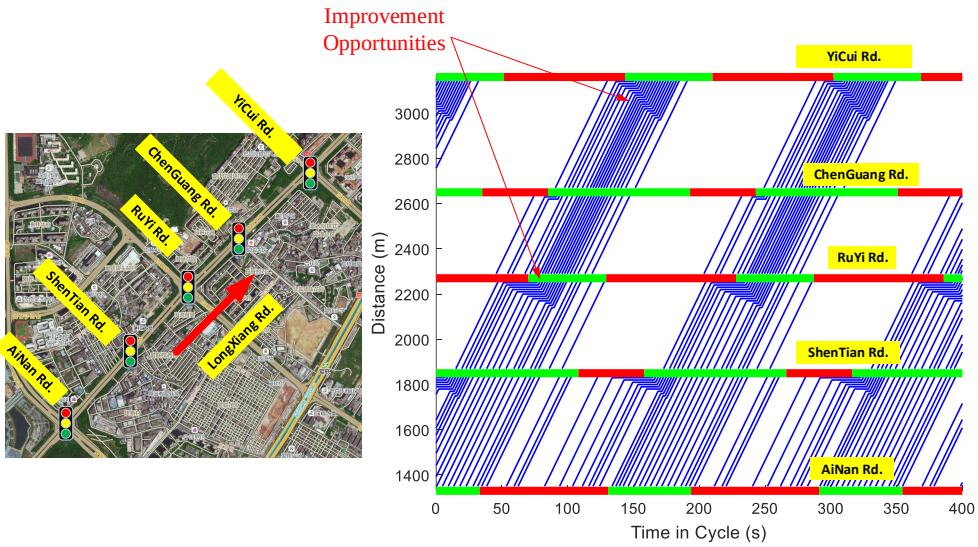

Figure 3.13: Time-Space diagram for the tested segment

From Figure 3.13, it can be seen that, in general, the signals were coordinated well with traffic traveling in free-flow speed for the most of the time. However, for Intersection ShenTian Rd. & LongXiang Rd. and Intersection YiCui Rd. & LongXiang Rd., vehicle delay exist and could potentially be reduced by adjusting offsets at these two intersections, indicating improvement opportunities at these two intersections.

3.5 Chapter Summary

With the rapid development of CV technology, paradigm shift may be brought to the traffic signal systems. The data from CVs provide invaluable opportunities to reduce or even eliminate the needs for conventional traffic detectors. In the near future with low penetration rates, data from CVs could be particularly useful to generate offline performance measure for traffic signal systems and adjust signal operation periodically, e.g., two weeks or a month. This potential is especially beneficial for improving existing signal operation.

In this chapter, an innovative procedure is developed to estimate hourly traffic volumes using data from CVs or trajectories data from navigation devices. For existing traffic signals, the traffic volumes are the key inputs to signal optimization, as well as to many other traffic engineering practices. Considering that CV deployments are still in their early stages, the focus of the proposed approach is to accommodate low CV penetration rates, for instance, below 10% in the City of Ann Arbor, MI.

In the proposed approach, the vehicle arrival process is modeled as a time dependent Poisson process and an EM procedure is derived for the estimation. The estimation procedure is tested with two case studies using real-world CV data from the SPMD project and vehicle trajectory data from navigation service users, respectively. Comparing with volume data collected manually and data from loop detectors, reasonable accuracy of the estimations was found. We believe that the proposed methodology would be

an important building block of utilizing CV data for adjusting or re-timing traffic signals.

Chapter 4

Eco-driving Advisory with V2I Information

4.1 Introduction

Energy consumption and Green House Gas (GHG) emission have been a long-time concern for the transportation sector. According to [101], the transportation sector consumed 28% of total energy usage and 67% of total petroleum usage in the US, second largest and largest among all sectors, respectively. The high petroleum consumption also leads to large GHG emission, with 28.2% of GHG and 32.9% of CO2 emission in the US. There is an urgent need to improve the performance of vehicular traffic in order to reduce fuel consumption and GHG emission.

The impacts of driving speed on fuel consumption and emission have

been long recognized [102, 103, 104]. For trips with same distance and travel time, different speed profiles could result in substantially different fuel consumption. It has be demonstrated that, even with simple speed advice, considerable improvement of fuel economy can be achieved [105, 106]. In fact, optimizing speed for improvement of fuel consumption is not a new concept with early studies traced back to [107, 108, 109]. Recent developments also include the incorporation of detailed engine model or terrain information into the optimization process [110, 111, 112], and the consideration of dynamically changing speed limits for fuel consumption minimization [113].

More recently, with the emerging CV technology, numerous studies have been conducted to optimize speed of CVs based on traffic and signal status information from RSEs at intersections. Rakha & Kamalanathsharma developed an eco-driving framework by integrating VT-Micro with a vehicle dynamics model [114]. Guan & Frey proposed a Dynamic Programming (DP) based approach to obtain optimal speed and gear choices based on the enumeration of possible vehicle arrival times at an intersection [115]. In [116], impacts from the traffic signals are considered as arbitrary terminal costs in the objective function to derive analytical solutions. Alsabaan et al. developed a simulation platform for the evaluation of eco-driving algorithms by integrating the INTEGRATION traffic model, VT-Micro fuel consumption and emission model , as well as a simple communication simulation model [117]. He et al. also studied the echo-driving problem, with consideration of the presence of vehicle queues. Li et al. also studied the fuel-optimal

eco-departure problem for optimal acceleration after stopping at intersection [118]. The problem was formulated as a nonlinear mixed-integer optimal control problem, considering both engine characteristics and gear transmission. The approximated solution is obtained through Legendre pseudo-spectral method.

Overall, research on optimizing driving speed with V2I information is in its early stage. While many studies rely on Dynamic Programming (DP) to solve the optimization problem for the purpose of evaluating vehicle performance in a controlled testing environment, the heavy computation load makes them difficult for on-board implementation. On the other hand, although driving history and fuel consumption data can now be easily collected with GPS units and On-board Diagnostics (OBD) scanners , such data are seldom explored to optimize fuel consumption.

In this chapter, an efficient algorithm is proposed to generate optimal speed profiles when driving through signalized intersections. Different from the majority of the existing work, here, the heterogeneity of drivers are considered by mining the historical driving and fuel consumption data. The historical data is utilized to calibrate parameters of the fuel consumption model as well as to generate acceleration and deceleration bounds of the driver. Therefore, the procedure could generate more personalized speed advisories to individual drivers. To illustrate and evaluate the proposed procedure, a case study is conducted using real-world data collected from the SPMD project, showing good potential of the proposed approach.

4.2 Problem Formulation and Fuel Consumption Model

4.2.1 Problem Formulation

The investigation scenario focuses on driving a CV through a signalized road with intersections deployed with RSEs. It is assumed that a speed advisory system is available on-board in the CV. The speed advisory system includes 4 main components: 1. an OBD reader that is able to collect and archive fuel consumption data from vehicle controller area network (CAN) bus; 2. a DSRC device for communicating with the RSEs; 3. a processing unit to analyze the historical driving data and traffic condition data at the intersection from a RSE, and generate speed advisory; and 4. a display unit for notifying the speed advisory to the driver. The traffic condition data from the RSE mainly consist of information of signal and queue status at an intersection, based on which the advisory system will determine the optimal speed profile satisfying the boundary constraints. The boundary constraints include the initial and the ending locations and speeds, as well as the travel time in between. An illustration of the investigation scenario and boundary constraints is shown in 4.1.

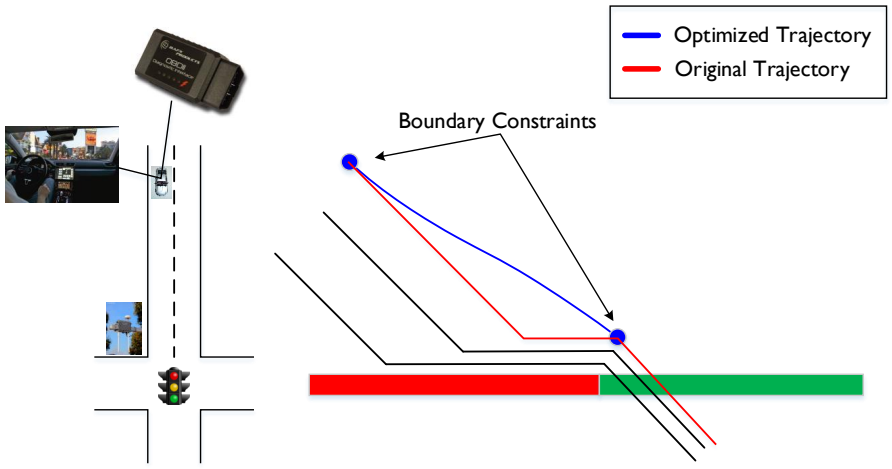

Figure 4.1: Investigation scenario and boundary point of vehicle approaching the intersection

The objective is to minimize total fuel consumption for driving between the two boundary points along the road, as:

$$\min : J = \int_0^T F_e(\dot{v},\ v)dt \tag{4.1}$$

Where F_e is the fuel consumption function, v is the vehicle speed, $\dot{v}$ is the vehicle acceleration/deceleration rate and T is the travel time between the two boundary points.

With the vehicle position x, as the state variable, we have the dynamics:

$$\dot{x} = v \tag{4.2}$$

The acceleration/deceleration rate is selected as the control variable, as:

$$u = \dot{v} = \ddot{x} \tag{4.3}$$

The boundary constraints are:

$$x(0) = 0,\ x(T) = x_T,\ v(0) = v_0,\ v(T) = v_T \tag{4.4}$$

Where x_T is the ending position, v_0 is the starting speed, and v_T is the ending speed.

The acceleration/deceleration rate is also bounded as:

$$u \in [a_L(v), a_U(v)] \tag{4.5}$$

Where $a_L(v)$ and $a_U(v)$ are the lower bound and upper bound of acceleration/deceleration rate depending on speed, respectively.

4.2.2 Mining Historical Data

A sample of the historical driving data is shown in Figure 4.2, from the SPMD project. In the project, historical data have been collected for each participant during his/her daily driving. For instance, data in Figure 4.2 are from a participant driving a Ford Fusion, in which instantaneous fuel consumption data can be accessed through CAN bus.

TxDevice	Trip	Time	MPG (scaled)	GPS Speed	Latitude	Longitude	Altitude
10164	966	51970	27	3.09	42.279879	-83.700163	199.55
10164	966	51980	27	3.06	42.279880	-83.700160	199.55
10164	966	51990	27	2.98	42.279883	-83.700158	199.55
10164	966	52000	27	2.95	42.279884	-83.700154	199.55
10164	966	52010	27	2.86	42.279886	-83.700153	199.55

Figure 4.2: Sample of historical data from the SPMD project

The historical data from the above selected driver are collected from Aug 2013 to Aug 2014, with around 1,439,000 data points archived. Using this data, relationship between instantaneous fuel consumption rate with speed and acceleration/deceleration rate can be constructed as a look-up table. The result is shown in Figure 4.3. In the figure, the region for fuel consumption or preferred acceleration/deceleration bounds shrink when the speed increases. This is a reasonable trend, considering the limitations of vehicle performance, and that drivers tend to decelerate/accelerate more frequently in lower speed than higher speed. Additionally, to avoid speeding over limit, we modify the acceleration to be 0 m/s^2 when vehicle speed reaches a preset value, i.e., a speed limit. In our research, the speed limit is set as 27 m/s for urban driving.

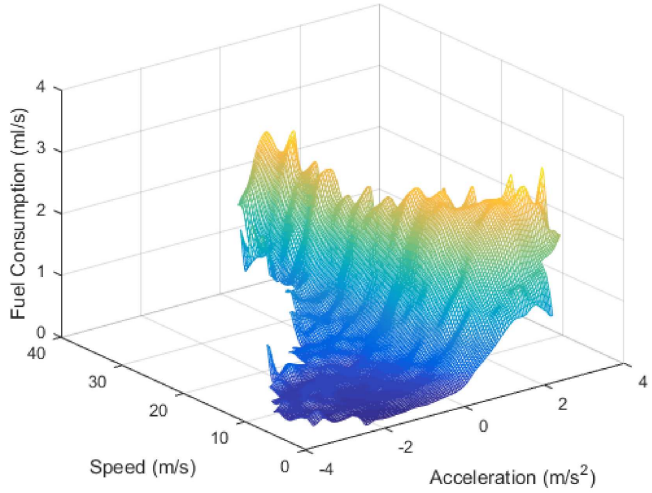

(a) Fuel consumption map

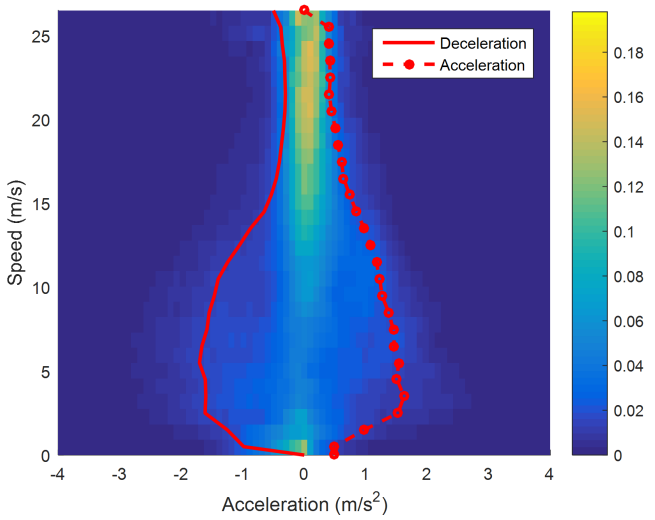

(b) Acceleration & deceleration bounds

Figure 4.3: Profiles obtained from historical driving data

With the fuel consumption map, one approach is to employ DP for solving the optimal control problem. However, the DP based approach is too

computationally expensive to be used for real-time applications. Therefore, instead of using DP with the look-up table, we utilize an approximated fuel consumption model so that an analytical solution can be derived.

4.2.3 A Simplified Fuel Consumption Model and Parameter Calibration

Here, the model proposed by [119] is adopted as the simplified fuel consumption model. The model estimates instantaneous fuel consumption rate F_e based on vehicle speed v and acceleration/deceleration rate $\dot{v}$. There are totally 3 terms, the first term accounting for idling cost, the second term for costs related with requested power output, and third term for penalty of excessive acceleration. The model is expressed as follows:

$$F_e(v, \dot{v}) = \alpha + \max\{c_1 v + c_2 v^3 + c_3 v\dot{v}), 0\} + c_4 v\dot{v}^2{}_{|\dot{v}\geq 0} dt \tag{4.6}$$

Where $\alpha,\ c_1,\ c_2,\ c_3$ and c_4 are the model parameters that need to be calibrated using the historical data by minimizing root mean square error (RMSE). Let $\beta = \{\alpha, c_1, c_2, c_3, c_4\}$, we aim at finding, β^* that:

$$\beta^* = \arg\min_{\beta} \sqrt{\frac{1}{N} \sum \left[F(v, \dot{v}|\beta) - \tilde{F}(v, \dot{v}|\beta)\right]^2} \tag{4.7}$$

Where $\tilde{F}(v, \dot{v}|\beta)$ is the observed fuel consumption rate, and N is the total

number of fuel consumption data points.

Since the fuel consumption model is piece-wise continuous, we can re-arrange the model and estimate parameters, similarly to the form of the piece-wise linear regression.

$$F_e(v,\dot{v}) = \alpha + c_1\left(v + \frac{c_2}{c_1}v^3 + \frac{c_3}{c_1}v\dot{v}\right)\times I\left(\dot{v} > -\frac{c_1}{c_3} - \frac{c_2}{c_3}v^2\right) + c_4\dot{v}^2 v \times I(\dot{v} > 0) \tag{4.8}$$

To minimize the objective function, we enumerate $\frac{c_2}{c_1}$ and $\frac{c_3}{c_1}$. With a given $\frac{c_2}{c_1}$and $\frac{c_3}{c_1}$, the rest of parameters can be fitted with linear regression. The illustration of the RMSE depending on $\frac{c_2}{c_1}$ and $\frac{c_3}{c_1}$ is shown in Figure 4.4. The calibrated parameters are listed in Table 4.1.

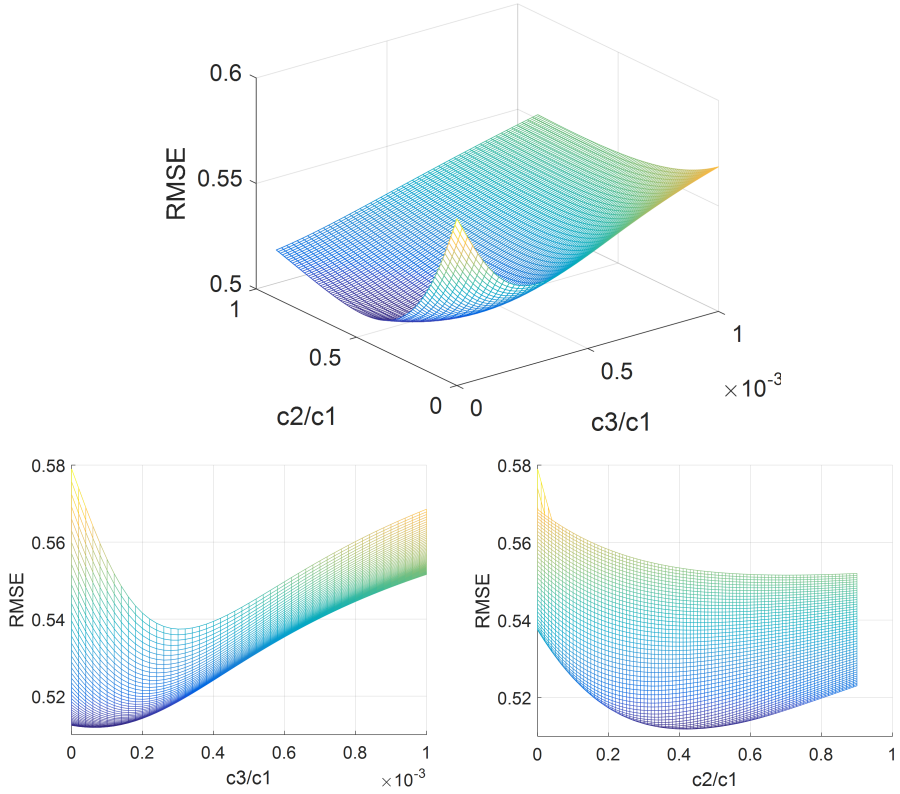

Figure 4.4: Illustration of RMSE for parameter calibration

	Calibrated Value
α	$0.4757\ ml/s$
c_1	$0.0976\ ml/m$
c_2	$0.0410\ ml * s^2/m^3$
c_3	$5.8547 * 10^{-6}\ ml * s^2/m^2$
c_4	$0.0165\ ml * s^4/m^3$

Table 4.1: Calibrated parameters

4.3 Solving Optimal Control Problem with PMP

With the simplified fuel consumption model, we then solve the optimal control problem using PMP [120]. With the terminal constraints, we can rearrange the objective as:

$$\begin{aligned}\max J &= \int_0^T -\alpha - \max\{c_1 v + c_2 v^3 + c_3 v\dot{v}), 0\} - c_4 v\dot{v}^2{}_{|\dot{v}\geq 0} dt \\ &\propto \int_0^T -\max\{c_2 v^3,\ -c_1 v - c_3 v\dot{v}\} - c_4 v\dot{v}^2{}_{|\dot{v}\geq 0} dt\end{aligned}$$

To solve the problem, we first define Hamiltonian as:

$$H(u) = -\max\{c_2 v^3,\ -c_1 v - c_3 v\dot{v}\} - c_4 v u^2{}_{|u\geq 0} + \lambda_1 v + \lambda_2 u \tag{4.9}$$

Where λ_1, λ_2 are the co-states.

Depending on the co-state λ_2 and speed v, $H(u)$ is a piece-wise continuous function of u with 3 regions, with two break points as:

$$u = a_c = -\frac{c_2 v^2 + c_1}{c_3},\ and\ u = 0$$

Where a_c is the deceleration rate when the vehicle decelerates using rolling resistance and aerodynamic force without brakes activated.

The Hamiltonian can be expressed as:

$$H(u) = \begin{cases} c_1 v + c_3 v u + \lambda_1 v + \lambda_2 u, & u < u_c \\ -c_2 v^3 + \lambda_1 v + \lambda_2 u, & u_c \leq u < 0 \\ -c_2 v^3 - c_4 v u^2 + \lambda_1 v + \lambda_2 u, & u \geq 0 \end{cases} \tag{4.10}$$

The optimal control u^*needs to satisfy following conditions:

$$u^* = \arg\max_u H(u) \tag{4.11}$$

$$\dot{\lambda}_1 = -\frac{\partial H}{\partial x} = 0 \tag{4.12}$$

$$\dot{\lambda}_2 = -\frac{\partial H}{\partial v} = \frac{\partial}{\partial v} \max\{c_2 v^3,\ -c_1 v - c_3 v u\} + c_4 u^2{}_{|\dot{v} \geq 0} - \lambda_1 \tag{4.13}$$

Depending on λ_2, six cases need to be consider for calculating the optimal control, u^*.

1. If $\lambda_2 > 0$, $\lambda_2 > 2c_4 v a_U$

$$u^* = a_U \tag{4.14}$$

$$\dot{\lambda}_2 = 3c_2 v^2 + c_4 u^2 - \lambda_1 \tag{4.15}$$

2. $\lambda_2 > 0$, $\lambda_2 < 2c_4 v a_U$

$$u^* = \frac{\lambda_2}{2c_4 v} \tag{4.16}$$

$$\dot{\lambda}_2 = 3c_2 v^2 + c_4 u^2 - \lambda_1 \tag{4.17}$$

3. $\lambda_2 = 0$

$$u \in [a_c, 0] \tag{4.18}$$

$$\dot{\lambda}_2 = -\frac{\partial H}{\partial v} = 3c_2 v^2 - \lambda_1 \tag{4.19}$$

In this state, if we have $\lambda_1 = c_1 + 3c_2 v^2$, then we can select $u = 0$ for cruising state. Otherwise, this is only a transient state.

4. $\lambda_2 < 0$, $\lambda_2 + c_3 v > 0$

$$u = a_c = -\frac{c_2 v^2 + c_1}{c_3} \tag{4.20}$$

Here, a jump exists for H_y, due to the piece-wise linearity of the function at a_c. We will use the right-side derivative as the approximation of H_y at this point.

$$\dot{\lambda}_2 = -\frac{\partial H}{\partial v} = 3c_2 v^2 - \lambda_1 \tag{4.21}$$

5. $\lambda_2 < 0$, $\lambda_2 + c_3 v = 0$

$$u \in (a_L, a_c] \tag{4.22}$$

$$\dot{\lambda}_2 = \ -c_1 - c_3 u - \lambda_1 \tag{4.23}$$

6. $\lambda_2 < 0$, $\lambda_2 + c_3 v < 0$

$$u = a_L \tag{4.24}$$

$$\dot{\lambda}_2 = \ -c_1 - c_3 u - \lambda_1 \tag{4.25}$$

Based on these conditions, we can then construct four types of speed profiles associated with different boundary conditions.

Type 1. Acceleration-then-Deceleration speed profile

In this profile, the vehicle will start from accelerating, and end with decelerating. The illustration of Type 1 profile is shown in Figure 4.5. In this profile, the co-state λ_2 will decrease from an initial positive value, with vehicle accelerating. Then, after λ_2 reaches 0, the vehicle will go to a switching point when it reaches a critical speed v_c, and starts to decelerate. Afterwards, λ_2 will remain negative till the end of the trip. For this type of profile, we need to ensure that $\lambda_1 > 3c_2 v_c^2$. Otherwise, if $\lambda_1 < 3c_2 v_c^2$, the co-state λ_2 will remain positive, instead of decreasing to 0. If $\lambda_1 = 3c_2 v_c^2$, the vehicle will

approach the switching point indefinitely, as: $\dot{\lambda}_2 \to 0$, $u \to 0$ with $t \to +\infty$. With $\lambda_1 > 3c_2v_c^2$, after the switching point, we have $\dot{\lambda}_2 = 3c_2v^2 - \lambda_1$, which will remain negative so that the vehicle will remain decelerating.

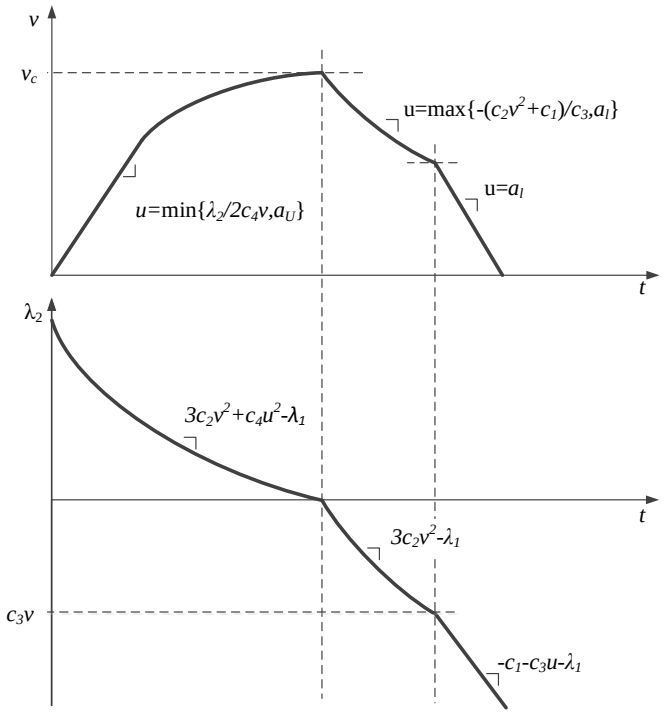

Figure 4.5: Acceleration-then-Deceleration speed profile

To find a Type 1 profile that satisfies the boundary conditions, the key is to find correct co-state $\lambda_1$and the switching speed v_c. The general idea is that, given a v_c and λ_1, one can construct the trajectory from the switching speed to starting speed in a backward fashion, and trajectory from switching speed to ending speed in a forward fashion. For a given v_c, we can enumerate λ_1 to

satisfy time constraint. Then, v_c can be enumerated to satisfy the distance constraint. The detailed algorithm is shown in Algorithm 4.1.

Algorithm 4.1 Searching for Type 1 Profile

```
1: v_c = v_T, δv > 0, δλ > 0
2: loop
3:     λ_1 = 3c_2 v_c^2 + δλ
4:     loop
5:         Construct acceleration portion from v_c to v_0, calculate T_1, x_1
6:         Construct acceleration portion from v_c to v_T, calculate T_2, x_2
7:         if T_1 + T_2 ≤ T then
8:             break
9:         else
10:            λ_1 = λ_1 + δλ
11:        end if
12:    end loop
13:    if v_c == max{v_0, v_T} and x_1 + x_2 > x_T then
14:        break;                    ▷ optimal profile is not Type 1 profile
15:    end if
16:    if x_1 + x_2 > x_T then
17:        break;                    ▷ find optimal Type 1 profile
18:    end if
19: end loop
```

Type 2. Acceleration only speed profile

In the second type of profile, the vehicle will accelerate throughout the whole trip. The illustration of acceleration only profile is shown in Figure 4.6. At the beginning, the co-state λ_2 will decrease from an initial positive value. However, instead of reaching 0, λ_2 will remain positive and start increasing after reaching a switching point. Correspondingly, the vehicle will keep accelerating throughout the trip. Note that in this profile, the switching

point is referred to the point where λ_2 switches from decreasing to increasing. At the switching point, we have:

$$\dot{\lambda}_2 = 3c_2v_c^2 + c_4\left[\min\{\frac{\lambda_2(t_c)}{2c_4v_c}, a_U\}\right]^2 - \lambda_1 = 0 \rightarrow \lambda_1 = 3c_2v_c^2 + c_4\left[\min\{\frac{\lambda_2(t_c)}{2c_4v_c}, a_U\}\right]^2$$

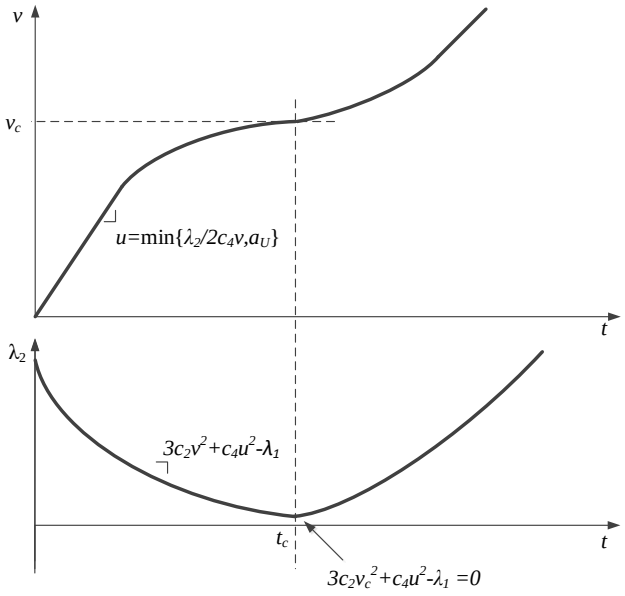

Figure 4.6: Acceleration only speed profile

To find a Type 2 profile that satisfies boundary conditions, the key is to find v_c and $\lambda_2(t_c)$ (and hence λ_1), at the switching point. Similarly to finding a Type 1 profile, given v_c, $\lambda_2(t_c)$, λ_1, we can construct the speed profile

from switching point to the two ends. For a given v_c, we will enumerate $\lambda_2(t_c)$ (equivalently λ_1), to satisfy travel time constraint. Then, v_c will be enumerated to satisfy the distance constraint. The detailed algorithm is shown in Algorithm 4.2.

Algorithm 4.2 Searching for Type 2 Profile

$v_c = v_T, \delta v > 0, \delta\lambda > 0, v_T > v_0$
loop
    $\lambda_2(t_c) = \delta\lambda$
    $\lambda_1 = 3c_2v_c^2 + c_4 \min\{\frac{\lambda_2(t_c)}{2c_4v_c}, a_U\}$
    loop
        Construct acceleration portion from v_c to v_0, calculate T_1, x_1
        Construct deceleration portion from v_c to v_T, calculate T_2, x_2
        if $T_1 + T_2 \leq T$ **then**
            break;
        else
            $\lambda_2(t_c) = \lambda_2(t_c) + \delta\lambda$
            $\lambda_1 = 3c_2v_c^2 + c_4 \min\{\frac{\lambda 2(t_c)}{2c_4v_c}, a_U\}$
        end if
    end loop
    if $x_1 + x_2 <= x_T$ **then**
        break; ▷ find optimal Type 2 profile
    else
        $v_c = v_c - \delta v$
    end if
    if $v_c < v_0$ **then**
        break ▷ optimal profile is not Type 2 profile
    end if
end loop

Type 3. Deceleration only speed profile

In the third type of profile, the vehicle will start from decelerating, then cruise, and finally end with decelerating. The illustration is shown in Figure

4.7. The vehicle starts from driving with a high speed, and an initial co-state λ_2 within the range of $(-c_3 v_c, 0)$. Depending on λ_1, we have two possibilities: 1. if $\lambda_1 = c_1 + 3c_2 v_c^2$, we have a cruising period, with $u = 0,\ \dot{\lambda}_2 = 0$; and 2. if $\lambda_1 > c_1 + 3c_2 v_c^2$, in other words, λ_2 remains negative when $\dot{\lambda}_2 = 0$, the vehicle will remain decelerating without cruising through out the trip. For profile without cruising period, we refer the point where λ_2 switches from increasing to decreasing as the switching point. For profile with cruising period, we have a switching segment with vehicle cruising, instead of a switching point.

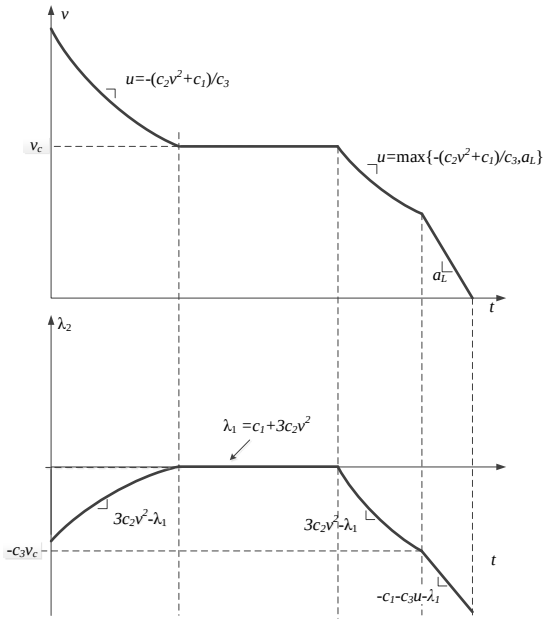

Figure 4.7: Deceleration only speed profile

To find a Type 3 profile, we apply a similar procedure. Given v_c and λ_1, we can construct the profile from the switching point or segment to the

two ends. Then, λ_1 is iterated to satisfy travel time constraint for a given v_c. Then, the v_c is iterated to satisfy distance constraint. The detailed algorithm is shown in Algorithm 4.3.

Algorithm 4.3 Searching for Type 3 Profile

```
1: v_c = v_0, δv > 0, δλ > 0, v_0 > v_T
2: loop
3:     λ_1 = 3c_2 v_c^2
4:     loop
5:         Construct dcceleration portion from v_c to v_0, calculate T_1, x_1
6:         Construct dcceleration portion from v_c to v_T, calculate T_2, x_2
7:         if T_1 + T_2 ≤ T then
8:             break
9:         else
10:            λ_1 = λ_1 + δλ
11:        end if
12:    end loop
13:    if λ_1 == 3c_2 v_c^2 and x_1 + x_2 + (T − T_1 − T_2)v_c < x_T then
14:        break;                    ▷ find optimal Type 3 profile w/ cruising
15:    else if x_1 + x_2 < x_T then
16:        break;                    ▷ find optimal Type 3 profile w/o cruising
17:    else
18:        v_c = v_c − δv;
19:    end if
20:    if v_c < v_T then
21:        break;                    ▷ optimal profile is not a Type 3 profile
22:    end if
23: end loop
```

Type 4. Deceleration-then-Acceleration speed profile

In this profile, the vehicle will start from decelerating, then end with accelerating. The illustration is shown in Figure 4.8. Similar to Type 3

profile, the vehicle also starts with a high speed, and a negative initial co-state λ_2 . In this case, we have $\lambda_1 < c_1 + 3c_2 v_c^2$, in other words, $\dot{\lambda}_2 > 0$ when λ_2 reaches 0. Then, the vehicle will enter acceleration state till the end of the trip. If $\lambda_1 < -c_1$, it is possible that at the beginning, the vehicle decelerates with brake activated, but then decelerates with brake deactivated. This is because that as $\dot{\lambda}_2 + c_3\dot{v} = -c_1 - \lambda_1 > 0$, it is possible $\lambda_2 + c_3 v$ could switch sign, instead of remaining negative. This case is also shown in the right part of Figure 4.8.

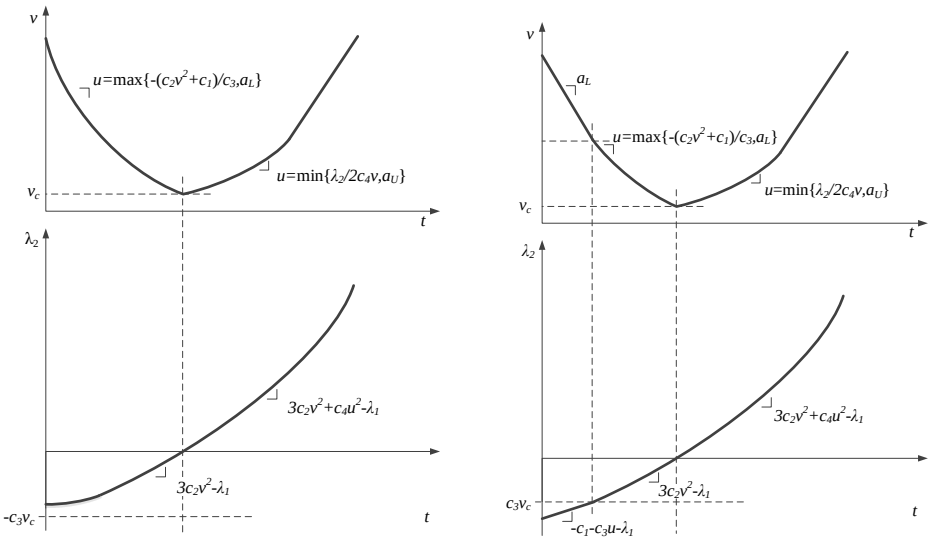

(a) Starting with brakes off (b) Starting with brakes on

Figure 4.8: Deceleration-then-Acceleration speed profile, starting with brakes off (A) and starting with brakes on (B)

To find a type 4 profile, similarly, given v_c and λ_1, we can construct the profile from the switching point to the two ends. Then, λ_1 is iterated to

satisfy time constraint for a given v_c, and v_c is iterated to satisfy distance constraint. The detailed algorithm is shown in Algorithm 4.4.

Algorithm 4.4 Searching for Type 4 Profile

```
1: v_c = min v_0, v_T, δv > 0, δλ > 0
2: loop
3:     λ_1 = 3c_2 v_c^2 − δλ
4:     loop
5:         Construct deceleration portion from v_c to v_0, calculate T_1, x_1
6:         Construct acceleration portion from v_c to v_T, calculate T_2, x_2
7:         if T_1 + T_2 ≤ T then
8:             break
9:         else
10:            λ_1 = λ_1 − δλ
11:        end if
12:    end loop
13:    if x_1 + x_2 < x_T then
14:        break;                          ▷ find optimal type 4 profile
15:    else
16:        v_c = v_c − δv
17:    end if
18: end loop
```

Overall Procedure

The flowchart for overall procedure is also shown in Figure 4.9. Essentially, the procedure will start with searching Type 1 profile, by setting $v_c = \min\{v_0, v_T\}$, and iterating λ_1. If the distance of the profile is smaller than total travel distance, the optimal profile will be a Type 1 profile, and we will increase v_c. Otherwise, if $v_0 < v_T$, we will try Type 2 profile, and enumerate v_c from v_T to v_0, to check if the distance constraint is satisfied. If $v_0 > v_T$, we will try Type 3 profile, and iterate v_c from v_0 to v_T. If neither

Type 2 or Type 3 profile could satisfy the distance constraint, the optimal profile will then be a Type 4 profile. We will then reduce v_c from $\min\{v_0, v_T\}$ to 0, until the distance constraint is satisfied.

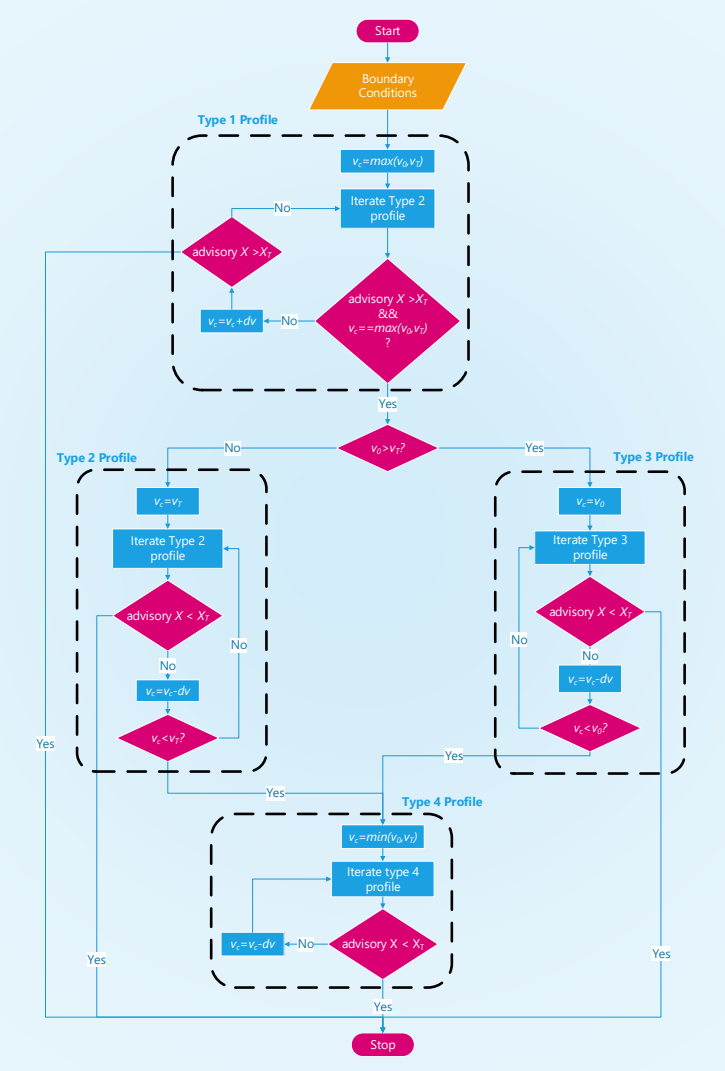

Figure 4.9: Overall procedure to generate optimal speed profile

4.4 Case Study

To evaluate the potential of the proposed procedure, a case study is conducted using data from SPMD project. A driver is selected from the SPMD project, and parts of his/her trajectories driving along a signalized road with 3 intersections are retrieved for analysis. The selected road is illustrated in Figure 4.10

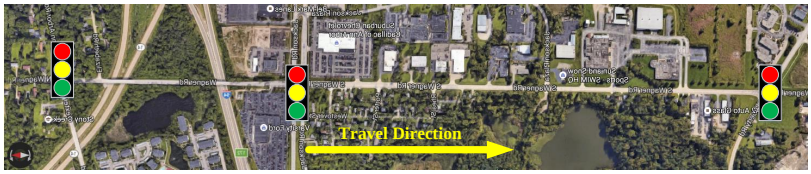

Figure 4.10: Illustration of the selected signalized road

Overall, 132 trips from the driver are selected for evaluation. The trajectories of the driver driving on the road are shown in Figure 4.11.

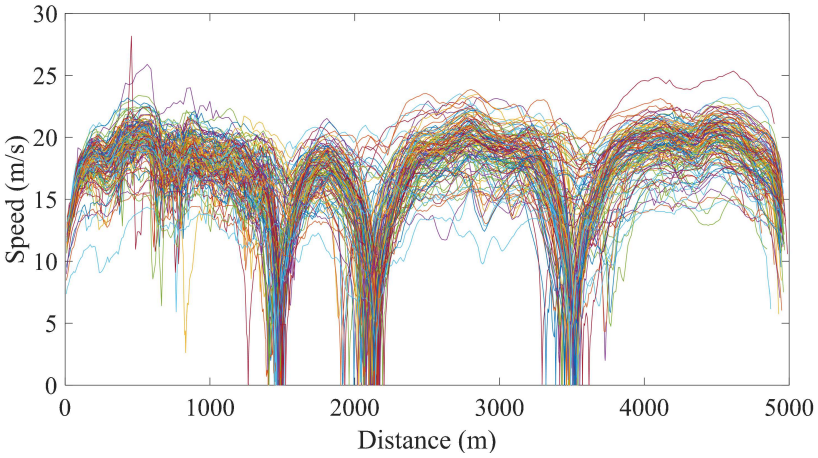

Figure 4.11: Illustration of vehicle trajectories on the selected road

For the driver approaching an intersection, boundary constraints need to be established to generate the speed advisory. The illustration of selecting boundary conditions is shown in Figure 4.1. The selection of the boundary condition is for the consideration that the optimized speed advisory will not compromise the driver's travel time budget while maintaining vehicle's physical position constrained by the queue in front. For each trajectory, the boundary points are first extracted, for vehicle driving through the selected segment. Then, the optimal trajectory is calculated for each part of the trajectories between two boundary points. The fuel consumption is then calculated using the look-up table, which would be more accurate than the analytical model.

To better illustrate the optimization, an example with comparison between the original trajectory and optimized trajectory is shown in Figure 4.12. As shown in the figure, the optimization intends to smooth the overall trajectory for better fuel economy. Also, note that no abrupt rate change exists during deceleration between two boundary points. This would suggest that the optimization intends to minimize or eliminate the activation of brake, but relies on rolling resistance and aerodynamic drag for decelerating. For this particular case, the fuel economy for the optimized trajectory is 26.61 MPG, and 24.12 MPG for the original trajectory, with 10.3% improvement from the optimization.

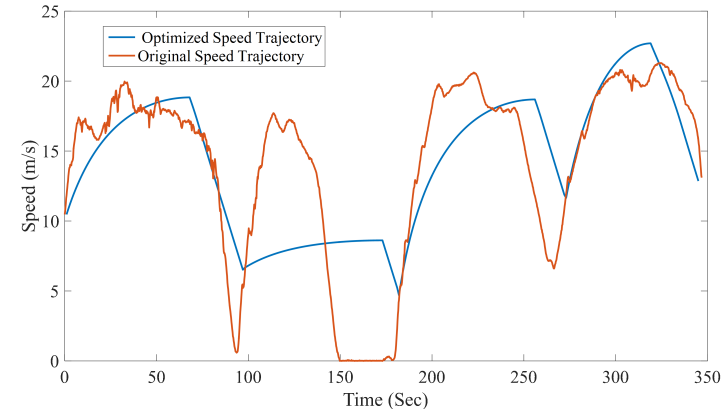

(a) Time-Speed Plot

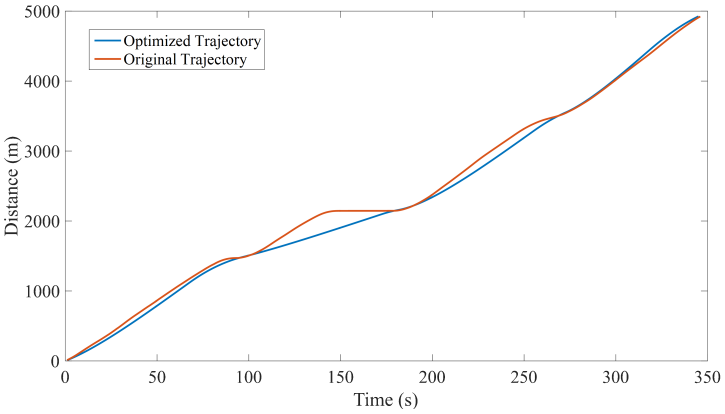

(b) Time-Distance Plot

Figure 4.12: Illustration of optimization by comparing optimized trajectory and original trajectory

The results for the optimized and original trajectories are listed in Figure 4.13, and also summarized in Table 4.2. As can be seen in the figure, the majority of the optimized trajectories outperform the original trajectories with better fuel economy. Notice that a few cases exist in which the optimization slightly under-perform the original trajectories. This is mainly due to the

difference between the analytical model with the look-up table. On average, the speed advisory improves the fuel economy by 10.5%, with 27.36 MPG for the optimized trajectories over 24.77 MPG for the original trajectories.

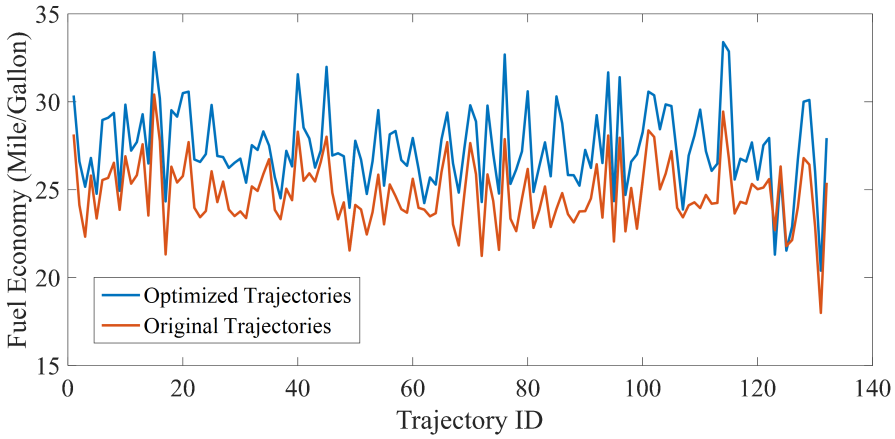

Figure 4.13: Fuel economy comparison between original and optimized trajectories

	Original Traj.	Optimized Traj.	Improvement
Average Fuel Economy (MPG)	24.77	27.36	10.5%

Table 4.2: Fuel economy for optimized and original trajectories

4.5 Chapter Summary

In this chapter, we propose a new approach to generate speed advisory for CV driving on signalized road for improving fuel economy. The

approach first analyzes historical driving data to generate personalized acceleration/deceleration bounds, as well as to calibrate parameters of the fuel consumption model. Then, an efficient algorithm is derived based on PMP to solve the optimal control problem.

To evaluate the proposed procedure, a case study is conducted using data from the SPMD project, focusing on a driver driving on a signal road with 3 intersections. Based on the case study, on average, the optimized speed advisory could improve the fuel economy by 10.5% from original trajectories without any advisories. The results indicate encouraging fuel-saving potential of the speed advisory system using V2I information.

Chapter 5

Conclusions and Future Research

5.1 Research Summary

The advents of CV technology are revolutionizing the transportation system. V2V and V2I communication not only provides opportunities to improve safety performance of vehicles, but also introduces significant potential to improve mobility and energy efficiency of the transportation system. With the focus on facilitating development and deployment of V2I systems at signalized intersections, this dissertation develops three innovative CV applications: 1. Automatic intersection map generation; 2. Traffic volume estimation; and 3. Eco-driving advisory with V2I information. Through analysis of real-world CV data collected in the SPMD project, encouraging results have

been obtained. Together, these three applications aim to leverage CV data for efficient and effective management of traffic signal systems.

Intersection Map Generation

In the first application, we developed a new approach to automatically generate intersection map using BSMs received by the RSEs. The proposed approach consists of three steps to estimate intersection map information: the pre-processing step to clean and categorize the BSM data, the estimation step to estimate approach and lane geometries, and the post-processing step to reorganize lane geometries. We applied the proposed approach to estimate map for five selected intersections from the SPMD project. The estimated maps were then compared with surveyed maps obtained from highly accurate LiDAR surveys, for the accuracy evaluation of the proposed approach.

Overall, encouraging results were obtained, albeit with some limitations. Using 1-month BSM data collected at each of the intersections, the estimation approach correctly identified most of the intersection structure regarding number of lanes for different movements. For the identified lanes, the accuracy of estimated lane geometries is 0.6 m on average, with the accuracy of the majority (90%) of the estimation within 1.2 m. Considering the robustness of the estimation, the accuracy of the worst estimations is 1.3 m on average, with majority (90%) within 2.2 m. The accuracy on average is well below the typical lane width of 3.6 m, while the worst estimations within each lane geometry are also with reasonable accuracy. Overall, the

evaluation would indicate the potential of using the estimated map for CV applications.

In addition to map estimation, we also investigated the feasibility of automatic SPaT-MAP association, i.e., associating vehicle movements with traffic signal phases, using signal status data and BSM data. A simple-yet-effective procedure was developed to estimate the association through matching vehicle departures with traffic signal status. A case study was conducted using data from one of the five intersections. In the case study, the proposed procedure was able to correctly associate vehicle movements to all applicable signal phases, validating the applicability of automatic SPaT-MAP association.

Overall, this application demonstrates the feasibility and potential of using CV data and signal status data to generate intersection map and lane-phase mapping automatically. The proposed procedure could be useful for deploying and maintaining V2I system at intersections in the near future.

Traffic Volume Estimation at Signalized Intersections

In the second application, we developed an innovative procedure to estimate traffic arrivals, particularly, traffic volumes, using data from the CVs. For traditional traffic signals, traffic volumes are the key inputs for optimizing signal settings. Considering CV deployments are still in their early stages, the focus of the proposed approach is to accommodate cases with low CV penetrations, for instance, 3% in the City of Ann Arbor, MI.

In our estimation algorithm, the traffic arrivals were modeled as a time dependent Poisson process and CV arrivals were treated as observations of the process. Then, an EM procedure was derived to estimate traffic volume, a key parameter of the process. To overcome the limitation of low CV penetration rates, it is proposed to aggregate historical CV data according to TOD periods. The proposed procedure was then evaluated with two case studies with real-world CV data, as well as GPS data from users of a navigation service.

In the first case study using CV data, the estimation yielded 10.1% to 12.3% MAPE, based on volume data collected manually from the field. In the second case study using GPS data from users of a navigation service, the estimation yielded 8.08% MAPE, based on volume data from loop detectors. Moreover, to illustrate the process of utilizing the estimation for traffic signal evaluation, the estimated data were utilized to generate TS-Diagram to evaluate the coordination qualities of traffic signals on an arterial road.

With this application, it is demonstrated that data from CVs with low penetrations can be utilized to generate performance measure for traffic signal system and adjust signal operation periodically, e.g., two weeks or a month, indicating great potential of CV data in assisting operation of existing traffic signals.

Eco-driving Advisory Generation with V2I Information

In the last application, an efficient procedure was developed to generate speed advisory for driving on signalized road based on traffic information from RSEs. In the proposed approach, historical driving data were first analyzed to obtain preferable acceleration and deceleration bounds, and to calibrate parameters for fuel consumption model. Then, an efficient algorithm was derived based on PMP to solved the optimal control problem for driving through signalized intersections with V2I information.

To evaluate the potential of the proposed system, a case study was conducted using data collected from the SPMD project. We selected a random driver and retrieved a part of his/her driving trajectories traveling through a signal road with 3 intersections. The trajectories were then optimized assuming that V2I information were available to the driver. On average, the optimized speed advisory improves the fuel economy by 10.5% from non-optimized driving, indicating encouraging potential of the speed advisory system.

5.2 Future Research

Several directions can be pursued for future research.

For intersection map generation, while the presented approach focuses on generating static maps using considerable amount of data (1-month data), in reality, the road networks are frequently affected by temporary changes such

as lane closures or geometry modifications due to constructions or traffic incidents. It would be interesting to investigate the feasibility of using CV data to identify dynamic changes of maps. This dynamic information could be extremely beneficial for real-time routing or driving assistance applications.

For the volume estimation application, the presented work is but the first step of exploring CV or trajectories data from navigation devices for assisting traffic signal operation and it can be extended in several directions. First, the proposed estimation is sensitive to interrupted traffic from adjacent parking lots or driveways which introduce significant noises to the vehicle trajectories. Thus, the proposed algorithm is mostly suitable for estimation at signalized intersections where no sink or source of traffic exists nearby the stop bar. Also, due to the assumption that no residual queue exists at start of signal cycles, the proposed approach is not suitable for estimation with oversaturated traffic conditions. We intend to address these limitations in our future work. Lastly, while the current focus is on estimating traffic arrival information, developing systematic approaches for traffic signal re-timing, regarding offsets, green splits, and cycle lengths as well as TOD schedules will be, another focus of our future work.

Another focus of our future research will be on jointly optimizing traffic signal operation and driving speeds of CVs. Currently, even though V2I communication enables information exchange between vehicles and infrastructure, the two systems are being operated separately. How to operate the two systems together as a holistic system to achieve their highest efficiency

could be another important direction for future research.

Bibliography

[1] D Bezzina and J Sayer. Safety pilot model deployment: Test conductor team report. *Report No. DOT HS 812 171*, 2014.

[2] Siva RK Narla. The evolution of connected vehicle technology: From smart drivers to smart cars to self-driving cars. *Institute of Transportation Engineers. ITE Journal*, 83(7):22, 2013.

[3] NTOC. 2012 national traffic signal report card. 2012.

[4] Nita Congress. The automated highway system: an idea whose time has come. *Public Roads*, 58(1), 1994.

[5] Sanghyun Cheon. An overview of automated highway systems (ahs) and the social and institutional challenges they face. *University of California Transportation Center*, 2003.

[6] Ram Kandarpa, Mujib Chenzaie, Matthew Dorfman, Justin Anderson, Jim Marousek, Ian Schworer, Joe Beal, Chris Anderson, Tim Weil, and Frank Perry. Final report: Vehicle infrastructure integration (vii) proof of concept (poc) test–executive summary. *US Department of Transportation, IntelliDrive (SM), Tech. Rep*, 2009.

[7] Jim Barbaresso, Gustave Cordahi, Dominie Garcia, Christopher Hill, Alex Jendzejec, and Karissa Wright. Usdot's intelligent transportation systems (its) its strategic plan 2015-2019. Technical report, 2014.

[8] Jon Masters. Making the right connections. *ITS International*, pages 9–11, 2016.

[9] The White House. Obama administration announces columbus, oh winner of the smart city challenge to pioneer the future of transportation, 2016.

[10] NHTSA. Advance notice of proposed rulemaking for v2v communications. Technical report, 2014.

[11] Olivia Marcus. Car-to-car communication may hit roads soon, 2015.

[12] Edward A Mueller. Aspects of the history of traffic signals. *IEEE Transactions on Vehicular Technology*, 19(1):6–17, 1970.

[13] Clay McShane. The origins and globalization of traffic control signals. *Journal of Urban History*, 25(3):379–404, 1999.

[14] Lawrence A Klein, Milton K Mills, and David RP Gibson. Traffic detector handbook: -volume ii. Technical report, 2006.

[15] Gordon M Sessions. Traffic devices: historical aspects thereof. 1971.

[16] Fo Vo Webster. Traffic signal settings. Technical report, 1958.

[17] Nathan H Gartner, John DC Little, and Henry Gabbay. Optimization of traffic signal settings by mixed-integer linear programming: Part i: The network coordination problem. *Transportation Science*, 9(4):321–343, 1975.

[18] Nathan H Gartner. A versatile program for setting signals on arteries and triangular networks john dc little* mark d. kelson. 1981.

[19] Nathan H Gartner, Susan F Assmann, Fernando Lasaga, and Dennis L Hous. Multiband–a variable-bandwidth arterial progression scheme. *Transportation Research Record*, (1287), 1990.

[20] Dennis I Robertson. Transyt: a traffic network study tool. 1969.

[21] Feng-Bor Lin. *Estimation of average phase durations for full-actuated signals*. Number HS-034 942. 1982.

[22] Feng-Bor Lin. Predictive models of traffic-actuated cycle splits. *Transportation Research Part B: Methodological*, 16(5):361–372, 1982.

[23] Rahmi Akcelik. Estimation of green times and cycle time for vehicle-actuated. 1994.

[24] Alexander Skabardonis. Determination of timings in signal systems with traffic-actuated controllers. *Transportation Research Record: Journal of the Transportation Research Board*, (1554):18–26, 1996.

[25] Montasir Abbas, Darcy Bullock, and Larry Head. Real-time offset transitioning algorithm for coordinating traffic signals. *Transportation Research Record: Journal of the Transportation Research Board*, (1748):26–39, 2001.

[26] Edward Smaglik, Anuj Sharma, Darcy Bullock, James Sturdevant, and Gary Duncan. Event-based data collection for generating actuated controller performance measures. *Transportation Research Record: Journal of the Transportation Research Board*, (2035):97–106, 2007.

[27] Yafeng Yin, Meng Li, and Alexander Skabardonis. Offline offset refiner for coordinated actuated signal control systems 1. *Journal of transportation engineering*, 133(7):423–432, 2007.

[28] Lihui Zhang and Yafeng Yin. Robust synchronization of actuated signals on arterials. *Transportation Research Record: Journal of the Transportation Research Board*, (2080):111–119, 2008.

[29] Jianfeng Zheng, Henry Liu, and Steve Misgen. Fine-tuning time-of-day transitions for arterial traffic signals. *Transportation Research Record: Journal of the Transportation Research Board*, (2488):32–40, 2015.

[30] Jianfeng Zheng, Henry Liu, Steve Misgen, and Guizhen Yu. Performance diagnosis tool for arterial traffic signals. *Transportation Research Record: Journal of the Transportation Research Board*, (2356):109–116, 2013.

[31] Christopher Day, Ross Haseman, Hiromal Premachandra, Thomas Brennan Jr, Jason Wasson, James Sturdevant, and Darcy Bullock. Evaluation of arterial signal coordination: methodologies for visualizing high-resolution event data and measuring travel time. *Transportation Research Record: Journal of the Transportation Research Board*, (2192):37–49, 2010.

[32] Christopher Day and Darcy Bullock. Computational efficiency of alternative algorithms for arterial offset optimization. *Transporta-*

tion Research Record: Journal of the Transportation Research Board, (2259):37–47, 2011.

[33] Henry X Liu, Xinkai Wu, Wenteng Ma, and Heng Hu. Real-time queue length estimation for congested signalized intersections. *Transportation research part C: emerging technologies*, 17(4):412–427, 2009.

[34] Henry X Liu and Wenteng Ma. A virtual vehicle probe model for time-dependent travel time estimation on signalized arterials. *Transportation Research Part C: Emerging Technologies*, 17(1):11–26, 2009.

[35] Jianfeng Zheng, Henry Liu, Steve Misgen, Kevin Schwartz, Bob Green, and Mike Anderson. Use of event-based traffic data in generating time-space diagrams for evaluation of signal coordination. *Transportation Research Record: Journal of the Transportation Research Board*, (2439):94–104, 2014.

[36] John McCracken. Demonstration project 93–making the most of today's technology. *Public Roads*, 59(3), 1996.

[37] Peter Koonce, Lee Rodegerdts, Kevin Lee, Shaun Quayle, Scott Beaird, Cade Braud, Jim Bonneson, Phil Tarnoff, and Tom Urbanik. Traffic signal timing manual. Technical report, 2008.

[38] SAE. Dedicated short range communications (dsrc) message set dictionary: J2735. 2009.

[39] John Harding, Gregory Powell, Rebecca Yoon, Joshua Fikentscher, Charlene Doyle, Dana Sade, Mike Lukuc, Jim Simons, and Jing Wang. Vehicle-to-vehicle communications: Readiness of v2v technology for application. Technical report, 2014.

[40] John B Kenney. Dedicated short-range communications (dsrc) standards in the united states. *Proceedings of the IEEE*, 99(7):1162–1182, 2011.

[41] Stefan Schroedl, Kiri Wagstaff, Seth Rogers, Pat Langley, and Christopher Wilson. Mining gps traces for map refinement. *Data mining and knowledge Discovery*, 9(1):59–87, 2004.

[42] Tao Guo, Kazuaki Iwamura, and Masashi Koga. Towards high accuracy road maps generation from massive gps traces data. In *2007 IEEE International Geoscience and Remote Sensing Symposium*, 2007.

[43] Lijuan Zhang, Frank Thiemann, and Monika Sester. Integration of gps traces with road map. In *Proceedings of the second international workshop on computational transportation science*, pages 17–22. ACM, 2010.

[44] Patrick Baier, Harald Weinschrott, Frank Dürr, and Kurt Rothermel. Mapcorrect: automatic correction and validation of road maps using public sensing. In *Local Computer Networks (LCN), 2011 IEEE 36th Conference on*, pages 58–66. IEEE, 2011.

[45] Fernando Torre, David Pitchford, Phil Brown, and Loren Terveen. Matching gps traces to (possibly) incomplete map data: bridging map building and map matching. In *Proceedings of the 20th International Conference on Advances in Geographic Information Systems*, pages 546–549. ACM, 2012.

[46] Yin Wang, Xuemei Liu, Hong Wei, George Forman, Chao Chen, and Yanmin Zhu. Crowdatlas: self-updating maps for cloud and personal use. In *Proceeding of the 11th annual international conference on Mobile systems, applications, and services*, pages 27–40. ACM, 2013.

[47] Xin Chen, Brad Kohlmeyer, Matei Stroila, Narayana Alwar, Ruisheng Wang, and Jeff Bach. Next generation map making: geo-referenced ground-level lidar point clouds for automatic retro-reflective road feature extraction. In *Proceedings of the 17th ACM SIGSPATIAL International Conference on Advances in Geographic Information Systems*, pages 488–491. ACM, 2009.

[48] Wenhuan Shi, Shuhan Shen, and Yuncai Liu. Automatic generation of road network map from massive gps, vehicle trajectories. In *Intelligent Transportation Systems, 2009. ITSC'09. 12th International IEEE Conference on*, pages 1–6. IEEE, 2009.

[49] Albert Steiner and Axel Leonhardt. Map-generation algorithm using low-frequency vehicle position data. In *Transportation Research Board 90th Annual Meeting*, number 11-0486, 2011.

[50] Stewart Worrall and Eduardo Nebot. Automated process for generating digitised maps through gps data compression. In *Australasian Conference on Robotics and Automation*, 2007.

[51] Sera Jang, Taehwan Kim, and Eunseok Lee. Map generation system with lightweight gps trace data. In *Advanced Communication Technology (ICACT), 2010 The 12th International Conference on*, volume 2, pages 1489–1493. IEEE, 2010.

[52] Lili Cao and John Krumm. From gps traces to a routable road map. In *Proceedings of the 17th ACM SIGSPATIAL International Conference on Advances in Geographic Information Systems*, pages 3–12. ACM, 2009.

[53] Gabriel Agamennoni, Juan I Nieto, and Eduardo M Nebot. Robust inference of principal road paths for intelligent transportation systems. *Intelligent Transportation Systems, IEEE Transactions on*, 12(1):298–308, 2011.

[54] Sophia Karagiorgou and Dieter Pfoser. On vehicle tracking data-based road network generation. In *Proceedings of the 20th international conference on advances in geographic information systems*, pages 89–98. ACM, 2012.

[55] Jun Li, Qiming Qin, Chao Xie, and Yue Zhao. Integrated use of spatial and semantic relationships for extracting road networks from floating car data. *International Journal of Applied Earth Observation and Geoinformation*, 19:238–247, 2012.

[56] Kiri Wagstaff, Claire Cardie, Seth Rogers, Stefan Schrödl, et al. Constrained k-means clustering with background knowledge. In *ICML*, volume 1, pages 577–584, 2001.

[57] Yihua Chen and John Krumm. Probabilistic modeling of traffic lanes from gps traces. In *Proceedings of the 18th SIGSPATIAL International Conference on Advances in Geographic Information Systems*, pages 81–88. ACM, 2010.

[58] ERIAC Uduwaragoda, AS Perera, and SAD Dias. Generating lane level road data from vehicle trajectories using kernel density estimation.

In *Intelligent Transportation Systems-(ITSC), 2013 16th International IEEE Conference on*, pages 384–391. IEEE, 2013.

[59] Sören Kammel and Benjamin Pitzer. Lidar-based lane marker detection and mapping. In *Intelligent Vehicles Symposium, 2008 IEEE*, pages 1137–1142. IEEE, 2008.

[60] Albert S Huang, David Moore, Matthew Antone, Edwin Olson, and Seth Teller. Finding multiple lanes in urban road networks with vision and lidar. *Autonomous Robots*, 26(2-3):103–122, 2009.

[61] Brian Bailey. A benchmark for data fusion, 2012.

[62] T Kardi. K-means clustering tutorials, 2006.

[63] Mahmuda Ahmed, Sophia Karagiorgou, Dieter Pfoser, and Carola Wenk. A comparison and evaluation of map construction algorithms using vehicle tracking data. *GeoInformatica*, 19(3):601–632, 2015.

[64] Chris Veness. Calculate distance and bearing between two latitude/longitude points using haversine formula in javascript, 2010. *URL http://www. movable-type. co. uk/scripts/latlong. html. Fetched January*, 2012.

[65] Yiheng Feng. *Intelligent Traffic Control in a Connected Vehicle Environment*. PhD thesis, UNIVERSITY OF ARIZONA, 2015.

[66] Kevin Gay and Valarie Kniss. Safety pilot model deployment lessons learned and recommendations for future connected vehicle activities. Technical report, USDOT FHWA-JPO-16-363, 2015.

[67] Seli James Agbolosu-Amison, Brian Park, and Mid-Atlantic Universities Transportation Center. Performance evaluation of dynamic gap-out feature using stochastic optimization method and software in the loop simulation. Technical report, Mid-Atlantic Universities Transportation Center, 2008.

[68] Joyoung Lee, Byungkyu Park, and Ilsoo Yun. Cumulative travel-time responsive real-time intersection control algorithm in the connected vehicle environment. *Journal of Transportation Engineering*, 139(10):1020–1029, 2013.

[69] Joyoung Lee, Byungkyu Brian Park, Kristin Malakorn, and Jaehyun Jason So. Sustainability assessments of cooperative vehicle intersection control at an urban corridor. *Transportation Research Part C: Emerging Technologies*, 32:193–206, 2013.

[70] Noah J Goodall, Brian L Smith, and Byungkyu Brian Park. Microscopic estimation of freeway vehicle positions from the behavior of connected vehicles. *Journal of Intelligent Transportation Systems*, 20(1):45–54, 2016.

[71] Qing He, K Larry Head, and Jun Ding. Pamscod: Platoon-based arterial multi-modal signal control with online data. *Transportation Research Part C: Emerging Technologies*, 20(1):164–184, 2012.

[72] Qing He, K Larry Head, and Jun Ding. Multi-modal traffic signal control with priority, signal actuation and coordination. *Transportation Research Part C: Emerging Technologies*, 46:65–82, 2014.

[73] Yiheng Feng, K Larry Head, Shayan Khoshmagham, and Mehdi Zamanipour. A real-time adaptive signal control in a connected vehicle environment. *Transportation Research Part C: Emerging Technologies*, 55:460–473, 2015.

[74] S Ilgin Guler, Monica Menendez, and Linus Meier. Using connected vehicle technology to improve the efficiency of intersections. *Transportation Research Part C: Emerging Technologies*, 46:121–131, 2014.

[75] Vicente Milanés, Jorge Villagra, Jorge Godoy, Javier Simó, Joshué Pérez, and Enrique Onieva. An intelligent v2i-based traffic management system. *Intelligent Transportation Systems, IEEE Transactions on*, 13(1):49–58, 2012.

[76] Christopher M Day and Darcy M Bullock. Opportunities for detector-free signal offset optimization with limited connected vehicle market penetration: A proof-of-concept study. *Transportation Research Record*, 2016.

[77] Juan C Herrera, Daniel B Work, Ryan Herring, Xuegang Jeff Ban, Quinn Jacobson, and Alexandre M Bayen. Evaluation of traffic data

obtained via gps-enabled mobile phones: The mobile century field experiment. *Transportation Research Part C: Emerging Technologies*, 18(4):568–583, 2010.

[78] Baik Hoh, Marco Gruteser, Ryan Herring, Jeff Ban, Daniel Work, Juan-Carlos Herrera, Alexandre M Bayen, Murali Annavaram, and Quinn Jacobson. Virtual trip lines for distributed privacy-preserving traffic monitoring. In *Proceedings of the 6th international conference on Mobile systems, applications, and services*, pages 15–28. ACM, 2008.

[79] Daniel B Work, Olli-Pekka Tossavainen, Sébastien Blandin, Alexandre M Bayen, Tochukwu Iwuchukwu, and Kenneth Tracton. An ensemble kalman filtering approach to highway traffic estimation using gps enabled mobile devices. In *Decision and Control, 2008. CDC 2008. 47th IEEE Conference on*, pages 5062–5068. IEEE, 2008.

[80] Mei Chen and Steven Chien. Dynamic freeway travel-time prediction with probe vehicle data: Link based versus path based. *Transportation Research Record: Journal of the Transportation Research Board*, (1768):157–161, 2001.

[81] Chumchoke Nanthawichit, Takashi Nakatsuji, and Hironori Suzuki. Application of probe-vehicle data for real-time traffic-state estimation and short-term travel-time prediction on a freeway. *Transportation Research Record: Journal of the Transportation Research Board*, (1855):49–59, 2003.

[82] Erik Jenelius and Haris N Koutsopoulos. Travel time estimation for urban road networks using low frequency probe vehicle data. *Transportation Research Part B: Methodological*, 53:64–81, 2013.

[83] Fangfang Zheng and Henk Van Zuylen. Urban link travel time estimation based on sparse probe vehicle data. *Transportation Research Part C: Emerging Technologies*, 31:145–157, 2013.

[84] Bruce R Hellinga and Liping Fu. Reducing bias in probe-based arterial link travel time estimates. *Transportation Research Part C: Emerging Technologies*, 10(4):257–273, 2002.

[85] Ashish Bhaskar, Edward Chung, and André-Gilles Dumont. Fusing loop detector and probe vehicle data to estimate travel time statistics

on signalized urban networks. *Computer-Aided Civil and Infrastructure Engineering*, 26(6):433–450, 2011.

[86] Ruey Long Cheu, Chi Xie, and Der-Horng Lee. Probe vehicle population and sample size for arterial speed estimation. *Computer-Aided Civil and Infrastructure Engineering*, 17(1):53–60, 2002.

[87] Shawn M Turner and Douglas J Holdener. Probe vehicle sample sizes for real-time information: The houston experience. In *Vehicle Navigation and Information Systems Conference, 1995. Proceedings. In conjunction with the Pacific Rim TransTech Conference. 6th International VNIS.'A Ride into the Future'*, pages 3–10. IEEE, 1995.

[88] Gurcan Comert and Mecit Cetin. Queue length estimation from probe vehicle location and the impacts of sample size. *European Journal of Operational Research*, 197(1):196–202, 2009.

[89] Gurcan Comert. Simple analytical models for estimating the queue lengths from probe vehicles at traffic signals. *Transportation Research Part B: Methodological*, 55:59–74, 2013.

[90] Gurcan Comert. Queue length estimation from probe vehicles at isolated intersections: Estimators for primary parameters. *European Journal of Operational Research*, 252(2):502–521, 2016.

[91] Peng Hao, Zhanbo Sun, Xuegang Jeff Ban, Dong Guo, and Qiang Ji. Vehicle index estimation for signalized intersections using sample travel times. *Transportation Research Part C: Emerging Technologies*, 36:513–529, 2013.

[92] Peng Hao, Xuegang Jeff Ban, Dong Guo, and Qiang Ji. Cycle-by-cycle intersection queue length distribution estimation using sample travel times. *Transportation research part B: methodological*, 68:185–204, 2014.

[93] Paul I Richards. Shock waves on the highway. *Operations research*, 4(1):42–51, 1956.

[94] Michael J Lighthill and Gerald Beresford Whitham. On kinematic waves. ii. a theory of traffic flow on long crowded roads. In *Proceedings of the Royal Society of London A: Mathematical, Physical and*

Engineering Sciences, volume 229, pages 317–345. The Royal Society, 1955.

[95] Mecit Cetin. Estimating queue dynamics at signalized intersections from probe vehicle data: Methodology based on kinematic wave model. *Transportation Research Record: Journal of the Transportation Research Board*, (2315):164–172, 2012.

[96] Eleni Christofa, Juan Argote, and Alexander Skabardonis. Arterial queue spillback detection and signal control based on connected vehicle technology. *Transportation Research Record: Journal of the Transportation Research Board*, (2356):61–70, 2013.

[97] Jing-Quan Li, Kun Zhou, Steven Shladover, and Alexander Skabardonis. Estimating queue length under connected vehicle technology: Using probe vehicle, loop detector, and fused data. *Transportation Research Record: Journal of the Transportation Research Board*, (2356):17–22, 2013.

[98] Carlos F Daganzo. A variational formulation of kinematic waves: basic theory and complex boundary conditions. *Transportation Research Part B: Methodological*, 39(2):187–196, 2005.

[99] Zhanbo Sun and Xuegang Jeff Ban. Vehicle trajectory reconstruction for signalized intersections using mobile traffic sensors. *Transportation Research Part C: Emerging Technologies*, 36:268–283, 2013.

[100] Jeff A Bilmes et al. A gentle tutorial of the em algorithm and its application to parameter estimation for gaussian mixture and hidden markov models. *International Computer Science Institute*, 4(510):126, 1998.

[101] US Energy Information Administration. Annual energy outlook, 2014.

[102] Eva Ericsson. Independent driving pattern factors and their influence on fuel-use and exhaust emission factors. *Transportation Research Part D: Transport and Environment*, 6(5):325–345, 2001.

[103] Kyoungho Ahn, Hesham Rakha, Antonio Trani, and Michel Van Aerde. Estimating vehicle fuel consumption and emissions based on instantaneous speed and acceleration levels. *Journal of transportation engineering*, 128(2):182–190, 2002.

[104] Yonglian Ding and Hesham Rakha. Trip-based explanatory variables for estimating vehicle fuel consumption and emission rates. *Water, Air and Soil Pollution: Focus*, 2(5-6):61–77, 2002.

[105] Matthew Barth and Kanok Boriboonsomsin. Energy and emissions impacts of a freeway-based dynamic eco-driving system. *Transportation Research Part D: Transport and Environment*, 14(6):400–410, 2009.

[106] Karsten Jakobsen, Sabrine CH Mouritsen, and Kristian Torp. Evaluating eco-driving advice using gps/canbus data. In *Proceedings of the 21st ACM SIGSPATIAL International Conference on Advances in Geographic Information Systems*, pages 44–53. ACM, 2013.

[107] Leonard Evans and Robert Herman. Automobile fuel economy on fixed urban driving schedules. *Transportation Science*, 12(2):137–152, 1978.

[108] AB Schwarzkopf and RB Leipnik. Control of highway vehicles for minimum fuel consumption over varying terrain. *Transportation Research*, 11(4):279–286, 1977.

[109] JN Hooker. Optimal driving for single-vehicle fuel economy. *Transportation Research Part A: General*, 22(3):183–201, 1988.

[110] Chaozhe R He and Gábor Orosz. Fuel consumption optimization of heavy-duty vehicles: An analytical approach. In *ASME 2014 Dynamic Systems and Control Conference*, pages V002T20A006–V002T20A006. American Society of Mechanical Engineers, 2014.

[111] Y Saboohi and H Farzaneh. Model for developing an eco-driving strategy of a passenger vehicle based on the least fuel consumption. *Applied Energy*, 86(10):1925–1932, 2009.

[112] Bart Saerens, Jeroen Vandersteen, Tim Persoons, Jan Swevers, Moritz Diehl, and Eric Van den Bulck. Minimization of the fuel consumption of a gasoline engine using dynamic optimization. *Applied energy*, 86(9):1582–1588, 2009.

[113] Bojin Liu, Dipak Ghosal, Chen-Nee Chuah, and H Michael Zhang. Reducing greenhouse effects via fuel consumption-aware variable speed limit (fc-vsl). *Vehicular Technology, IEEE Transactions on*, 61(1):111–122, 2012.

[114] Hesham Rakha and Raj Kishore Kamalanathsharma. Eco-driving at signalized intersections using v2i communication. In *Intelligent Transportation Systems (ITSC), 2011 14th International IEEE Conference on*, pages 341–346. IEEE, 2011.

[115] Tianyi Guan and Christian W Frey. Predictive fuel efficiency optimization using traffic light timings and fuel consumption model. In *Intelligent Transportation Systems-(ITSC), 2013 16th International IEEE Conference on*, pages 1553–1558. IEEE, 2013.

[116] Engin Ozatay, Umit Ozguner, Simona Onori, and Giorgio Rizzoni. Analytical solution to the minimum fuel consumption optimization problem with the existence of a traffic light. In *ASME 2012 5th Annual Dynamic Systems and Control Conference joint with the JSME 2012 11th Motion and Vibration Conference*, pages 837–846. American Society of Mechanical Engineers, 2012.

[117] Maazen Alsabaan, Kshirasagar Naik, and Tarek Khalifa. Optimization of fuel cost and emissions using v2v communications. *Intelligent Transportation Systems, IEEE Transactions on*, 14(3):1449–1461, 2013.

[118] Shengbo Eben Li, Shaobing Xu, Xiaoyu Huang, Bo Cheng, and Huei Peng. Eco-departure of connected vehicles with v2x communication at signalized intersections. *IEEE Transactions on Vehicular Technology*, 64(12):5439–5449, 2015.

[119] Rahmi Akcelik and Mark Besley. Operating cost, fuel consumption, and emission models in aasidra and aamotion. In *25th conference of australian institutes of transport research (CAITR 2003)*, pages 1–15, 2003.

[120] Gerald L Thompson. *Optimal Control Theory: Applications to Management Science and Economics*. Springer, 2006.